

UNIVERSIDADE DE LISBOA INSTITUTO SUPERIOR TÉCNICO



Design of soil biocementation strategies using biological activity monitored with biosensors

Inês Costa Feijão Borges

Supervisor: Doctor Maria Rafaela Pinheiro Cardoso

Co-Supervisor: Doctor Susana Isabel Pinheiro Cardoso de Freitas

Thesis approved in public session to obtain the PhD Degree in Civil Engineering

Jury final classification: Pass with Distinction

2025



UNIVERSIDADE DE LISBOA INSTITUTO SUPERIOR TÉCNICO

Design of soil biocementation strategies using biological activity monitored with biosensors

Inês Costa Feijão Borges

Supervisor: Doctor Maria Rafaela Pinheiro Cardoso

Co-Supervisor: Doctor Susana Isabel Pinheiro Cardoso de Freitas

Thesis approved in public session to obtain the PhD Degree in Civil Engineering

Jury final classification: Pass with Distinction

Jury

Chairperson: Doctor Helena Margarida Machado da Silva Ramos, Instituto Superior Técnico, Universidade de Lisboa

Members of the Committee:

Doctor João Pedro Estrela Rodrigues Conde, Instituto Superior Técnico, Universidade de Lisboa Doctor Maria Rafaela Pinheiro Cardoso, Instituto Superior Técnico, Universidade de Lisboa Doctor Grainne El Mountassir, Department of Civil and Environmental Engineering, University of Strathclyde, Glasgow, Reino Unido

Doctor Paulo José da Venda Oliveira, Faculdade de Ciências e Tecnologia, Universidade de Coimbra Doctor Rui Pedro Carrilho Gomes, Instituto Superior Técnico, Universidade de Lisboa

Funding Institutions

Fundação para a Ciência e a Tecnologia – FCT

Abstract

This thesis contributes to the advancement of the study on biocementation, which is an environmentally friendly

technique used for soil stabilization in geotechnical engineering. It is divided into three main parts, each focused

on a n important topic of the design of solutions for the use of this technique, namely: (i) bacteria and clay

mineral interaction, (ii) monitoring using a novel biosensor, and (iii) the development of a biocementation

chamber for laboratory tests, to prepare more homogeneous samples.

The first part investigates the impact of clay minerals on biocementation, by studying calcium carbonate

precipitation and S. pasteurii growth in the presence of kaolin and bentonite with different quantities. Optimal

clay percentages range from 5% to 10% for kaolin and 5% for bentonite considering bacterial survival and the

amount of biocement precipitated. The study highlights the importance of considering clay-bacteria interaction

and practical treatment fluid access. Overall, clay minerals play a crucial role in promoting biocementation

effectiveness, being a potential additive to enhance treatment.

The second part is focused on optimizing a biosensor for monitoring biocementation by measuring the amount

of urease enzyme present in pore fluids. Key optimization factors include the operational range, cross-reactions,

portability, user-friendliness, soil particle interference, and economic management. The biosensor, optimized for

detecting purified urease from C. ensiformis, yielded calibration curves valid for different concentration ranges.

It successfully estimated urease concentration in enzyme induced calcite precipitation (EICP) treated sand

samples, confirming its potential to be used for predicting biocement content. Despite sensor's limitations, its

use as monitoring tool for biocementation is promising and has the potential to become an important design

tool.

The third part details the development of a new biocementation chamber and its application in treating sand

samples with EICP. The chamber allows for permeability measurement and intact specimen extraction for

mechanical characterization, offering advantages over conventional methods. Analysis of treated samples

revealed a lightly biocemented level. SEM images indicate calcite presence and with smoother textures observed

in biocemented samples. Mechanical tests showed a decrease in friction angle after treatment, alongside

increased compressibility, highlighting a particle-level phenomenon.

Although still some challenges remain unsolved, this thesis contributes to advancing our understanding of

biocementation and its practical applications in geotechnical engineering.

Keywords:

Biocementation; Clay-bacteria; Biosensor; Monitoring; Biocementation chamber

Resumo

Esta tese contribui para o avanço do estudo da biocimentação, que é uma técnica ecológica utilizada para a

estabilização de solos em engenharia geotécnica. Está dividida em três partes principais, cada uma centrada num

aspeto importante do dimensionamento de soluções para a utilização desta técnica, nomeadamente: (i)

interação entre bactérias e minerais argilosos, (ii) monitorização utilizando um novo biossensor, e (iii)

desenvolvimento de uma câmara de biocimentação para ensaios laboratoriais e preparar amostras mais

homogéneas.

Uma primeira parte investiga o impacto dos minerais argilosos na biocimentação, estudando a precipitação de

carbonato de cálcio e o crescimento de S. pasteurii na presença de caulinite e bentonite em diferentes

quantidades. As percentagens ótimas de argila variam entre 5% e 10% para a caulinite e 5% para a bentonite,

tendo em conta a sobrevivência bacteriana e a quantidade de biocimento precipitado. O estudo realça a

importância de considerar a interação argila-bactéria e o acesso prático ao fluido de tratamento. No geral, os

minerais de argila desempenham um papel crucial na eficácia da biocimentação, sendo um potencial aditivo para

melhorar o tratamento.

A segunda parte centra-se na otimização de um biossensor para monitorizar a biocimentação através da medição

da quantidade de enzima urease presente nos fluidos dos vazios. Os principais fatores de otimização incluem a

gama de funcionamento, as reações cruzadas, a portabilidade, a facilidade de utilização, a interferência das

partículas do solo e a gestão económica. O biossensor, otimizado para detetar a urease purificada de C.

ensiformis, definiu curvas de calibração válidas para diferentes gamas de concentração. Estimou com sucesso a

concentração de urease em amostras de areia tratadas com precipitação de calcite induzida por enzima (EICP do

termo em inglês), confirmando o seu potencial para ser utilizado na previsão do teor de biocimento. Apesar das

limitações do sensor, a sua utilização como ferramenta de monitorização da biocimentação é promissora e tem

potencial para se tornar uma importante ferramenta de dimensionamento.

A terceira parte descreve em pormenor o desenvolvimento de uma nova câmara de biocimentação e a sua

aplicação no tratamento de amostras de areia com EICP. A câmara permite a medição da permeabilidade e a

extração de amostras intactas para caraterização mecânica, oferecendo vantagens em relação aos métodos

convencionais. A análise das amostras tratadas revelou um nível de biocimentação ligeiro. As imagens de SEM

indicam a presença de calcite, observaram-se texturas mais suaves nas amostras biocimentadas. Os testes

mecânicos mostraram uma diminuição do ângulo de atrito após o tratamento, juntamente com um aumento da

compressibilidade, evidenciando um fenómeno ao nível das partículas.

Embora ainda existam alguns desafios por resolver, esta tese contribui para o avanço da nossa compreensão da

biocimentação e das suas aplicações práticas na engenharia geotécnica.

Palavras-chave:

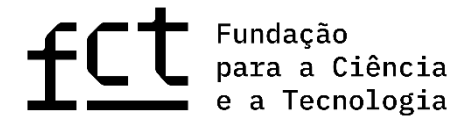
Biocimentação; Argila-bactérias; Biossensor; Monitorização; Câmara de biocimentação

iii

À Ana Quintela.

Funding

The funding was given by FCT I.P through PhD individual grant reference SFRH/BD/144257/2019 and projects BIOSOIL (PTDC/ECI-EGC/32590/2017) and CALCITE (PTDC/ECI-EGC/1086/2021) that allowed to perform all experimental tests presented in this thesis.



Agradecimentos

Às minhas orientadoras, Professora Rafaela e Professora Susana, pela orientação. Um agradecimento especial à Professora Rafaela por tudo o que me ensinou e agradeço o mote, que me ofereceu sem saber, para me agarrar ao manuscrito com convicção, "Maria levantou-se e partiu apressadamente".

Às minhas mentoras do INESC e do iBB, a Débora e a Sofia, obrigada por todo o conhecimento passado e por todo o apoio no laboratório. Um especial agradecimento à Débora, pois a nossa amizade saltou os muros do INESC. A todas as pessoas destes institutos que me ajudaram nestes dois mundos, que de estranhos passaram a familiares ao longo destes anos.

Aos meus colegas e amigos, à Mariana, ao Victor, à Solange, ao Francisco, à Filipa e à Joana obrigada pela partilha de conhecimento no laboratório e por todos os almoços e conversas longas nos corredores.

Aos técnicos do laboratório, em especial ao Sr. José Alberto e ao Jorge, e à secretária de secção Dona Leonor, obrigada pelo apoio e pelo ânimo.

À minha família, mãe, pai, Rita e Tesla, por todo o suporte emocional e financeiro. Obrigada!

Aos meus sexta-feira 13, Pedro, Gustavo, Inês, Miguel e Miguel, por todo o suporte emocional e amizade de vários anos.

À minha família Tostinha, em especial à Sónia, ao Tiago, à Alicia, ao Bruno, à Miryan, ao Pedro, ao Paiva, ao Airton, ao Cachinho, à Teresa, à Bea, à Elisa, ao Rui, à Cristiani, ao Thomas e à Susana, e a todos os outos membros da família, cheguei aqui graças ao apoio dos Tostinhas.

Aos meus companheiros dos Toastmasters, principalmente à Raquel que me deu a conhecer o clube, obrigada por todo o feedback e dedicação.

E finalmente, a todas as mulheres em STEM, às que me abriram caminho, às que caminham comigo e àquelas a quem eu desejo que o caminho seja facilitado.

Contents

Abs	strac	t	i
Res	sumo)	iii
Fur	nding	ξ	vii
Agı	rade	cimentos	ix
List	of f	igures	xv
List	t of t	ables	xix
List	t of s	ymbols	xx
	aptei		
1	-	Objectives	
		•	
2		Thesis organization	
3	(General aspects of biocementation	
	3.1	Biocementation	2
	3.2	MICP vs EICP	3
	3.3	Biocement minerals	3
	3.4	Applications	3
	3.5	Environmental aspects	4
Cha	aptei	1 Interactions between clay minerals, bacteria growth a	nd urease activity on
bio	cem	entation of soils	7
1	(General overview	7
2	(Clay and bacteria interaction on biocementation	8
3	ı	Materials and methods	10
	3.1	Soil characterization	10
	3.2	Reagents and solutions	12
	3.3	Equipment	12
	3.4	Procedures	13
4	ı	Biocementation on sand in the presence of clay minerals	14

	4.1	Soil samples preparation and set-up	14
	4.2	Treatment protocols	15
	4.3	Evaluation of biocement treatment and clay presence	15
	4.4	Results and discussion	16
5		Liquid samples prepared with S. pasteurii and clay minerals	23
	5.1	Tests performed	23
	5.2	Results and discussion	24
6		Discussion	28
7		Final considerations	29
	7.1	Conclusion	29
	7.2	Future studies	30
Cha	pte	r 3 Urease biosensor as monitoring tool for biocementation	31
1		General overview	31
2		Monitoring tools for biocementation treatment in civil engineering field	32
3		Biosensor to detect urease	36
	3.1	Biosensor principle	36
	3.2	Lab-on-a-chip	37
	3.3	Immunoassays	41
	3.4	Detecting urease (background)	41
4		Materials and methods	43
	4.1	Reagents	43
	4.2	Equipment	44
	4.3	Procedures	45
5		Immunoassay optimization	49
	5.1	Overview	49
	5.2	Gold pads assays (preliminary tests)	49
	5.3	Optimization process on MR-platform	50
	5.4	Calibration curve and final procedure	54
6		Using the biosensor as monitoring tool	56
	6.1	Overview	56

	6.2	Methods used for preparing and testing soil samples	. 57
	6.3	Results	. 58
	6.4	Discussion	. 59
7		Costs analysis	. 61
8		Discussion	. 62
9		Final considerations	. 63
	9.1	Conclusion	63
	9.2	Future studies	. 64
Cha	apte	er 4 Biocementation chamber and hydro-mechanical characterization of E	ICP
tre	ated	d samples	65
1		General overview	65
2		Sample preparation for laboratory tests	. 66
	2.1	Cylindrical standard samples preparation	. 66
	2.2	Characterization of samples homogeneity	. 67
	2.3	Background from the group (Biocementation chamber)	. 68
3		Experimental results from biocementation literature review	. 69
	3.1	. Hydro-mechanical behaviour	. 69
	3.2	Shear Strength	71
	3.3	Compressibility	72
4		Materials and sample preparation	72
	4.1	Soil characterization	72
	4.2	Treatment solutions	73
	4.3	Standard sample preparation procedures	73
5		Biocementation chamber developed	73
	5.1	Set-up	73
	5.2	Sand sample preparation	. 76
	5.3	Treatment protocols using the set-up developed	76
	5.4	Sample extraction from the new chamber for triaxial tests	. 78
6		Tests on biocemented samples	79
	6.1	Overview	79

6.2	Triaxial test	80
6.3	Oedometer test	80
6.4	Permeability test	80
6.5	Calcium carbonate content (CCC)	81
6.6	Scanning electron microscopy (SEM)	82
7 Ho	omogeneity of biocement distribution	82
7.1	Calcium carbonate content (CCC)	82
7.2	Scanning electron microscopy (SEM)	84
8 Hy	ydro-mechanical characterization	89
8.1	Triaxial test	89
8.2	Oedometer tests	95
8.3	Permeability tests	96
9 Di	iscussion	96
10 Fir	nal considerations	101
10.1	Conclusions	101
10.2	Future studies	102
Chapter 5	5 Final considerations	103
Referenc	es	105

List of figures

Figure 1.1 – SEM images of uncemented sand (top) and microbially cemented sand (bottom) (DeJong et al., 2006)
Figure 1.2 – SEM images of the synthetized calcium carbonate polymorphs: (a) calcite; (b) vaterite and (c
aragonite (Ševčík et al., 2018)
Figure 1.3 – Comparison of typical sizes of soil particles and bacteria, geometric limitations, and approximate
limits of the treatment (DeJong et al., 2010).
Figure 2.1 – Grain size distribution of soils: APAS 20 sand, white kaolin and Mg-bentonite
Figure 2.2 – XRD pattern for kaolin (left) and bentonite (right) (Gingine, 2017).
Figure 2.3 – FTIR Spectrum for kaolin (left) and bentonite (right) (Gingine, 2017).
Figure 2.4 – Spectrophotometer U2000 from Hitachi (left) and electrical conductivity cell 50 70 from Crison (right
Figure 2.5 – Scheme (left) and photograph (right) of the experimental set-up
Figure 2.6 – Soil samples prepared with 5% of (top) kaolin and (bottom) bentonite for all protocols: Bact, dH2O
pH 9 and FS1
Figure 2.7 – SEM images of S00 samples for Bact (left) and FS (right) protocols
Figure 2.8 – SEM images of samples for Bact protocol for 1 % (top), 5 % (middle) and 20 % (bottom) of clay fo
kaolin (left) and bentonite (right)
Figure 2.9 – SEM images of samples for FS protocol for 1 % (top) and 20 % (bottom) of clay for kaolin (left) and
bentonite (right)
Figure 2.10 – SEM images of samples for dH2O protocol for 5 % (top) and 20 % (bottom) of clay for kaolin (left
and bentonite (right)
Figure 2.11 –SEM images of samples for pH9 protocol for 5 % (top) and 20 % (bottom) of clay for kaolin (left) and
bentonite (right)
Figure 2.12 – Pore size distribution curves for 5% of each clay (SK kaolin, SB bentonite): (a) overall view, (b
enlargement for the smallest pore sizes for kaolin (c) enlargement for the smallest pore sizes for bentonite 2
Figure 2.13 – Calcium carbonate content (CCC) for samples prepare with different clay percentages and the
resulting (Cardoso, et al., 2023)
Figure 2.14 – 20 mL NH4-YE medium with clay and bacteria cells after 24 hour of growth (top) and plates prepared
to count the colony-forming units (CFUs) for each medium sample after 72 hours growth at 30°C dilution of 10
(bottom)
Figure $2.15 - \Delta OD_{600}$ over time for sample without anti-flocculant (top) and with anti-flocculant (bottom) with
the adjusted logistic function (FL)
Figure 2.16 – Urease activity measured over time on samples: 00; B01; K01; B05 and K05
Figure 3.1 – (left) SEM image showing an active calcite bond which bridges two grains of sand and an inactive
calcite bond (Terzis & Laloui, 2018) and (right) Microscope images showing the precipitation of irregularly shape
CaCO₃ crystals and the fixation of bacterial cells during the precipitation process. (Wang et al., 2019)

Figure 3.2 – (left, top) EDS spectra collected on <i>S. pasteurii</i> control cells and (left, bottom) <i>S. pasteurii</i> cells clearly
showing presence of crystalline deposits on the cell-wall showing presence of Ca and (right) XRD plot indicate
the formation of calcite and vaterite polymorphs (Ghosh et al., 2019)
Figure 3.3 – Unconfined compression strength plotted against calcite precipitation for different treatments (A
Qabany & Soga, 2013)
Figure 3.4 – The geoelectrical resistivity measurements before (top) and during (bottom) treatment indicate the
approximate area, which is affected by biogrouting. (van Paassen, 2011)35
Figure 3.5 - Biosensor operating principle: main subsystems (Vargas-Bernal et al., 2012)
Figure 3.6 – Magnetoresistive chip based read-out platform
Figure 3.7 – Components of the biochip platform: (1) power supply/battery; (2) control and acquisition board; (3
inductor and (4) biochip port and support
Figure 3.8 – Biorecognition steps on the magnetoresistive biosensor (Adapted from Germano et al. (2009)) 39
Figure 3.9 – Biochip (6.3 X 7.4 mm) mounted on a PCB next to three microscope pictures (40X, 160X and 800)
magnifications) of the fabricated piece (Valentim, 2016)
Figure 3.10 – (left) Schematic representation of the microfluidic platform components showing how the
alignment and sealing of the channel is achieved and (right) photo of pressure platform including the PCB aligned
with the platform support and with the PDMS U-channel, in detail the PDMS element with the U-Shaped channel
filled with coloured fluid (Martins et al., 2010)
Figure 3.11 – Scheme of direct and sandwich immunoassays to detect urease
Figure 3.12 – Gold pads assays with signal (left) and without (right) (Ferreira Cardoso, 2015)
Figure 3.13 – Calibration curve for urease quantification using the MR platform and performing a direct
immunoassay (Albuquerque, 2017)
Figure 3.14 – (left) Magnetic concentration DynaMag-2 magnet from ThermoFisher Scientific and (right) magnetic
separation process
Figure 3.15 – NE-300 Just Infusion Syringe Pump. 45
Figure 3.16 – Scheme of the immunoassay procedure
Figure 3.17 - Biochip Platform Interface V3.2 showing graphical representation of the transfer curve
corresponding to the 17th sensor of a biochip
Figure 3.18 – Scheme of the measuring steps on the MR platform: baseline, saturation and binding 48
Figure 3.19 – Biochip Platform Interface V3.2 plots outputted of a positive signal on the 16th sensor (left) and a
negative signal on the 2nd sensor (right) of a biochip
Figure 3.20 – Gold pad assay with a visible positive signal (the visivle two white circles on top) and no spot
indicating a negative signal (the abstance of the two white circles on bottom)
Figure 3.21 – Calibration curves of the sensor varying the concentration of antibody (DAB): (a) 10 μ g/mL; (b)
20 μg/mL; (c) 50 μg/mL and (d) 70 μg/mL
Figure 3.22 – Signal for 20 mg/mL of urease varying the capture antibody concentration
Figure 3.23 – Calibration curve to detect urease at lower concentrations between 3 and 10 mg/mL. Capture
antibody at 100 µg/mL (volume:1 µL) and detection antibody at 50 µg/mL (volume:75 µL)53

Figure 3.24 – Target solutions being prepared right before of taking the supernatant of sample solution step	for
the samples of the feeding solution components.	. 54
Figure 3.25 – Calibration curves of the sensor using the magnetoresistive platform: CC10-30 (left) and CCunde	r10
(right)	. 55
Figure 3.26 – Set-up to prepare biocemented treated soil samples	. 57
Figure 3.27 – Relationship between the urease concentration in the inflow and the urease concentration in	the
outflow	. 59
Figure 3.28 – Calcium carbonate content vs urease concentration of the inflow.	. 59
Figure 3.29 – Calcium carbonate content plotted vs urease concentration fixed by the soil (inside the soil)	. 60
Figure 4.1 – Cross-section along longitudinal centre line through the centre injection well of the large so	cale
BioGrout experiment showing CaCO₃ content (%) (van Paassen et al., 2009)	. 67
Figure 4.2 – Image of tomography on a biocemented sand sample (Roy et al., 2023)	. 68
Figure 4.3 – Steel chamber: (a) set-up; (b) mould; (c) top and bottom pieces; and (d) steel chamber attack	hed
(adapted from Centeno Dias et al. (2020))	. 69
Figure 4.4 – Relationship between unconfined compression strength (top) and normalized permeability (botto	om)
with calcium carbonate content from several studies (Yu et al., 2021)	. 70
Figure 4.5 – Synthesis of consolidated drained triaxial test: (top) cohesion (kPa) and (bottom) friction angle ra	atio
as a function of formed calcium carbonate content (%) (adapeted from Yu et al. (2021))	. 71
Figure 4.6 – Gain size distribution of the sand	. 72
Figure 4.7 – Scheme of the set-up with the biocementation chamber	. 74
Figure 4.8 – Biocementation chamber top (left) and side (right) views	. 75
Figure 4.9 – AutoCAD scheme of the biocementation chamber.	
Figure 4.10 – Geotextile.	. 76
Figure 4.11 – Demoulded sample after biocementation treatment (left) and (right) sample on the tria	
equipment (right)	. 78
Figure 4.12 – Scheme of constant water height permeability test performed in the new biocementation chamles	ber.
	. 81
Figure 4.13 – Sample division for calcium carbonate content determination.	. 81
Figure 4.14 – Relationship the calcium carbonate content and between the position of the sample (Top, Mic	ldle
and Bottom)	. 83
Figure 4.15 – SEM images for 3 amplifications of control protocols: FU2T (top) and H2O (bottom)	
Figure 4.16 – SEM images for 3 amplifications of 1EU12B protocol: top sample (top), middle sample (centre)	and
bottom sample (bottom).	
Figure 4.17 – SEM images for 3 amplifications of 1EU2T protocol: top sample (top), middle sample (centre)	
bottom sample (bottom)	
Figure 4.18 – Energy dispersive X-ray spectroscopy (EDS) results on H2O (left) and FU2T (right)	
Figure 4.19 – Energy dispersive X-ray spectroscopy (EDS) results on 1EU12B sample top (left), middle (midd	
and bottom (right)	•

Figure 4.20 – Energy dispersive X-ray spectroscopy (EDS) results on 1EU2T sample top (left), middle (middle) and
bottom (right)88
Figure 4.21 – Triaxial undrained test results: deviator stress vs. axial strain for H2O (left), 1EU2T (middle) and
1EU12B (right) protocols92
Figure 4.22 – Triaxial undrained test results: pore pressure vs. axial strain for H2O (left), 1EU2T (middle) and
1EU12B (right) protocols92
Figure 4.23 – Triaxial undrained test results: Mohr circles for peak and critical states with CSL representation for
H2O (left), 1EU2T (middle) and 1EU12B (right) protocols
Figure 4.24 – Triaxial undrained test results: effective stress paths with CSL representation for H2O (left), 1EU2T
(middle) and 1EU12B (right) protocols
Figure 4.25 – Triaxial undrained test results: deviator stress vs. axial strain (top); pore pressure vs. axial strain
(centre) and effective stress paths for confinement stresses (bottom) for the confinement stresses of 100 kPa
(left), 150 kPa (centre) and 200/250 kPa (right)
Figure 4.26 – Compressibility curves of H2O, 1EU2 and 1EU12 protocols
Figure 4.27 – Relationship between permeability and calcium carbonate content for treated samples on the
biocementation chamber compared to other studies (adapted from Yu et al. (2021))
Figure 4.28 – Relationship friction angle ratio of critical and peak sates and calcium carbonate content compared
to other studies (adapted from Yu et al. (2021))99
Figure 4.29 – Mohr circles for critical states with CSL representation expected for the treated sand in comparison
with that measured for the untreated sand (top) and corresponding schemes of biocement (gray) distribution on
sand particle (yellow) for each hypotheses (bottom)

List of tables

Table 2.1 – Solis specifications of APAS 20 sand, white kaolin and Mg-bentonite	10
Table 2.2 – Summary of all tests reformed on kaolin and bentonite (Gingine, 2017)	12
Table $2.3-$ Final porosity of the soil samples (computed by knowing the dry volumetric weight and solid	particles
density)	14
Table 2.4 – Visual observation of samples after mould extraction	16
Table 2.5 – Mineralogical analysis before and after biocementation treatment	20
Table 2.6 – Calcium carbonate content and the variation for Bact and dH2O protocols	23
Table 2.7 – Colony-forming units (CFUs) enumerated in each dilution.	25
Table 2.8 – Parameters used to adjust the logistic function	26
Table 3.1 – Results of the gold pads tests.	50
Table 3.2 – Key optimization steps on the procedure of the biosensor assay for detecting urease	50
Table 3.3 – Signal measures and the confidence interval at 95% on the MR platform for the calibratio	n of the
sensor varying the concentration of antibody (DAB)	51
Table 3.4 – Parameter of the calibration curves: CC10-30 and CCunder10	55
Table 3.5 – Biocementation treatment protocols on sand samples and tests performed	58
Table 3.6 – Calcium carbonate content and urease concentration inside the sand samples	60
Table 3.7 – Costs analysis for the optimized sandwich immunoassay to detect urease	62
Table 4.1 – Protocols of biocementation treatment performed using the biocementation chamber	77
Table 4.2 – Timeline of the protocols of biocementation treatment performed using the biocem	nentation
chamber	77
Table 4.3 – Protocols used to investigate the homogeneity of biocement in the treated samples	78
Table 4.4 – Tests performed in each protocol of biocementation treatment performed using the biocem	nentation
chamber	79
Table 4.5 – Calcium carbonate content (CCC) for several protocols and positions: Top, Middle and Botto	om 82
Table 4.6 – Critical and peak states data for all protocols and confinement stresses of the triaxial tests pe	rformed.
	89
Table 4.7 – Friction and dilatancy angles for the different protocols of the triaxial tests	91
Table 4.8 – Oedometer parameters for H2O, 1EU2 and 1EU12 protocols	95
Table 4.9 – Permeability of the biocementation samples	96
Table 4.10 – Summary of all tests for 1EU12B, 1EU2T and H2O protocols	97
Table 4.11 – Cam Clay parameters that can be used for the design of biocemented soil solutions.	100

List of symbols

λ	Elastoplastic compressibility	c cohesion		
κ	Swelling compressibility	C. ensij	formis Canavalia ensiformis (Jack bean)	
γ_d	Dry volumetric weight	CC	Calibration curve	
σ	Electrical conductivity	Cc	Elastoplastic compressibility index	
σ	Normal stress	CCC	Calcium carbonate content	
σ_a	Axial strain	CFUs	Colony-forming units	
σ_y'	Yielding stress	СН	Fat clay	
$ au_c$	Tangential stress of critical stage	CO _{2-eq}	Dioxide carbonate equivalent	
$ au_p$	Tangential stress at peak	C _s index	elastic compressibility index or Swelling	
ϕ'	Friction angle	CSL	Critical State Line	
$\phi_{ m c}'$	Critical frictional angle	d ₅₀	Mean particle size	
$\phi_{ m p}'$	Peak frictional angle	DC	Direct current	
Δh	Loss of water head	dH2O	Distilled water	
Δu	Variation of pore pressure	e	Void ratio	
Ψ	Dilatancy angle	EDS	Energy-dispersive X-ray spectroscopy	
τ	Shear stress	EICP	Enzyme induced calcite precipitation	
Α	Cross section area	ELISA	Enzyme-linked immunosorbent assay	
AC	Alternate current	FL	Logistic function	
ASM	American Society for Microbiology	FS	Feeding solution	
ASTM	American Society for Testing and Materials	Gs	Soil particles density	
ATCC	American Type Culture Collection	HS	Held shape	
В	Bentonite	INESC I	D Instituto de Engenharia de	
B. past	eurii Bacillus pasteurii	Sistem	as e Computadores: Investigação e	
Bact	Biocementation treatment	Desenvolvimento		

BSA

Bovine Serum Albumin

INESC I	MN Instituto de Engenharia de	q	Deviator stress		
Sistem	·	q	Flow rate		
	ecnologias	RT	Room temperature		
IPA	Isopropyl Alcohol	S	APAS 20 sand		
k	Saturated permeability	S. past	teurii Sporosarcina pasteurii		
K	Kaolin	SEM	Scanning electron microscope		
L	Length of water pathway	SM	Silty sand		
LoC	Lab-on-a-chip	SP	poorly graded sand		
m	Mass		· · · · ·		
M_{c}	Slope of the critical state line	TEM	Transmission electron microscope		
MICP	Microbially induced calcite precipitation	uc	Urease concentration		
MIP	Mercury intrusion porosimetry	UCS	Unconfine compression strength		
ML	Silt with low plasticity	US	Urease solution		
MNPs	Magnetic nanoparticles	V	Velocity		
MR	Magnetoresistive	V	Voltage		
m _s	Solid mass	V_{v}	Void volume		
NHS	Did not hold shape	XRD	X-ray diffraction		
NP	Portuguese standard				
OC	Overconsolidation				
OD ₆₀₀	Optical density at 600 nm				
p Mean stress					
PB Twe	Phosphate buffer 0.1 M pH 7.4 Tween 20				
PB Phosphate buffer 0.1 M pH 7.4					
РСВ	PCB Printed circuit bord				
PDMS	PDMS Polydimethylsiloxane				
рН9	H9 Tris buffer 0.13 M pH 9				

PVC

Polyvinyl chloride

Chapter 1

Introduction

1 Objectives

The main goal of this thesis is to investigate some aspects related with biocementation as soil improvement technique, aiming at contributing to its broad use in geotechnical engineering applications. The research performed is divided into three main parts, each focused on important practical aspects when using this technique, namely:

- Investigate the influence of clay minerals on biocementation, aiming at understanding if this technique can be used in more types of soils;
- Optimize a biosensor to quantify urease enzyme, aiming at using it as monitoring tool for the treatment, or at least for its design;
- Develop a new chamber for applying this treatment in the laboratory, aiming at preparing homogeneous samples for systematic experimental characterization of the hydro-mechanical behaviour of the biocemented material.

2 Thesis organization

This thesis is organized in three main chapters, each investigating distinct aspects of biocementation treatment while sharing a common focus. Every chapter represents an independent research topic, collectively contributing to the understanding and advancement of biocementation techniques. The chapters begin with a literature review tailored to the topics addressed in each respective chapter. Subsequently, a practical delineation of materials and standard methods is presented consistently across all chapters. The organization of innovative methods and results is adapted to each chapter, ensuring a logical flow that facilitates comprehension. Finally, a discussion section and concluding remarks are included in each chapter, summarizing reflections and key findings.

Chapter 2, entitled "Interactions between clay minerals, bacteria growth and urease activity on biocementation of soils", investigates how clay minerals affect biocementation. The study presented an analysis of calcium carbonate precipitation in sandy soil and evaluated the growth and urease activity of *S. pasteurii* in the presence of two clays: white kaolin and Mg-bentonite. This study offers valuable insights into clay-bacteria interactions during biocementation, using standard tests on soil samples and bacterial growth media. The use of such standard characterization tools to investigate the effects of clay presence on the results represents an innovative approach.

Chapter 3, entitled "Urease biosensor as monitoring tool for biocementation", aims at developing a Lab-on-chip to be used as a monitoring tool for biocementation. This biosensor quantifies urease enzyme in the pore fluids,

being optimized in this work following processes addressing factors like operational range, cross-reactions, portability, user-friendliness, soil particle interference, and economic management. The tests of this biosensor's efficacy in soil samples are presented in this chapter, in which some limitations of its use are also identified.

Chapter 4, entitled "Biocementation chamber and hydro-mechanical characterization of EICP treated samples", focuses on the development of a new biocementation chamber inspired by an infiltration column. It details the treatment of small sand samples with enzyme induced calcite precipitation (EICP) to ensure uniform biocement distribution and allows subsequent permeability and triaxial strength characterization, along oedometer tests.

3 General aspects of biocementation

3.1 Biocementation

Biocementation is a technique to produce calcium carbonate (biocement) using biological entities such as enzyme or bacteria. This technique has been studied since the end on 20th century (Stocks-Fischer et al., 1999). When applied in soils, the biocement bonds the grains and clogs the soil pores, improving the hydro-mechanical properties of this material. This treatment reduces the permeability and increases the stiffness and strength of the soil. Biocementation occurs when urease enzyme, urea (CO(NH₂)₂) and a calcium source (Ca²⁺) are combined. Urease enzyme catalyses the hydrolysis of urea (Equation (1.1)) and the combination of the calcium ion from a calcium source supplied and the carbonate ion causes the precipitation of calcium carbonate (Equation (1.2)).

$$CO(NH_2)_2 + 2H_2O \rightarrow CO_3^{2-} + 2NH_4^+$$
 (1.1)

$$CO_3^{2-} + Ca^{2+} \rightarrow CaCO_3 \downarrow \tag{1.2}$$

Figure 1.1 compares a treated and a not treated sand sample with biocementation technique, where it is possible to observe the biocement bonds connecting the grains in the treated sample. The images were obtained from scanning electron microscopy (SEM).

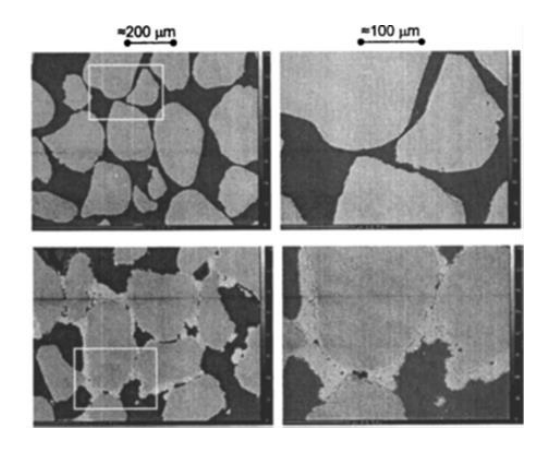


Figure 1.1 – SEM images of uncemented sand (top) and microbially cemented sand (bottom) (DeJong et al., 2006)

Urease (EC 3.5.1.5) was discovered and identified to be responsible for the hydrolysis of urea, also known as ureolysis, in the 19th century. This enzyme is found in plants, bacteria, fungi, algae and invertebrates. Depending on the urease source, there are several types of ureases with different protein structures (Krajewska, 2018).

3.2 MICP vs EICP

Biocementation treatment is known as microbially induced calcite precipitation (MICP) or enzyme induced calcite precipitation (EICP), depending on the source of urease enzyme. EICP usually uses purified urease in solution directly introduced in the soil, either injected or mechanical mixed. On the other hand, in MICP the ureolytic agent is a urease-producing bacteria (UPB), already existing or added to the soil. To use this source of urease, it is necessary to provide conditions to keep bacteria alive and active in the soil. These bacteria keep producing urease as long as adequate conditions are provided. This means that using bacteria as urease source is more economically viable than purified urease. The enzyme is commercially available in powder form, being estimated that using bacteria is fifty times cheaper than using enzyme (Ivanov et al., 2019).

3.3 Biocement minerals

Considering the precipitated biocement, there are three crystals polymorphs of anhydrous calcium carbonate: vaterite, aragonite, and calcite (Figure 1.2). The production of the polymorphs of calcite, aragonite and vaterite depend both on their growing environments and bacterial strains (Wei et al., 2015). Calcite mineral structure is more thermodynamically stable (almost cubic) than aragonite and vaterite. Calcite is the only insoluble form in water and therefore the intended form of biocement to be precipitated to ensure durability. Aragonite (several needles) occurs less commonly in nature because it is the least thermodynamically stable polymorph. Vaterite (spherical shape) can rapidly transform to calcite and aragonite in aqueous solution. Experimental evidence has demonstrated that vaterite can transform to aragonite in 60 minutes at 60° C and to calcite in 24 hours at room temperature (Ni & Ratner, 2008).

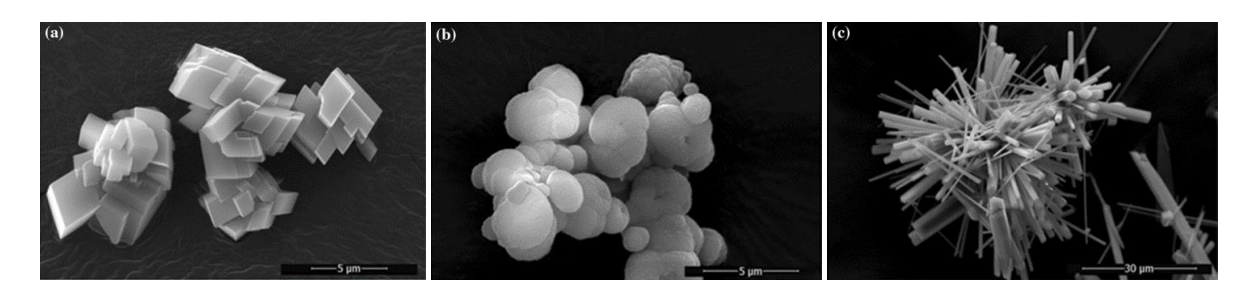


Figure 1.2 – SEM images of the synthetized calcium carbonate polymorphs: (a) calcite; (b) vaterite and (c) aragonite (Ševčík et al., 2018)

3.4 Applications

The ground improvement applications are the ones that are more relevant to the present work, nevertheless the biocement has several other applications in various field areas, for example self-healing concrete and restoring patrimony.

The pores size of the soil is the principal limitation, due to the space compatibility for the bacteria to move. Bacteria size is usually in the range of 0.5 to 4 μ m (Mitchell & Santamarina, 2005), and therefore, considering only geometric limitations, it is possible to identify the most suitable soil types to be treated. As presented in Figure 1.3, sandy soils are the most suitable for the treatment because the pore troughs allow the unhindered microbial motion and easy feeding solution transport (DeJong et al., 2010). The volume of voids in gravel soils is usually high, minimizing the effectiveness. Clay and silt soils have the potential to be treated by *ex-situ* mixing of the solutions (Islam et al., 2020; Morales et al., 2019).

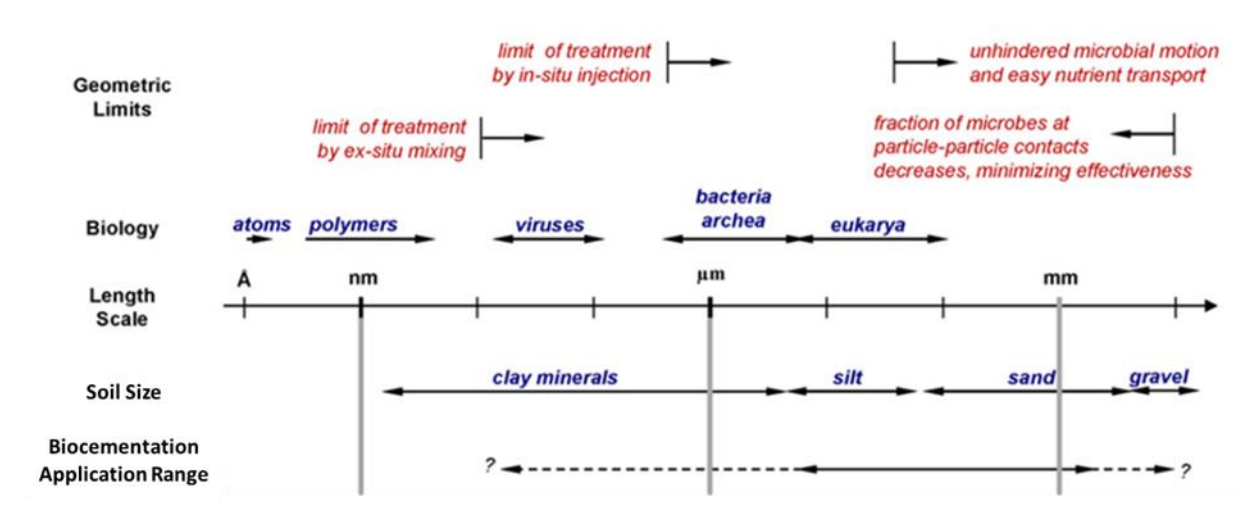


Figure 1.3 – Comparison of typical sizes of soil particles and bacteria, geometric limitations, and approximate limits of the treatment (DeJong et al., 2010).

Biocementation technique has several applications in geotechnical engineering both in laboratory and in large scale or in field works, such as (i) enhancing stability for retaining walls, embankments, slopes and dams (Borges et al., 2020; Cardoso et al., 2023); (ii) reducing the permeability in dams and dykes (Chu et al., 2013); (iii) increasing the bearing capacity of foundations and underground constructions (Filet et al., 2020; van Paassen, 2011); (iv) protecting to wind erosion by binding of the dust particles on exposed surfaces (Gomez et al., 2015); (v) strengthening slopes to prevent water erosion and failure in coastal area and rivers (Salifu et al., 2016); (vi) reducing the liquefaction potential of soil (Montoya et al., 2014); (vii) increasing the resistance to petroleum and natural gas extraction borehole degradation during drilling and extraction (Margesin et al., 2000).

3.5 Environmental aspects

Most traditional soil improvement techniques, such as shotcrete and jet grounding, require the use of large quantities of Portland cement. Cement production consumes energy to extract, heat, grind and transport (Habert et al., 2010). C8/10 concrete releases 75.6 kg CO_{2-eq} /ton, even with a low content of cement, such as this conventional low strength concrete (Røyne, 2017). Biocement has the potential to reduce, considerably, the production of greenhouse gas emissions in a range of 70-85%. This is the main environmental advantage of resorting to biocement instead of traditional concrete. According to Røyne (2017), biocement releases between 11.6 - 24.4 kg CO_{2-eq} /ton of greenhouse gas emissions.

The implementation of biocementation processes needs a consideration of potential chemical by-products and associated hazards. Compounds such as urea, ammonia, ammonium, hydroxide, and chlorine ions, which are involved in the biocementation reaction, must be carefully collected and disposed of to prevent environmental contamination. For instance, applying biocementation treatment to $1000~\text{m}^3$ of sand could lead to significant pollution, with an estimated contamination of over $100~\text{km}^3$ of air with ammonia and $4.5\times10^6~\text{m}^3$ of drinking water with ammonium (Ivanov et al., 2019), based on European Union standards (Anker et al., 2018). This highlights the importance of adhering to regulatory limits and implementing proper waste management practices to mitigate potential environmental impacts associated with biocementation processes.

In MICP, where bacteria are employed, careful consideration must be given to strain selection to ensure biosafety. This considers in using non-pathogenic bacteria and controlling the introduction in ecosystems. If possible, opting for the use of enzymes or not living bacteria are the best options to minimize potential risks to both human health and the environment (Ivanov et al., 2019).

Chapter 2

Interactions between clay minerals, bacteria growth and urease activity on biocementation of soils

1 General overview

The majority of data presented in this chapter has already been published in Applied Clay Science journal, by Cardoso et al. (2023) entitled "Interactions between clay minerals, bacteria growth and urease activity on biocementation of soils".

This chapter aims to investigate the influence of clay minerals on biocementation by studying the amount of calcium carbonate precipitated in a selected sandy soil and measuring how the growth and urease activity of *Sporosarcina pasteurii* (*S. pasteurii*) in medium are affected by the presence of two different types of clays minerals: white kaolin and bentonite (Mg-bentonite). These clays minerals were chosen to represent soils with non-active and active clay types, respectively. Although fundamental aspects related to electrochemical reactions and the chemical species involved in this soil treatment technique were not explored, this study offers valuable insights into clay-bacteria interaction in the context of biocementation. These insights were found through standard tests conducted on soil samples and on the growth medium of *S. pasteurii*. The use of such standard characterization tools to investigate the effects of clay presence on the results represents an innovative approach.

Section 2 begins with a comprehensive literature review concerning clay and bacteria interaction in general and detailed for *S. pasteurii*, the most used bacterium species for biocementation treatment.

Section 3 is focused on the main materials and methods employed on the chapter, which comprises soil characterization, reagents and solution s preparation with the clays, briefly describing the equipment used for bacteria growth less common in civil engineering scoop. Additionally, section 3 describes procedures both standard and adopted from literature, including the process employed to produce lyophilized bacteria as an alternative to live bacteria.

Section 4 describes the tests conducted on sand samples prepared with fixed clay contents. It comprises two parts: the first details sample preparation and treatment protocols, while the second covers test descriptions, results, and discussion.

Section 5 analyses the *S. pasteurii* and clay interaction, comprehending deeply the influence of clay on the *S. pasteurii* growth and on urease activity.

Section 6 presents a discussion comprising the results from soil and liquid samples.

Section 7 presents the final considerations, where the main outputs from the chapter are highlighted and future studies are suggested.

2 Clay and bacteria interaction on biocementation

Microbially induced calcite precipitation (MICP) has mainly been applied in clean sandy soils due to their large pores, which are compatible with the vital space required by bacteria (Mitchell & Santamarina, 2005), measuring approximately 0.5 to 4 μ m. Sandy soils exhibit high permeability, enabling access for the feeding solution, a solution containing urea and a calcium source. The reduced pore size of clayey soils makes this access unachievable. When selecting suitable soils for biocementation treatment, their natural saturated coefficient of permeability should be above 10^{-5} m/s (Terzis & Laloui, 2019b), a range typically found in sandy soils with very small percentages of fine materials (particles with diameters smaller than 0.075 mm). This criterion is essential because the procedure starts with the injection of the biocementation treatment fluid into the soil under low pressures, and fluids need to flow to permeate all volume, ensuring uniform distribution for effective treatment and promoting homogeneity.

Although typically considered unsuitable for natural clayey soils, biocementation treatment can be applied to such soils if they are first disaggregated before compaction. In this case, compaction occurs after mixing the soil with biocementation treatment fluids instead of water (Islam et al., 2020; Morales et al., 2019). Trapped air and the resulting void ratio from compaction provide essential space for bacteria survival. This treatment enhances the strength of compacted clay aggregates, particularly cohesion and tensile strength, making it effective in reducing cracking resulting from the desiccation of compacted clayey soils (Liu et al., 2020), including those rich in bentonite (Vail et al., 2019).

Bacterial adhesion to soil particle surfaces is crucial to initiate the biocementation process. Cardoso et al. (2018) used a microstructural approach to elucidate biocementation in clayey soils. It was observed that clay particles coated sand particles, interfering on bacterial adhesion and impeding the formation of continuous calcite layers. This phenomenon is dependent on the clay content present in the soil voids. Sun et al. (2019) investigated the impact of varying kaolin clay percentages on biocementation in sandy soils, identifying 7.5 % clay by weight as the maximum limit which clay particles would clog the pores of the sand (d₅₀ = 0.3 mm). This study confirmed bacterial activity by detecting biocement below this clay percentage, which was similar to the biocement found in the absence of clay. The production of calcium carbonate increased with increasing kaolin content until reaching 7.5 % kaolin, after which it declined. This trend was attributed to bacteria's ability to attach to both clay minerals and sand particles, therefore enhancing the available surface area for bacterial adhesion. Zhao et al. (2021) conducted biocementation treatment on column infiltration. The samples were prepared using bentonite percentages up to 5%, mixed in fine, medium and coarse sands. The quantity of precipitated calcium carbonate increased with rising bentonite percentages on all types of sand. The authors explained this observation as both bacteria and calcium ions were retained in the soil due to the volume expansion of bentonite on hydration, leading to a reduction in permeability. Consequently, biocementation treatment fluids remained in soil pores for longer, therefore extending reaction times.

Other fields have been exploring bacteria-clay adhesion. For instance, the combination of bacteria with fine materials, such as clay particles, zeolites and stone powder, has been successful in producing aggregates for self-healing concrete and mortar (Bhaskar et al., 2017). Clays have demonstrated the ability to immobilize bacteria, as observed in bentonite clay buffers by Stroes-Gascoyne (2010). Ma et al. (2021) explored biocementation for sealing cracks in concrete, by injecting a mixture of bentonite and bacteria into the cracks, using a bentonite slurry to protect bacteria from fluid dragging forces during multistaged injections.

Cardoso et al. (2018) and Morales et al. (2019) emphasized the importance of investigating biocementation in clayey soils by considering the chemical interactions between clay minerals and the chemicals present in the feeding solution. Clay soils experience significant volume changes in response to fluids with different chemical properties (such as swelling or collapse), which could impact the available space for bacteria. Zhao et al. (2021) reached a similar conclusion while investigating sand-bentonite mixtures. However, it's crucial to also consider pH in studying these volume changes, as highlighted by Cardoso et al. (2018) and Sun et al. (2019).

In addition to the physical straining of bacteria within clay pores, a complete understanding of biocementation must also consider electrochemical interactions and biological phenomena. Bacteria carry a surface charge, often negative, which, in the context of biocementation, promotes the fixation of calcium ions. As a result, bacteria cell walls serve as nucleation sites for the formation of calcium carbonate (L. Ma et al., 2020). This charged bacterial surface also interacts with clay particles, which also carry a negative charge, as well as with cations present in the pore fluids. This interaction explains the immobilization of bacteria by clays, such as when organized clay clusters form around bacteria to minimize repulsion forces due to electrochemical interactions (Cuadros, 2017; Mueller, 2015).

Indeed, bacteria can interact with clay minerals in various ways, including aggregation, flocculation, dissolution, and changes in specific surface area and layer charge, sometimes accelerating mineral transformation (Cuadros, 2017; Vandevivere et al., 1994; Zhu et al., 2011). Some studies on bacteria found in lakes and deep sea environments (Fomina & Skorochod, 2020) have suggested cation exchange between bacteria and clay minerals, as if the bacteria were obtaining nutrients from the clay minerals.

Sporosarcina pasteurii is the most used bacterium species in soil biocementation treatment due to its high urease activity, common presence in soils, and non-pathogenic nature (Lapierre et al., 2020). However, the electrochemical interaction with clay minerals and the biological mechanisms related to enzyme production by these urease-producing bacteria remain poorly understood. Sun et al. (2019) explored the effect of Al₂O₃ and FeCl₂ present in clays on bacteria growth and concluded that they negatively impacted urease activity, primarily through pH changes, although deeper chemical interactions were not investigated.

Burdalski et al. (2022) studied biocementation considering *S. pasteurii* activity in different soils and found that cells growth and the type and amount of biocement produced were sensitive to the minerals present in the soils and feeding solutions, especially in the presence of interchangeable cations. No additional references were found in the literature concerning the urease enzyme produced by *S. pasteurii*. Further research is needed to clarify the interaction between urease enzyme, particularly, and other proteins, generally, produced by bacteria species

used in biocementation treatments and various clay minerals. This would aid in designing treatments tailored to different soil types and potentially incorporating clay as an additive to enhance efficiency and expanding the range of treatable soils. Clay-bacteria interaction has been observed in nature with other species and clay minerals (Cuadros, 2017; Mueller, 2015).

3 Materials and methods

3.1 Soil characterization

APAS 20 sand, white kaolin and Mg-bentonite were used to prepare soil samples, the three soils are commercially available, Table 2.1 presents the soils specifications and the grain size distribution of the three soils are showed in Figure 2.1. The clay minerals were identified by X-Ray Diffraction (XRD), as shown in Figure 2.2. Kaolin clay is composed of kaolinite, quartz, and muscovite minerals, while bentonite clay is composed of sepiolite, quartz, and microcline minerals. Fourier transform infrared spectroscopy (FTIR) is a complementary method to XRD. The FTIR spectrum for both clays are represented in Figure 2.3. X-ray fluorescence spectrometry (XRF) was employed to determine the elemental composition of the specimens. Table 2.1 presents the summary of all tests reformed on kaolin and bentonite (Gingine, 2017).

Table 2.1 – Solis specifications of APAS 20 sand, white kaolin and Mg-bentonite.

Name	Sand	Kaolin	Bentonite
Description	APAS 20 Sand	White kaolin	Mg-bentonite
Unified Soil Classification System (USCS)	Poorly graded clean sand (SP)	Low plasticity silt (ML)	High plasticity clay (CH)
Specific gravity (G₅)	2.68	2.61	2.74
Liquid limit (w∟)	-	49 %	300 %
Plastic limit (w _P)	-	30 %	51 %
Plasticity index (PI)	-	22 %	249 %
Activity number (PI%/Clay%)	-	0.55	4.36
Natural water content	0 %	2 %	14%
Main minerals	Quartz, Zircon and Tourmaline	Kaolinite, Quartz and Muscovite	Montmorillonite, Quartz and Microcline
Specific surface area	-	20 m ² /g	800 m ² /g

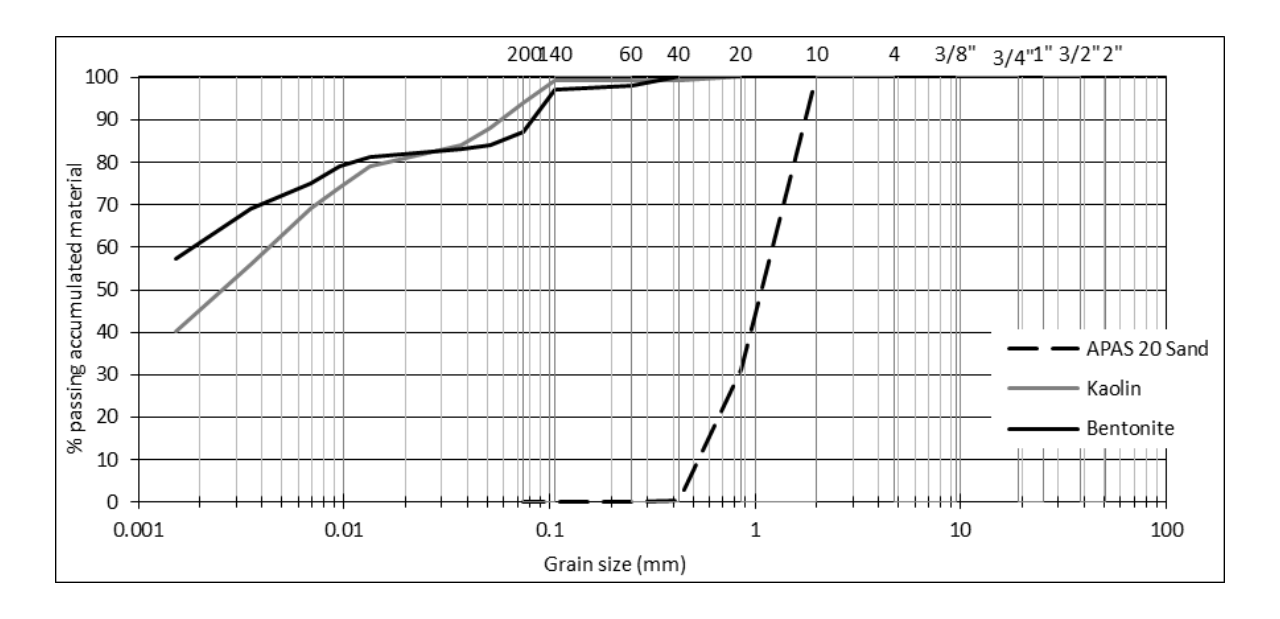


Figure 2.1 – Grain size distribution of soils: APAS 20 sand, white kaolin and Mg-bentonite.

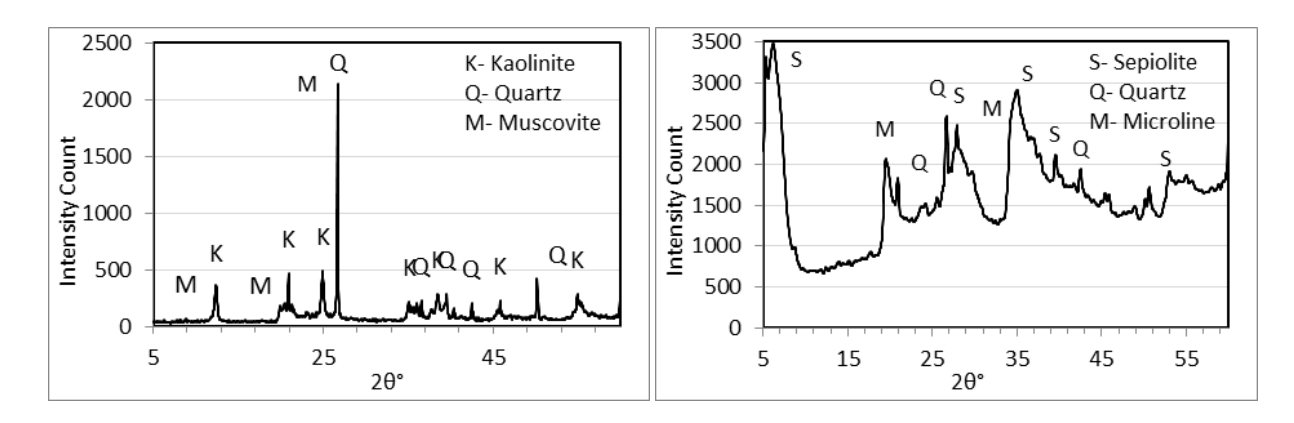


Figure 2.2 – XRD pattern for kaolin (left) and bentonite (right) (Gingine, 2017).

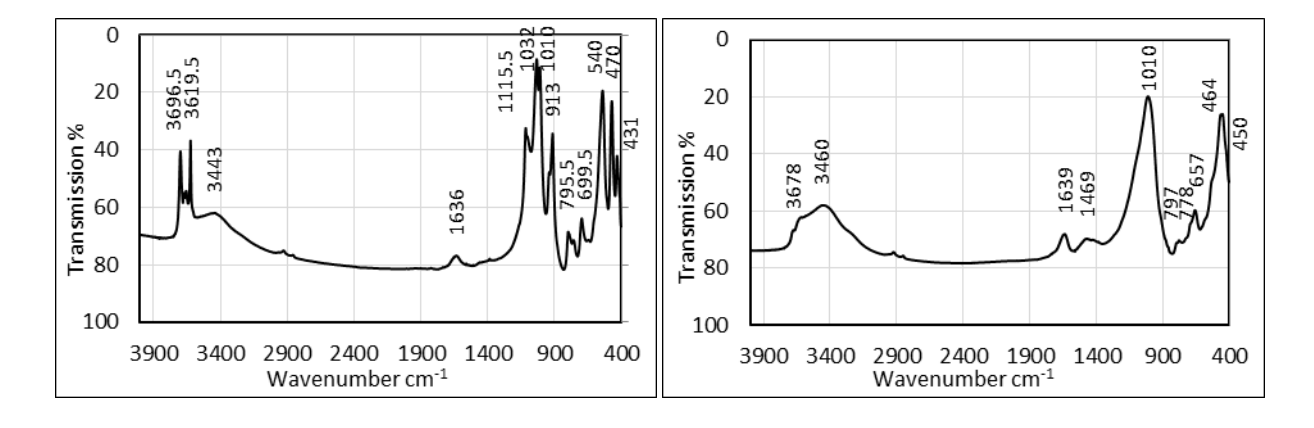


Figure 2.3 – FTIR Spectrum for kaolin (left) and bentonite (right) (Gingine, 2017).

Table 2.2 – Summary of all tests reformed on kaolin and bentonite (Gingine, 2017).

	XRD	FTIR	XRF
	Minerals	Molecules/Compounds	Elements
Kaolin	Kaolinite – Al ₂ Si2O ₅ (OH) ₄ Quartz – SiO ₂ Muscovite- Al ₃ Si ₃ O ₁₀ (OH) _{1.8} F _{0.2}	Bands matching Kaolin, Si-O band, Hematite, hydroxyl linkage (absorbed water).	Major – Si, Al Minor – Na, Fe, Mg, K, Ca, Ti, Cr, Mn, Ni, Cu, Zn, Pb, Zr
Bentonite	Sepiolite – Mg ₄ Si ₆ O ₁₅ (OH) ₂ ·6H ₂ O Quartz – SiO ₂ Microline – KAlSi ₃ O ₈	Bands matching Sepiolite and Bentonite, SiO band, hydroxyl linkage (absorbed water).	Major – Si, Mg Minor – Al, Na, K, Ca, Ti, Mn, Rb, Sr, Zr

3.2 Reagents and solutions

Sporosarcina pasteurii, formally named *Bacillus pasteurii* (*S. pasteurii* and *B. pasteurii*) was the bacterium species selected from American Type Culture Collection (ATCC strain #11859).

NH4-YE medium, recommended by ATCC to grow *S. pasteurii* was autoclaved in stock concentrations, it was composed by yeast extract at 20.0 g/L, ammonium sulphate, (NH₄)₂SO₄, at 10.0 g/L and tris buffer (pH 9.0) at 0.13 M. Additionally, NH4-YE medium for plate (Petri dish) growth included the addition of 20.0 g/L of agar.

The NH4-YE growth medium with clay particles at 30 g/L and 150 g/L were prepared fowling the same recommendation. Stock solutions were prepared by mixing clay with distilled water or antifoulant solution, which was composed by sodium hexametaphosphate at 3.3 g/L and sodium carbonate at 0.7 g/L (NP_E-196, 1996).

Tris buffer solution was prepared at 0.13 M with distilled water with pH 9 adjusted.

Feeding solution was composed by urea at 0.5 M, calcium chloride at 0.5 M, ammonium chloride at 10 g/L, sodium bicarbonate at 2.12 g/L, yeast extract at 2 g/L and ammonium sulphate at 1 g/L, with pH 7.

3.3 Equipment

A spectrophotometer is an equipment that measures the intensity of light at different wavelengths, providing information about the absorption or transmission properties of a substance in a sample. The spectrophotometer U2000 from Hitachi is shown in Figure 2.4 (left). This equipment is used to monitor bacteria growth, as optical density increases with increasing number of cells present in the fluid analysed.

An electrical conductivity probe is a device used to measure the electrical conductivity of a solution, which in this work was electrical conductivity cell 50 70 from Crison and is presented in Figure 2.4 (right). This equipment is used to monitor urease activity, as the concentration of ammonium ion increases while urea hydrolysis is under progress.





Figure 2.4 – Spectrophotometer U2000 from Hitachi (left) and electrical conductivity cell 50 70 from Crison (right)

3.4 Procedures

3.4.1 Bacteria growth

S. pasteurii were grown at 30° C, at 250 rpm and under aerobic conditions on a 1:5 ratio (1 part bacteria to 5 parts air) in NH4-YE medium, as suggested by ATCC. The cells concentration adopted for the treatments was $^{\sim}10^{7}$ cells/mL (Al Qabany & Soga, 2013), which corresponds to an optical density at 600 nm (OD₆₀₀) of approximately 1, measured on the spectrophotometer. Fresh *S. pasteurii* were employed on tests in medium with clay, specifically on growing *S. pasteurii* in medium with clay and on determining the urease activity in the presence of clay.

3.4.2 Bacteria lyophilization

Lyophilization or dry freezing consist of dehydrated at low temperature. These bacteria can be stored for extended periods without losing viability, their dried state facilitates handling and transportation, and they can be easily rehydrated as required, offering flexibility in experimental set-ups and field applications (Terzis, 2017). They were produced and applied in this thesis to enable the preparation of a stock of ready-to-use bacteria, similar to what is usual when using enzymes.

The procedure used to lyophilize *S. pasteurii* (adopted from Terzis & Laloui, 2018) starts with freshly grown cells at OD_{600} =1. The cells were centrifuged (3000 rpm, 20 minutes), re-suspended in a 10% sucrose solution, stored in boiling tubes with perforated lids, frozen at -80°C for 1 hour, and dried at -40°C under vacuum for at less 24 hours. Then the boiling tubes with the lyophilized bacteria were closed with parafilm to avoid moister from entry and stored at 4°C. Right before being used, the bacteria were re-suspended in growth media, and the OD_{600} was checked. If the OD_{600} fell within the range of 0.8 to 1.2, indicating the bacterial concentration was suitable, the bacteria solution was immediately used. Lyophilized *S. pasteurii* were employed on soil treatment, specifically on Bact protocol described later.

3.4.3 Urease activity

Urease activity was determined by a conductivity method (Harkes et al., 2010). 0.5 mL of bacteria solution was added to 4.5 ml of urea solution stock concentration at 1.11 M (ratio 1:10), making the reaction concentration

of 1 M urea after dissolution. The electrical conductivity changes were recorded over 5 minutes at 20 °C (room temperature). Finally, the correlation in Equation (2.1) was used to determine the hydrolysis activity of urease (Whiffin, 2004).

$$1 mS/min = 11 mM urea hydrolysed/min$$
 (2.1)

3.4.4 Calcium carbonate content

The calcium carbonate content (CCC) was determined using acid washing method adapted from Portuguese standard (NP-E196-1996, 1966). The dry mass of the sand sample was measured using an oven at 105° C for 24 hours before the test (m_1) and then the soil was placed in hydrochloric acid (HCl, 0.5 M) until the reaction was complete. Then it was washed with distilled water, filtered and dried again in an oven at 105° C for 24 hours to measure the final mass (m_2) The calcium carbonate content is the ratio between the dry mass lost after the test (mass of biocement which is acid soluble) and the initial dry mass of the sample, calculated according to Equation (2.2).

$$CCC\% = \frac{m_1 - m_2}{m_1} \times 100 \tag{2.2}$$

4 Biocementation on sand in the presence of clay minerals

4.1 Soil samples preparation and set-up

The soil samples were prepared with APAS 20 sand (S) mixed with varying proportions of two different clay minerals, kaolin (K) or bentonite (B): 0%, 1%, 5%, 10%, and 20%. These proportions were determined based on the ratio of the dry masses of clay to sand. The sample without clay (S00) was the reference, it was prepared with void ratio e = 0.895, corresponding to a dry volumetric weight of $\gamma_d=14.1~kN/m^3$ and a void volume $V_v=1.35~cm^3$ This void ratio corresponds to a relative density of $d_r=50\%$ and a porosity of 47.5%, which decreases with increasing amounts of dry clay, as outlined in Table 2.3.

Table 2.3 – Final porosity of the soil samples (computed by knowing the dry volumetric weight and solid particles density)

Name of the sample	S00	SK01	SK05	SK10	SK20	SB01	SB05	SB10	SB20
Porosity (%)	47.5	46.9	44.8	42.1	36.6	47.0	44.9	42.4	37.2

The research set-up consisted of a plastic container, with a PVC geogrid, a metallic filter mesh and a filter paper placed on the bottom. The soil samples were prepared on cylindrical PET moulds, filling them to a height of 2.0 cm and a cross-sectional diameter of 1.35 cm, resulting in a volume of 2.86 cm³. These moulds were positioned on top the geogrid, metallic mesh and filter paper, as illustrated in Figure 2.5. The samples were assembled by mixing the soil with the respective treatment solution, placed in the tube mould and then the main container was fielded up with treatment solution.

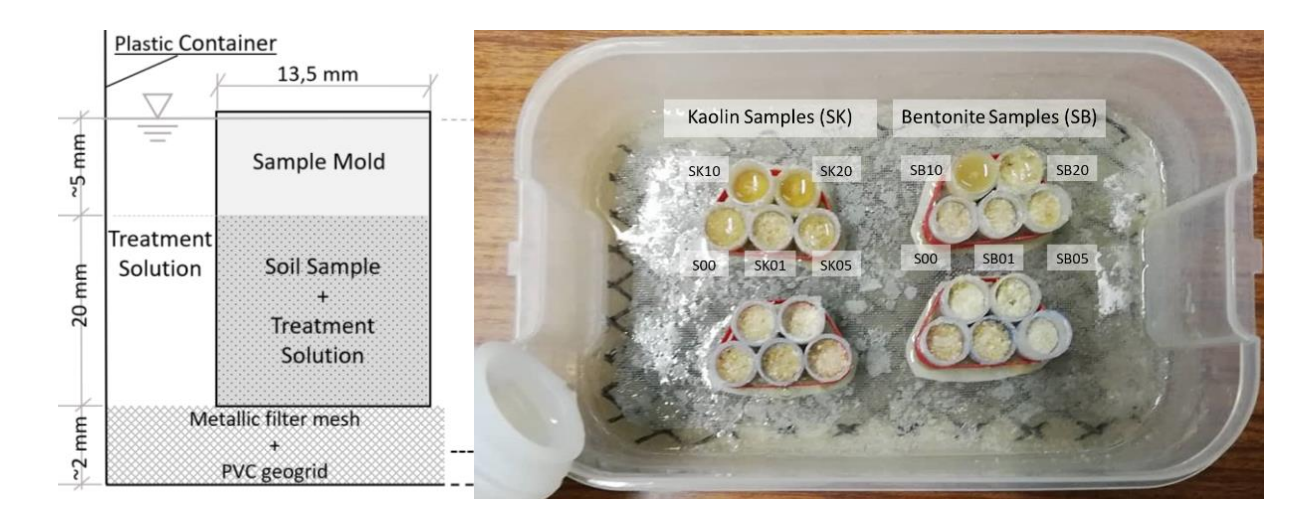


Figure 2.5 – Scheme (left) and photograph (right) of the experimental set-up.

4.2 Treatment protocols

Four treatment protocols were investigated: biocementation solution (lyophilizated *S. pasteurii*, procedure on section 3.4.2, and feeding solution on the plastic container, Bact), only feeding solution (FS), Tris buffer 0.13 M pH 9 (pH 9) and distilled water (dH2O). Bact protocol intend to study the biocementation treatment effects, FS the potential role of native bacteria, pH 9 the chemical effects and dH2O served as a control. The samples were assembled by mixing the soil with the protocol solution. It was used a volume equal to the volume of the voids $(V_v = 1.35 \ ml)$ of the untreated samples, S0O, in order to reach full saturation once the soil is placed in the mould. All samples were then placed in a main container, which was filled with the protocol solution to submerge the samples completely.

All samples were submerged at 20°C (room temperature) for 72 hours in the treatment fluid, and then all the liquid of the container was purged. The samples were drained by gravity and dried in air before being carefully extracted from the moulds.

For the particular case of the Bact protocol, this process was repeated a total of three times. On each time 1.35 ml of rehydrated S. pasteurii were irrigated in the soil on the top of the sample, using a pipette to distribute drops homogeneously in the entire area, and the plastic container was filled with fresh feeding solution for another 72 hours (treatment was performed in 3 sets of 72 hours).

4.3 Evaluation of biocement treatment and clay presence

Several tests were conducted to evaluate the efficacy of the biocement treatment and the impact of clay presence. The test performed were visual observation and in more detail on scanning electronic microscope (SEM), determination of calcium carbonate content (CCC), mercury intrusion porosimetry (MIP) and X-ray diffraction (XRD).

The presence of clay and clay and biocement are responsible for some cohesion and are easily detected by naked eye, so visual observation of the sample integrity was the first step for evaluating the efficiency of biocementation treatment on sand mixed with clay.

The images captured through scanning electron microscopy (SEM, Hitachi SEM model S2400) provide direct information about the presence of calcium carbonate minerals when visible. SEM associated with the technique of energy-dispersive X-ray spectroscopy (EDS) allows for the identification of chemical elements, such as calcium, carbon, and oxygen.

The calcium carbonate content was determined on all samples prepared with the protocols dH2O and Bact according with the procedure detailed on section 0.

Mercury intrusion porosimetry tests (MIP) were conducted on cubic 1x1x1 cm³ of soil samples using AutoPore IV 9500 equipment to analyse pore size distribution before and after the protocol implementation. Prior to testing, the samples were air-dried for a minimum of 48 hours to mitigate the shrinkage effect on soil structure, given the small percentage of clay present. Samples S00, SK05 and SB05 treated with Bact protocol and samples SK05 and SB05 treated with dH2O and pH9 protocols were the samples tested.

X-ray diffraction spectrometry (XRD) is a technique that allows checking the presence of a certain mineral, which permits to confirm the presence of calcite mineral and other calcium carbonate minerals on the Bact protocol. XRD spectrometry was performed on sand, kaolin and bentonite soils and also on samples S00, SK05 and SB05 treated with Bact protocol.

4.4 Results and discussion

The soil samples were carefully extracted from the moulds. Some samples held their shape (HS) and same did not (NHS), Table 2.4 presents these observations. The presence of the biocement in the sample of sand without clay added (S00) treated with Bact protocol was responsible for the stability observed, while disaggregation occurred for all the other S00 samples prepared without biocementation treatment, as expected, due to the absence of bonds between the sand particles. The disaggregation of the sample without clay added prepared with feeding solution discards the relevance of biocementation performed by native bacteria.

S00 SK01 SK05 **SK20 SB01 SB05 SB10 SB20** Protocol **SK10** NHS **Bact** HS HS HS NHS HS HS HS NHS dH2O NHS NHS HS HS HS HS HS HS HS рН9 NHS NHS HS NHS HS HS HS HS HS

HS

NHS

NHS

HS

HS

HS

Table 2.4 – Visual observation of samples after mould extraction

NHS HS - Held shape; NHS - Did not hold shape

NHS

HS

FS

Disaggregation occurred in samples containing 1% of each clay, except when subjected to biocementation treatment and when 1% bentonite was combined with distilled water. This can be attributed to the insufficient clay content to coat the particles adequately and promote cohesion. However, the exception observed with 1% bentonite in the presence of distilled water may be attributed to its higher swelling capacity in this fluid, resulting in a more uniform particle coating. The swelling effect was reduced under high pH conditions and in the presence of the feeding solution, leading to clay behaviour similar to that observed on kaolin and subsequent disaggregation.

The observed cohesion can be caused by the presence of clay minerals coating the particles, however the performance may be significantly altered in the presence of biocement if physical bonds are established between particles. Figure 2.6 presents images of 5% of clay for all protocols (Bact, dH2O, pH9 and FS), in which these differences on cohesion are evident. A stiff white coat was visible only when Bact protocol was applied, confirming the formation of biocement in the precipitate.



Figure 2.6 – Soil samples prepared with 5% of (top) kaolin and (bottom) bentonite for all protocols: Bact, dH2O, pH 9 and FS.

SEM images allowed the visualization of the crystals whose morphology can be associated with crystals from feeding solution, clay minerals and calcium carbonate minerals. These minerals are distinct only when small percentage of clay was added, being the coating of the particles indistinct for clay percentages above 5%. Figure 2.7 presents SEM images of samples without clay for Bact and FS protocols and Figure 2.8, Figure 2.9, Figure 2.10 and Figure 2.11 present SEM images of samples for Bact, FS, dH2O and FS protocols, respectively, with kaolin (left) and bentonite (right).

The presence of calcium carbonate is visible in the samples of sand with biocementation treatment without clay (S00 Bact, Figure 2.7 (left)). The presence of crystals from the feeding solution, after drying, are notable on the FS protocol images (Figure 2.7 (right) and Figure 2.9), because there was no washing step at the end. On samples SK01 and SB01 prepared with FS protocol, various mineral shapes were observed However, on Bact protocol for

low clay percentages were observed irregularly shaped crystals with occasional imprints, which indicates the presence of cells.

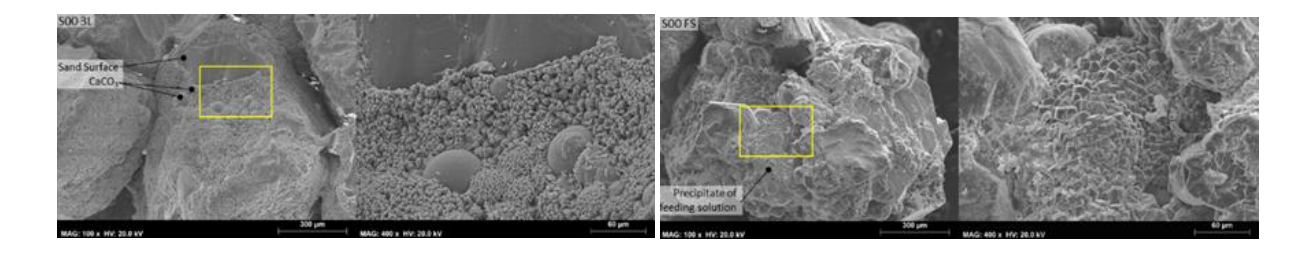


Figure 2.7 – SEM images of S00 samples for Bact (left) and FS (right) protocols.

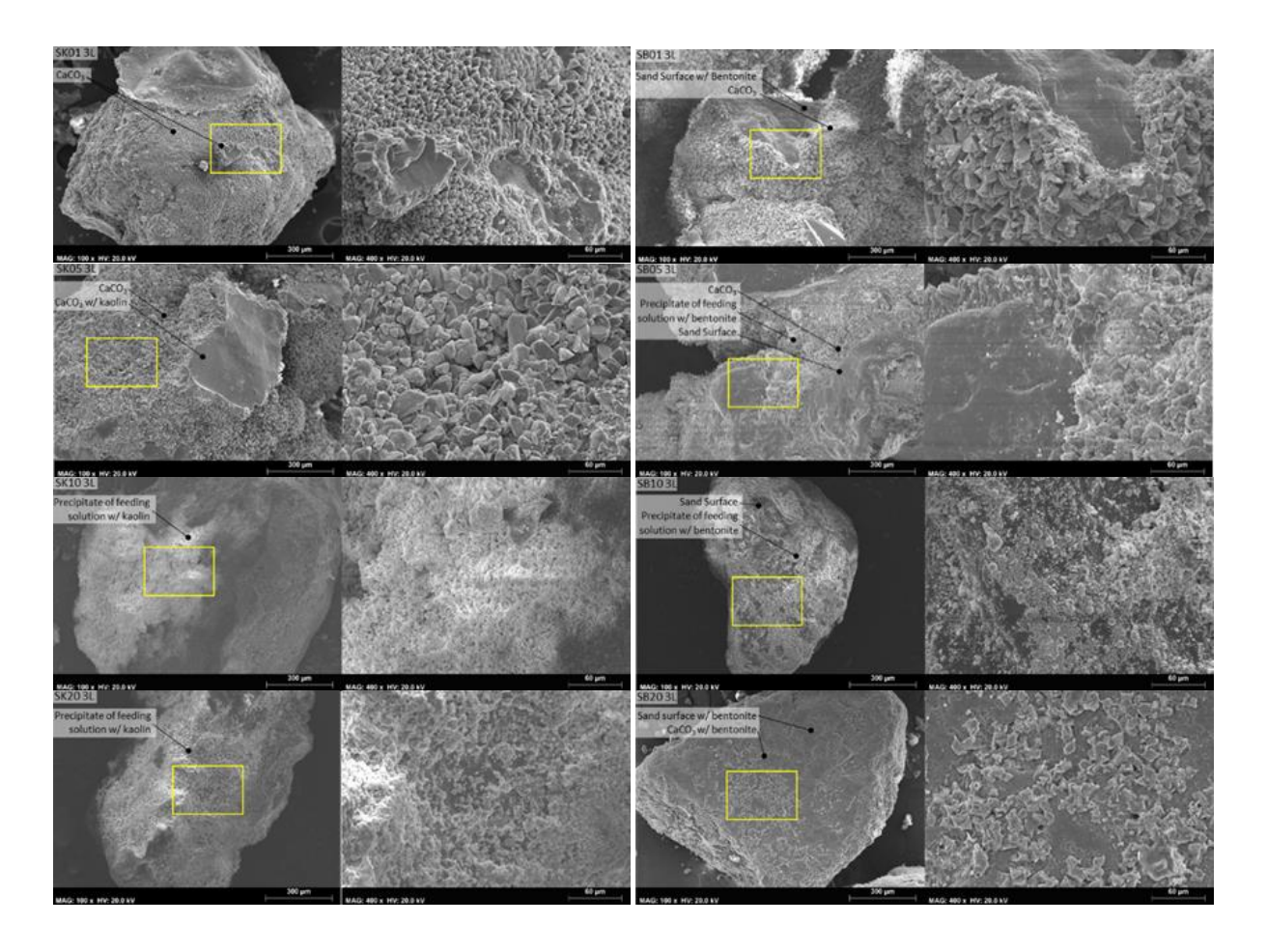


Figure 2.8 – SEM images of samples for Bact protocol for 1 % (top), 5 % (middle) and 20 % (bottom) of clay for kaolin (left) and bentonite (right).

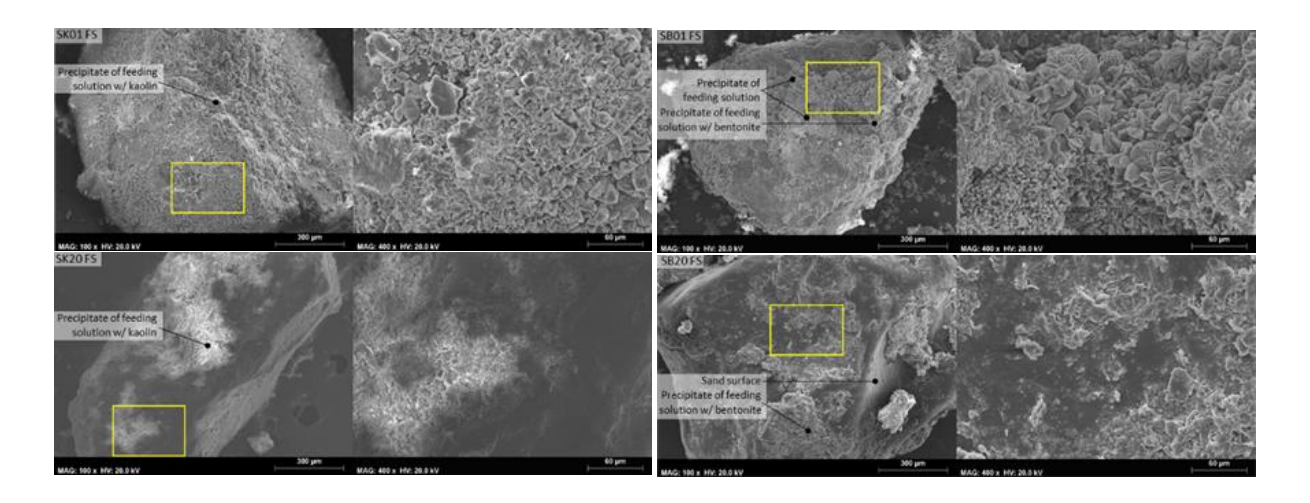


Figure 2.9 – SEM images of samples for FS protocol for 1 % (top) and 20 % (bottom) of clay for kaolin (left) and bentonite (right).

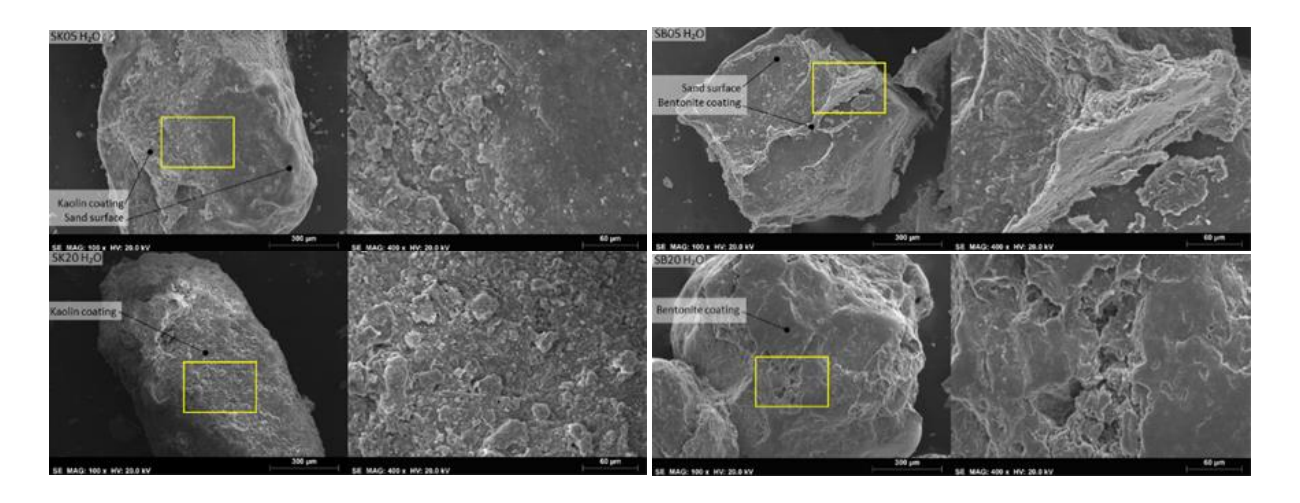


Figure 2.10 – SEM images of samples for dH2O protocol for 5 % (top) and 20 % (bottom) of clay for kaolin (left) and bentonite (right).

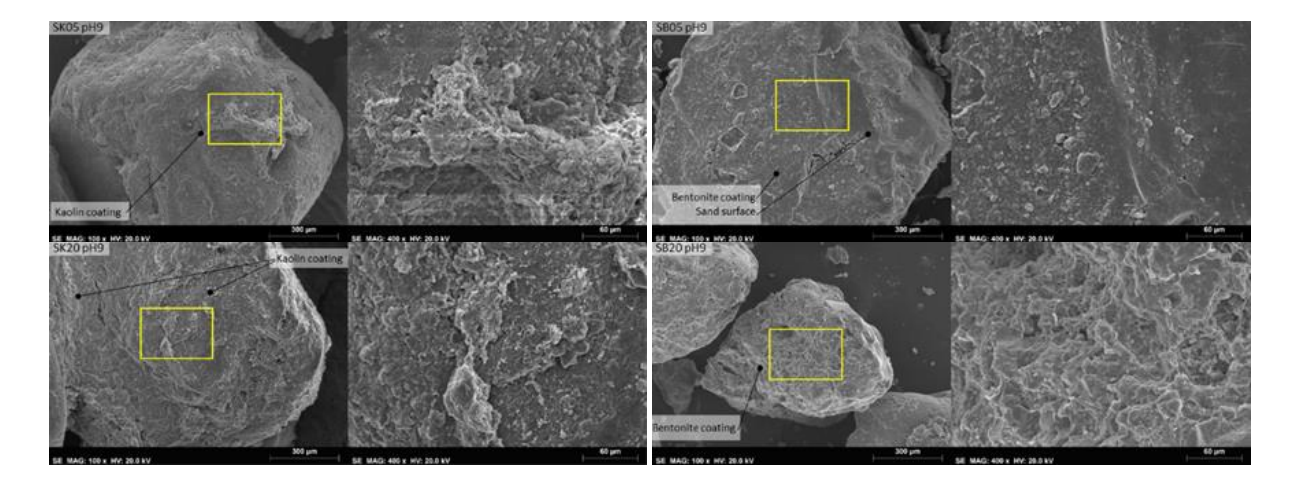


Figure 2.11 –SEM images of samples for pH9 protocol for 5 % (top) and 20 % (bottom) of clay for kaolin (left) and bentonite (right)

For 1% of clay samples with Bact protocol (Figure 2.8 (top)) the sizes of the minerals coating the sand particles are larger in the presence of bentonite than in the presence of kaolin. Considering the scale in the figures, they are around 10 μ m and 20 μ m for the kaolin and bentonite, respectively. This difference in size is probably a consequence of the pH on the clay minerals, it is observed that pH affects more the bentonite's volume than the kaolin's volume (Figure 2.11).

Probably, the visible crystals are precipitated $CaCO_3$ formed under different chemical conditions. The morphology of $CaCO_3$ can vary due to interactions with organic compounds (Li et al., 2010) or reactions between clay minerals and the feeding solution (Cardoso et al., 2020). These chemical reactions introduce complexity, leading to similar irregular textures seen in samples treated with the feeding solution protocol, particularly noticeable in samples with bentonite (Figure 2.9).

When the percentage of clay increases above 5% (Figure 2.8 (bottom)) the coating becomes indistinct in terms of minerals shape. In this case it was only possible to observe a heterogeneous mass of minerals coating the grains, resulting from clay interaction with the feeding solution, eventually with some irregularities which can be calcium carbonate crystals but not confirmed.

From EDS analysis performed for Bact and FS protocols, it was possible to detect calcium, carbon, oxygen, chlorine and aluminium, so the coat observed on sand particles is feeding solution precipitated, calcium carbonate and clay minerals. Similar results were found for the samples prepared with kaolin. Silicon was also detected in the specimens with low clay percentages, corresponding to the uncoated sand particles.

The XRD analysis revealed that in the biocemented samples containing 5% clay, only calcite was detected in sample SB05. However, in samples S00 and SK05, both vaterite and calcite were detected. This outcome serves as confirmation of biocement formation. Despite conducting XRD analysis, no differences were observed between analysis performed on samples before and after the biocementation treatment. This lack of variation suggests that it was difficult to detect any potential mineral changes experienced by the clays due to chemical or biological exposure. The challenge in detecting these changes arises from the small amounts of clay present within the sand particles, which may have been insufficient for the XRD analysis to accurately identify alterations.

Table 2.5 – Mineralogical analysis before and after biocementation treatment

Soil	Before biocementation treatment	After biocementation treatment
Sand	Quartz, Microcline, Alite and Muscovite	Quartz, Vaterite, Calcite and Microcline
Kaolin	Kaolinite, Quartz and Muscovite	Quartz, Vaterite, Calcite, Kaolinite and Microcline
Bentonite	Montmorillonite, Quartz and Microcline	Calcite, Quartz and Microcline (Montmorillonite not checked)

Figure 2.12 presents the pore size distribution of the soil samples prepared with 5% of each clay, SK05 and SB05, for the Bact, pH9 and dH2O protocols. *S. pasteurii* average sizes is around 2 μ m (Ghosh et al., 2019), also identified in Figure 2.12. The plot shows that the size of the pores changed after the treatment.

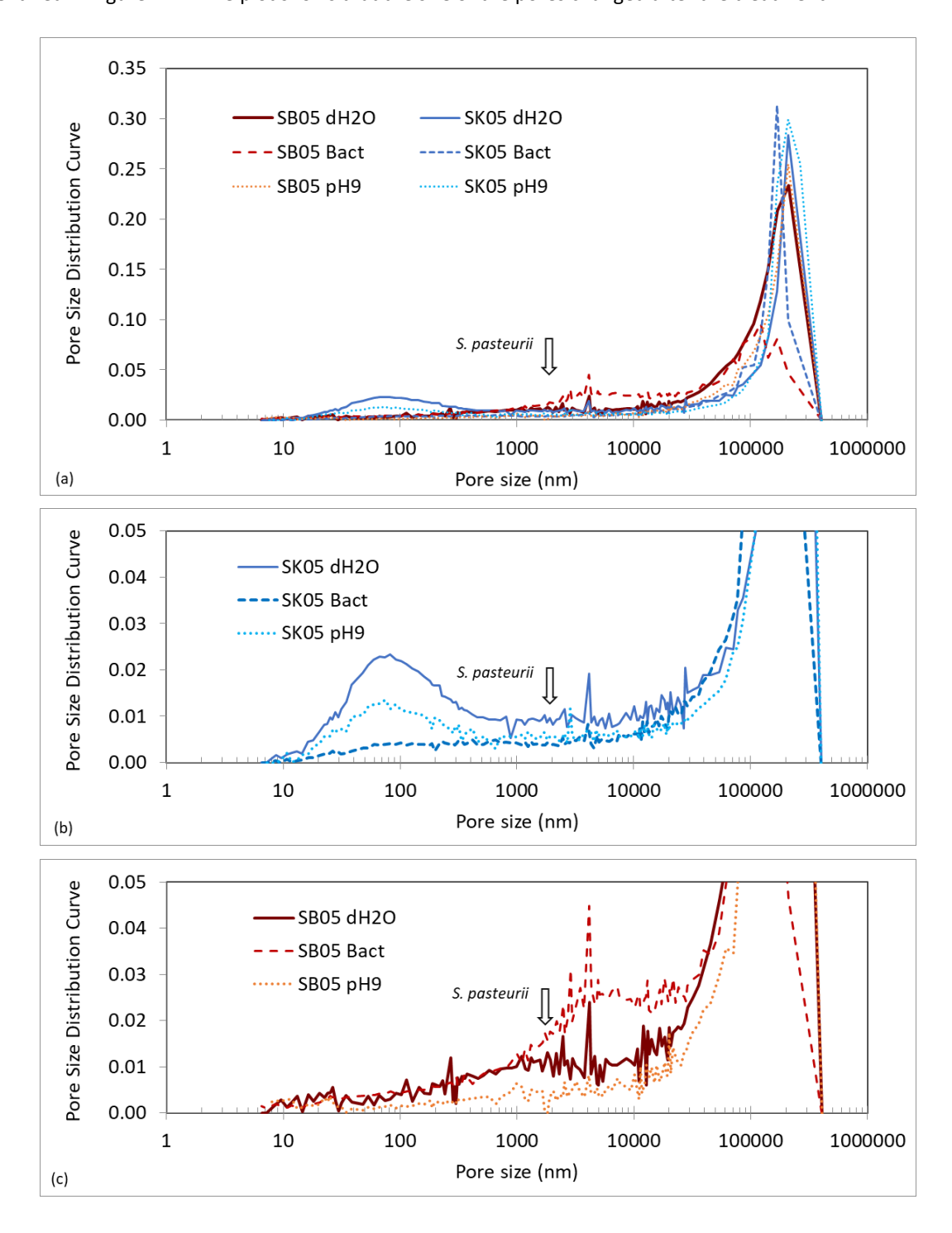


Figure 2.12 – Pore size distribution curves for 5% of each clay (SK kaolin, SB bentonite): (a) overall view, (b) enlargement for the smallest pore sizes for kaolin (c) enlargement for the smallest pore sizes for bentonite.

The biocementation treatment led to a reduction in the size of large pores for both clay types of samples. The large pores were not affected by pH changing, confirmed by the consistent peak at 200 μ m for both clays on pH9

samples. This reduction in pore size is observed on Bact samples, leading to the conclusion that this reduction is caused by biocement precipitation between the sand particles.

For the kaolin sample prepared with dH2O protocol, two distinct peaks were observed in Figure 2.12 (a), a large very sharp around 200 μ m, and a smaller around 100 nm. The larger pore size corresponds to the voids between sand particles, while the smaller one corresponds to the pores between clay aggregates. After the treatment, the pore size distribution exhibited a single peak at 180 μ m indicating pore clogging and a reduction in both large and small pores. The reduction in small pores between clay aggregates could also be influenced by pH, as evidenced by the flattening of the curve in this dimension range for the pH9 sample. It is suggested that biocement may have clogged pores between clay aggregates, particularly in the case of kaolin samples

For bentonite Bact sample, there was a significant increase in pore size distributions around the smaller diameters, indicating that the biocementation treatment caused notable changes. In contrast, for kaolin Bact sample, the number of pores around smaller sizes decreased, resulting in a flattened curve. However, in bentonite Bact sample, the presence of biocement may have led to rearrangement on pores distribution, reducing pores size around 200 µm to values around the smaller pores' sizes.

The different reactions of the two clay minerals to the presence of *S. pasteurii* would be explained by clay-bacteria interaction and pH effect. Morales et al. (2019) have observed the appearance of pores around 200 µm diameter created by bio-mediated aggregation, indicating that this process interferes with soil structure at a biochemical level, however the clay minerals in their sandy soil were not identified. Deep investigation is required to understand how clay-bacteria interaction affect the microstructure of clayey soils and this topic requires further deeper investigation, not done here.

Finally, the percentage of calcium carbonate content was determined on all types of samples with Bact and dH2O protocols. Table 2.6 presents the results and the difference between the two protocols, discarding the error caused by dissolution of clay minerals and eventual material loss during the measurements. Figure 2.13 presents the results in terms of clay percentage.

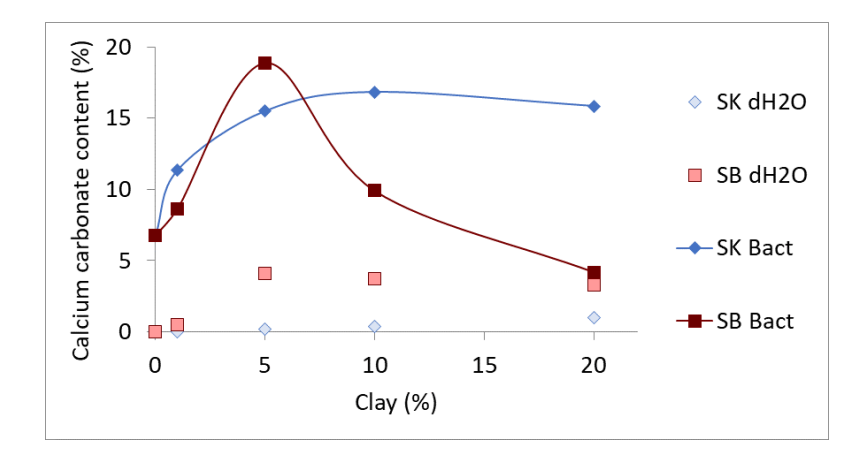


Figure 2.13 – Calcium carbonate content (CCC) for samples prepare with different clay percentages and the resulting (Cardoso, et al., 2023)

Protocol	S00	SK01	SK05	SK10	SK20	SB01	SB05	SB10	SB20
Bact	6.8 %	11.3 %	15.5 %	16.8 %	15.8 %	8.7 %	18.9 %	9.9 %	4.2 %
dH2O	0.0 %	0.0 %	0.2 %	0.4 %	1.0 %	0.5 %	4.1 %	3.7 %	3.3 %
ΔCCC	6.8 %	11.3 %	15.3 %	16.5 %	14.8 %	8.2 %	14.8 %	6.2 %	0.9 %

Table 2.6 – Calcium carbonate content and the variation for Bact and dH2O protocols.

The CCC increased with addition of clay, reaching a peak at 10% for kaolin and 5% for bentonite. The marked peak observed for bentonite indicates that *S. pasteurii* may be more sensitive to the presence of this clay mineral than to kaolin, which is somehow expected due to the higher activity of bentonite minerals and was observed in pore size distribution (Figure 2.12) with the increment of number of pores with diameter closer to bacteria size. A possible explanation for the results found for the larger percentages of this clay may be this clogging effect, preventing bacteria fixation to the sand particles and even to the clay aggregates. Sun et al. (2019) referred that there was no more room for the bacteria to grow for high percentages of clay clogging the large pores, however it should be added that the access of the feeding solution is also more difficult due to this pore clogging effect, significantly reducing permeability. Another aspect to consider is if the presence of the clay causes some inhibition of bacterial activity, more evident when clay increases above a given value, which will be discussed later.

5 Liquid samples prepared with S. pasteurii and clay minerals

5.1 Tests performed

Kaolin and bentonite were added to the NH4-YE medium to study their effect on *S. pasteurii* growth. Sodium hexametaphosphate and sodium carbonate were used as anti-flocculent agents (NP_E-196, 1996) to prevent clay aggregation during bacteria cells growth, and therefore avoiding interference with optical density (OD₆₀₀). Similar growth medium was prepared without these reagents to understand if the changes in OD₆₀₀ measurements could be explained by the formation of clay aggregates or if the anti-flocculent agents were affecting the growth of cells. All the values are presented as increments in OD₆₀₀ relative to the measurement made right before starting the growth and are called as Δ OD₆₀₀. All OD₆₀₀ values in solutions containing clay particles are expected to be higher than in those measured without clay due to the presence of additional colloids in suspension. Nevertheless, the increment of OD₆₀₀ values (Δ OD₆₀₀) can be caused either by *S. pasteurii* growth or by the disaggregation of clay aggregates, and therefore the comparison between the results measured with and without anti-flocculent agent help characterize better the influence of clay.

The clay concentrations on the growth medium were 30 g/L or 150 g/L, corresponding to percentages of 1% and 5% in the weight of clay in the prepared soil samples, respectively. This amount corresponds to the mass of dry clay existing in the void volume of the small samples prepared only with sand particles (47.4% porosity, total void volume 1.35 mL). The intention was to simulate the liquid in the voids of the soil samples.

NE-YE growth with clay was added the amount of cell corresponding to an OD_{600} of 0.1 on a NH4-YE growth medium, as it is common practice when growing *S. pasteurii*. It was not possible to prepare fluid samples for clay percentages above 5%, particularly for bentonite, because the NH4-YE medium transformed into a paste.

The 20 mL NH4-YE medium with clay and bacteria cells were grown in an Erlenmeyer flask with 100 mL capacity to guarantee an aeration ratio of 1:5, for 24 hours (\pm 1 hour) at 30° C at 250 r.p.m (these are the same conditions used to grow *S. pasteurii*). The OD₆₀₀ readings were made about every hour for 24 hours, excepted on the night period. The first reading at time zero serve as reference for Δ OD₆₀₀. The results were repeated twice for each fluid solution.

After the 24 hours of growth, plates were prepared according with American Society for Microbiology (ASM) Standard (Wise, 2006) at dilutions of 10¹, 10³ and 10⁵ times. The plates were left to grow at 30°C for 72 hours.

Urease activity on *S. pasteurii* in the presence of clay minerals was measured to understand their influence following the procedure described in section 3.4.3. Fresh *S. pasteurii* were grown following the standard procedure detailed in section 3.4.1, on a NH4-YE medium without clay, util reaching OD₆₀₀=1.

The solutions to be tested with the clay minerals were prepared, from this bacteria batch, without clay (reference) and with kaolin and bentonite at 30 g/L and 150 g/L. This procedure has ensured that the same number of cells were present in all solutions at the beginning. Urease activity was measured in all solutions over 22 days and the solutions were stored at room temperature ($20 \pm 1^{\circ}$ C). A similar procedure was made with NH4-YE medium without S. pasteurii, on solution with and without the clay minerals, to discard any possible chemical interaction between the clay particles and the urea.

5.2 Results and discussion

Figure 2.14 presents some photographs of the 20 mL NH4-YE medium with clay and bacteria cells after 24 hour of growth and the plates prepared to visualize the formation of colonies in the presence of the clay minerals. Table 2.7 displays the results of colony-forming units (CFUs) enumerated in each dilution. It is evident that the cells remained viable after 24 hours in NH4-YE medium with clay, regardless of the presence of anti-flocculant, as CFUs were observed in every sample. However, the plate results were inconclusive. According to ASM Standard (Wise, 2006), when enumerating CFUs, plates with between 20 to 300 (or 25 to 250) CFUs can be used to calculate the number of CFUs/ml of the original sample. For this study, only the 1BH and 5KH sample results met this criterion. The NH4-YE medium used for all plates was without clay, following 24 hours in the medium with clay, the cells adapted to the presence of clay minerals. This is a possible justification for the lower CFUs in samples with clay minerals than 00 and 00H samples.

Table 2.7 – Colony-forming units (CFUs) enumerated in each dilution.

	Dilutions	00 Bact	00H Bact	K01 Bact	K01H Bact	K05 Bact	K05H Bact	B01 Bact	B01H Bact
CFUs	10¹ times	>300	>300	>300	>300	>300	>300	>300	>300
	10 ³ times	>300	>300	<20	<20	<20	76	<20	204
	10⁵ times	<20	<20	<20	<20	<20	<20	<20	<20
$ imes 10^5$ CFUs/ml		-	-	-	-	-	0.76	-	2.04

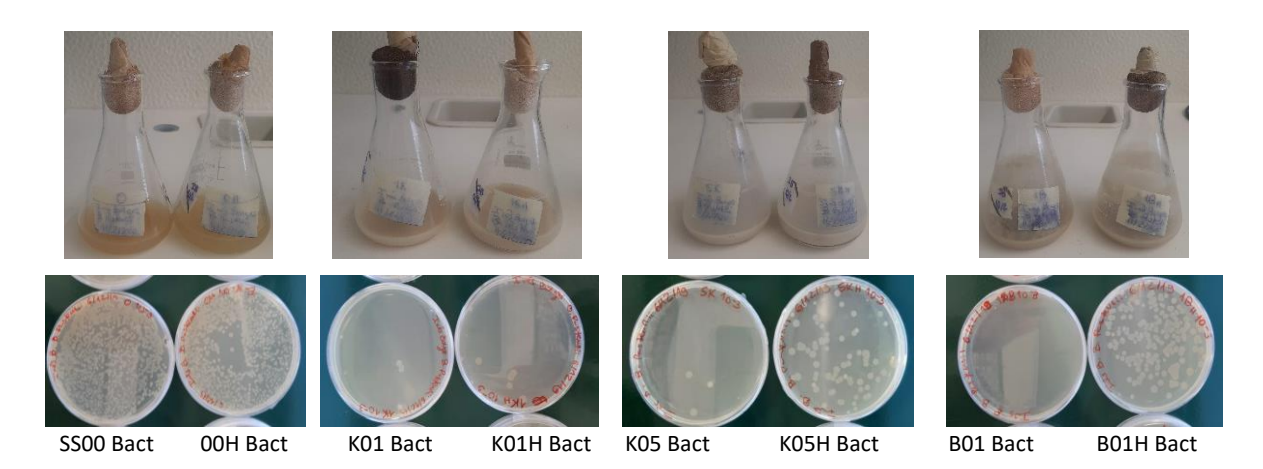


Figure 2.14 - 20 mL NH4-YE medium with clay and bacteria cells after 24 hour of growth (top) and plates prepared to count the colony-forming units (CFUs) for each medium sample after 72 hours growth at 30°C dilution of 10^3 (bottom).

The evolution over time of the optical density (ΔOD_{600}), which monitors cells growth in the NH4-YE medium with and without the clays, and with or without the anti-flocculent agent, is presented in Figure 2.15. Table 2.8 presents the parameters used to adjust the logistic function (FL), to the obtained data. Logistic function is presented on Equation (2.3) where L is the maximum value and k and x_0 are constants. These parameters were calibrated numerically to approximate coefficient of determination (R²) to 1.

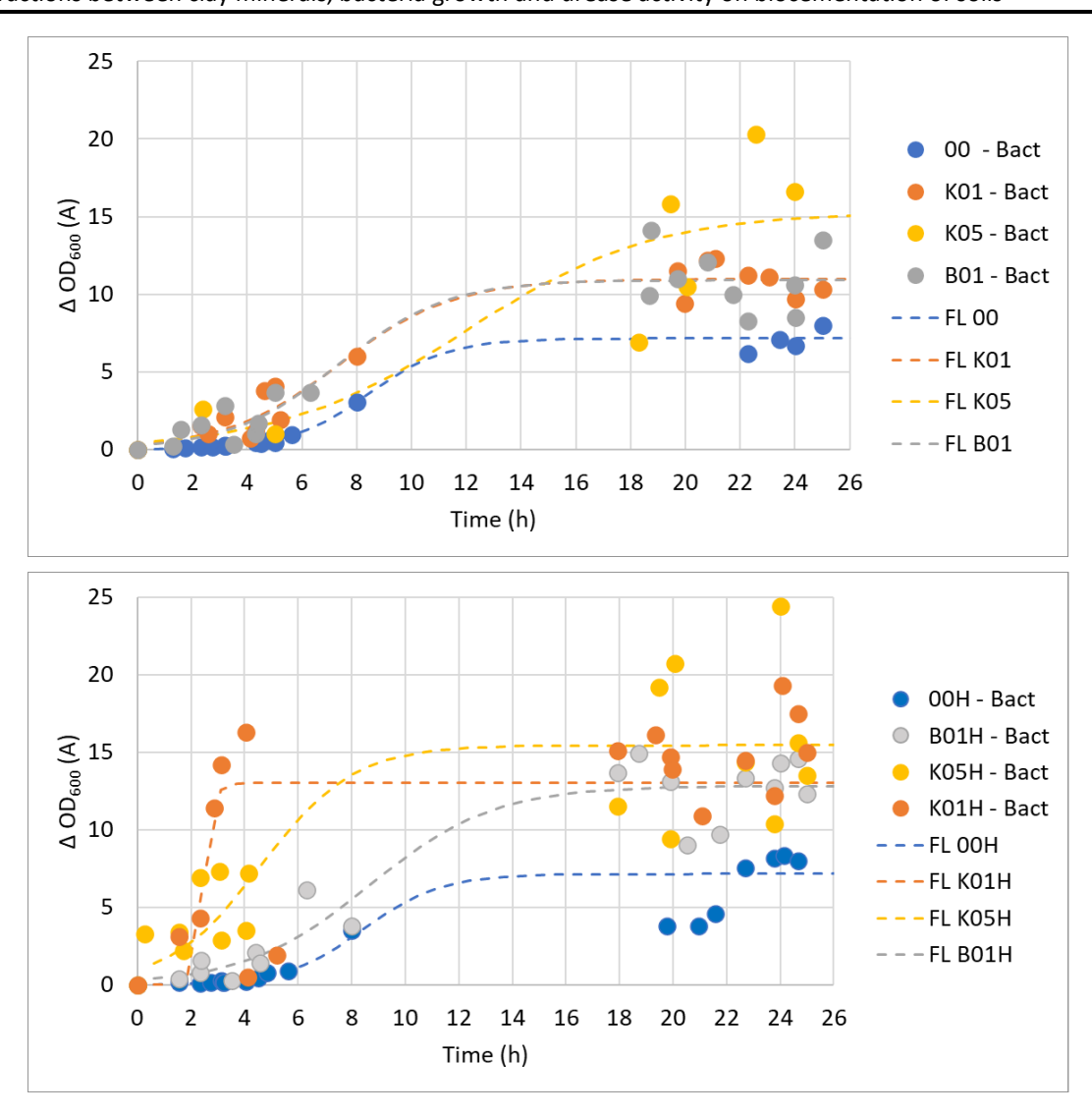


Figure $2.15 - \Delta OD_{600}$ over time for sample without anti-flocculant (top) and with anti-flocculant (bottom) with the adjusted logistic function (FL)

Table 2.8 – Parameters used to adjust the logistic function.

Sample	00	00H	K01	K01H	K05	K05H	B01	B01H
Protocol	Bact							
L	7.1	7.1	11	13	26.2	15.4	10.9	12.8
k	0.7	0.7	0.5	5.2	0.4	0.6	0.5	0.4
X 0	8.4	8.4	7.4	2.5	20.1	4.6	7.3	8.7
R ²	0.97	0.85	0.92	0.5	0.8	0.71	0.87	0.9

$$f(x) = \frac{L}{1 + e^{-k(x - x_0)}}$$
 (2.3)

The final ΔOD_{600} on samples 00 and 00H is similar, therefore the anti-flocculent did not affect the normal growth of *S. pasteurii*. In samples with clay the increment of OD_{600} in time appeared to be faster in the presence of the

anti-flocculent agent, probably due to the larger dispersion of the particles in the medium. The comparation between samples with and without anti-flocculent indicates that the final Δ OD₆₀₀ is caused mainly by cells growth rather than by the presence of the clay aggregates. This is because the changes on clays particles volume or their aggregation due to chemical interaction appears to have low signification in Δ OD₆₀₀ values when analysing the liquid samples prepared without any bacteria. However, this must be investigated further in specific tests, not performed at this stage.

Bacteria continued to grow in the presence of the two clay minerals, evidenced by increasing ΔOD_{600} values over time. ΔOD_{600} values for 1% kaolin and bentonite were similar. Slightly larger values for 5% kaolin were scattered. The presence of clay particles resulted in discrepancies in OD_{600} measurements compared to their absence. This occurred due to the higher relative density of clay particles, about 2.7 times higher than bacteria cells, which led to more movements during OD_{600} measurements in samples containing clay particles.

Notably, *S. pasteurii* can grow up to significant ΔOD_{600} values. For instance, Lapierre et al. (2020) recorded ΔOD_{600} as high as 25 after optimizing the growth medium composition. For instances, growth is not restricted by physical constraints due to high bacterial density. Instead, it is limited by toxicity resulting from bacterial activity in a closed environment (Stanier et al., 1958).

Finally, Figure 2.16 presents the plot of the measurements performed to find the urease activity along time over 22 days. In the first days, a higher urease activity was found for the sample 00, the *S. pasteurii* solution without any clay, however the activity decreased sharply after 6 days of age, reducing significantly after 12 days. For the samples where both clay minerals were present, the urease activity after 6 days remained stable or increased, which indicates that the clay minerals contributed to increase urease activity. Higher activity was obtained for 1% kaolin, followed by 5% bentonite, 1% bentonite and 5% kaolin. The values remained approximately constant after 13 days, and for this reason, the readings stopped after 22 days.

In general, a few days are acceptable for the survival of *S. pasteurii* at room temperature, and this is visible on sample 00 on Fig. 10. The presence of the clays appeared to stimulate urease activity after a 3-day period. The number of cells was not measured at the end of this test, nor were the minerals present in the fluid analysed, so there is no further information explaining the clay-bacteria interaction and clay influence on urease activity.

The control solution, without *S. pasteurii*, confirmed that electrical conductivity variation, used to measure urease activity, was zero along few days. Ensuring that any chemical reaction between the clays and the urea was affecting the urease activity measurements.

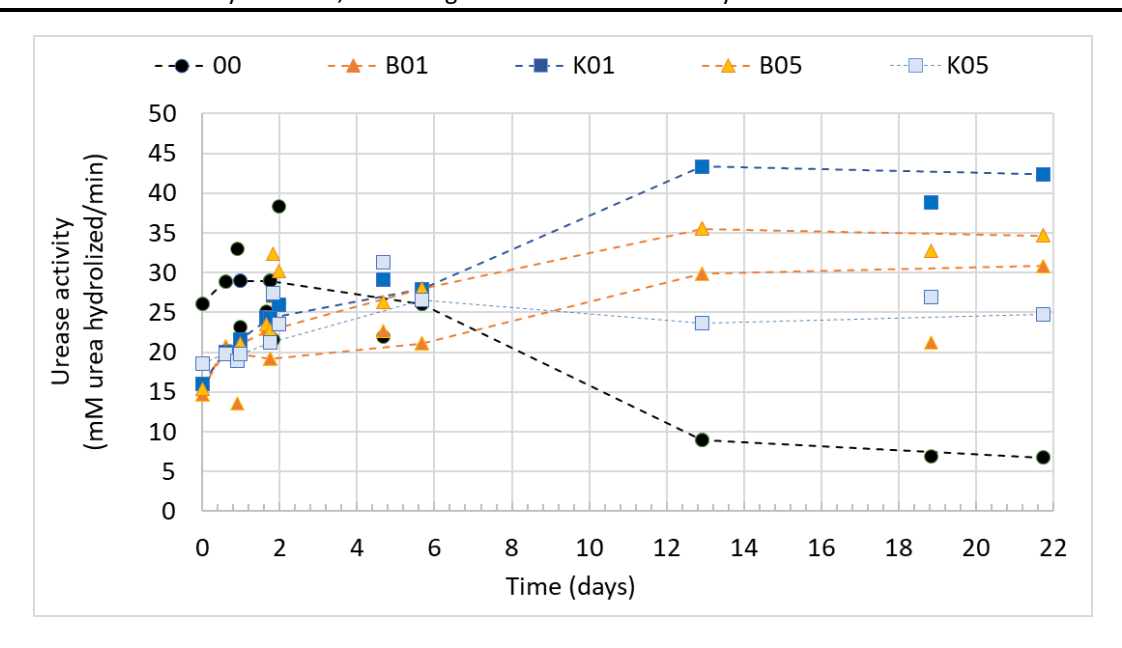


Figure 2.16 – Urease activity measured over time on samples: 00; B01; K01; B05 and K05

6 Discussion

The analysis of the precipitated calcium carbonate (CCC) in soil samples up to 5% of bentonite and 10% of kaolin revealed an increase compared to the biocement measured in the treated sand without clay. Notably, a distinct CCC peak was observed for bentonite, followed by a sudden drop, whereas the reduction in CCC with increasing clay percentage was less marked for kaolin.

These results confirm the interference of clay minerals in biocementation. However, it remains unclear whether this interference is related to physical aspects such as the presence of clay minerals provide surfaces for bacterial adhesion to soil particles, and both are in competition for space in soil voids, or if there are biochemical factors to consider related with clay-bacteria interaction. Clay-bacteria interaction was evident in tests on liquid samples, where growth ratios (ΔOD_{600}) were higher in the presence of clay compared to its absence. However, further testing is necessary to validate this observation. Additionally, clay presence appeared to influence *S. pasteurii* survival, as evidenced by the urease activity measurements in the presence of clays compared to their absence (Figure 2.16).

The urease activity values remained consistently high over 13 days in the presence of clays, contrasting with the rapid decline observed over 6 days in the absence of any clay. Notably, in these tests, 1% kaolin performed better than 5%, while 5% bentonite was better than 1%. This could potentially be explained by element transfer from the clay surface to the cell membrane via water.

Although mineral analysis conducted post-treatment failed to detect changes in the soil minerals, further analysis is necessary. It is important to note, thus lacking information about clay-bacteria interaction for 10% and 20% clay concentrations. However, it is likely that the presence of higher clay percentages may have a negative effect, as suggested by the CCC values, which estimates the precipitated amount of calcium carbonate.

For kaolin, the most suitable percentage for enhancing biocementation appears to range between 5% and 10%, as indicated by the maximum CCC observed at 5%-10% kaolin concentration, nevertheless, bacteria growth was almost identical for 1% and 5% and urease activity was higher for 1%. On the other hand, for bentonite, the maximum CCC was observed at 5%, suggesting that 5% bentonite is the optimal percentage for maximizing urease activity in biocementation.

Results from liquid sample tests suggest that the presence of clays applies a long-term influence, as evidenced by the constant urease activity over time, as if clay would act as a protective agent for urease enzyme. This effect is particularly noticeable for kaolin at lower concentrations, but both percentages of bentonite also kept high urease activity over an extended period. These findings align with observations in nature involving other bacteria and clay minerals (Cuadros, 2017; Mueller, 2015), being the first time, it is investigated in the context of biocementation and using *S. pasteurii*.

7 Final considerations

7.1 Conclusion

The influence of kaolin and bentonite clays was evaluated for a biocementation treatment, where Sporosarcina pasteurii was used as urease source. The evaluation focused on measuring the amount of calcium carbonate precipitated in samples of a sandy soil prepared with known percentages of kaolin and bentonite, and evaluating bacterial growth and urease activity in fluids with compositions mimicking those of the pore fluids. The comprehensive analysis confirms that clay minerals impact biocementation physically contributing to reduce pore volume, and therefore the amount of treatment fluids. This reduction is caused by the presence of the mineral itself and eventually can be affected by some volume change caused by the interaction with the treatment fluids.

The analysis also confirmed that clay-bacteria interaction have influence on biocementation treatment. In fact, the presence of clay on pores fluids space was shown beneficial for *S. pasteurii* growth and long-term urease activity, which can somehow compensate limitations imposed on the void volume reduction by clays. Having this balance in consideration, for the studied conditions, was found that the maximum clay percentage is between 5% to 10% for the kaolin and 5% for the bentonite. Due to its higher calcium carbonate content, kaolin proven more beneficial than the bentonite used. The optimal amount of bentonite for biocementation is lower than that of kaolin because bentonite exhibits higher reactivity. The reactivity acts reducing the amount of bentonite necessary to interact with a fixed quantity of bacteria, being unclear if it interferes with growth space. Possibly bentonite minerals also react more with the feeding solution, but this was not investigated.

The clay activity and clay-bacteria interaction were proven to have impact on biocementation efficiency. In addition, further enhancement possibilities of the treatment are introduced by knowing that clay presence favours bacteria activity. For example, specific clays could be included as an additive when treating clean sands to improve the efficiency of biocementation. If urease activity is kept higher in clayey environments, clay

addiction will allow increasing the precipitation of biocement, which avoids the injection of extra living cells on soils.

The interaction between bacteria and soil particles, specifically clay particles, must be considered in addition to practical aspects related to treatment fluid access. The maximum percentage has been estimated considering pore clogging reducing permeability and therefore access to treating solutions. The research carried out completes this information, considering that clay favours the precipitation of calcium carbonate by promoting urease activity along time.

7.2 Future studies

This studied aids in identifying the existence of a balance between advantages and disadvantages of clay's presence on biocementation treatment. A deeper understanding of aspects leading to the results achieved is suggested as a future study. Investigating the adsorption of bacteria on minerals, the fundamental mechanisms governing the bacteria—mineral interaction, including sorption and ions exchange would help in biocementation with clay addition. Certainly, there is a maximum clay percentage on biocementation to optimize the precipitation of biocement, nevertheless the mineral composition of the clays should be considered as well.

Clay naturally exists on soils, so using it as biocementation treatment addictive would be a big step in making this environmentally friendly soils reinforcement technique more efficient. The biological mechanisms explaining this beneficial influence must be investigated in the future.

Chapter 3

Urease biosensor as monitoring tool for biocementation

1 General overview

Part of data presented in this chapter has already been published in the Proceedings of the 8th International Symposium on Deformation Characteristics of Geomaterials (IS-PORTO 2023), by Borges et al. (2023) entitled "Towards a monitoring tool to quantify urease during biocementation treatment at microscale".

This chapter aims to test a biosensor for detecting urease enzyme (Lab-on-chip device) which was developed previously in the group, aiming at using it as a monitoring tool of biocementation process. Concerning the existing developments on the biosensor to detect urease enzyme and the past experience of the group, several optimization processes were tested. The optimization focused on the following key factors: (i) the range of operation; (ii) the biological and chemical cross-reactions; (iii) the portability, (iv) the easy to use for a non-expert user, (v) the presence of soil particles and (vi) the management of resources (economically). The last factor is explored in further detail by the first time in this work. In this chapter the biosensor was tested as a monitor toll in samples collected from the soil, with some limitations.

Section 2 begins with a comprehensive literature review concerning the existing and potential monitoring tools that can be used for monitoring biocementation. The analysis confirms that detecting urease concentration is a novel aspect.

Section 3 describes the most relevant aspects related with using biosensors and lab-on-chip devices. It presents the background work of the biosensor developed in the research group for detecting urease enzyme, explaining its operating principles.

Section 4 focuses on the main materials and methods employed on the chapter, which comprises several reagents and solutions, equipment less common in civil engineering scoop and procedures mainly related with the operation of the urease detection biosensor.

Section 5 reports all the steps involved on immunoassay optimization, explaining the challenges on the processes to obtain a calibration curve using a sandwich immunoassay.

Section 6 presents a test where the biosensor was used as monitoring tool for biocementation and where urease enzyme was detected on the outflow fluid after treating a sandy soil with purified urease (*Canavalia*).

Section 7 explores the costs involved when using the biosensor for a measurement.

Section 8 proposes protocols and good practices to use the biosensor as monitoring toll for biocementation technique.

Section 9 presents the final considerations, where the main outputs from the chapter are highlighted and future studies are suggested.

2 Monitoring tools for biocementation treatment in civil engineering field

A robust monitoring strategy is planned to consider real-time or time-lapse intervals information providing information about the progress of what is being monitored and not just isolated results. In civil engineering, monitoring is essential for evaluating project progress, ensuring quality, and addressing issues promptly. It enhances safety, reduces risks, and leads to efficient, successful project outcomes, meeting standards while minimizing unexpected challenges. In biocementation treatment, monitoring is also crucial for ensuring project success. This process, using living microorganisms and chemicals to improve soil properties, requires precise control and evaluation, allowing for design adjustments during treatment if needed.

Monitoring strategies for biocementation treatment can be categorized in three aspects: (i) qualitative or quantitative; (ii) done in situ or on laboratory and (iii) performed on soil or on liquid samples.

Qualitative monitoring primarily focuses on identifying the presence of biocement and its effects on soil structure and physical properties. In contrast, quantitative monitoring focus in measuring specific relevant details. It involves assessing changes in physical soil properties including permeability, mechanical strength, and the presence of biocement, as well as changes in biocementation agents. This comprehensive approach provides valuable data regarding the distribution of biocement within the soil and its impact on the desired soil properties.

Microscopy technique is an example of a qualitative method, as it enables the observation and examination of mineral shapes, sizes, bacterial colony locations, and soil grain bonds. Scanning Electron Microscopy (SEM) and optical microscopy have been utilized for this purpose. In Figure 3.1 (right), an active and inactive bond is presented, proving the monitoring capability of SEM (Terzis & Laloui, 2018). Optical microscope allows to observe living samples, enhancing the study of CaCO₃ crystal growth. An example is present in Figure 3.1 (left) (Wang et al., 2019) presenting images captured on a microfluidic device where the treatment fluids were mixed to observe crystal precipitation.

Spectrometry techniques can effectively detect specific chemical elements and minerals. Energy-Dispersive X-ray Spectroscopy (EDS), illustrated in Figure 3.2 (right) (Ghosh et al., 2019), is used to confirm the presence of elements like calcium, carbon, and oxygen, present in CaCO₃, but cannot detect this mineral by itself. On the other hand, X-ray Diffraction Spectrometry (XRD) is employed to confirm the presence of minerals such as calcite, as illustrated in Figure 3.2 (left) (Ghosh et al., 2019).

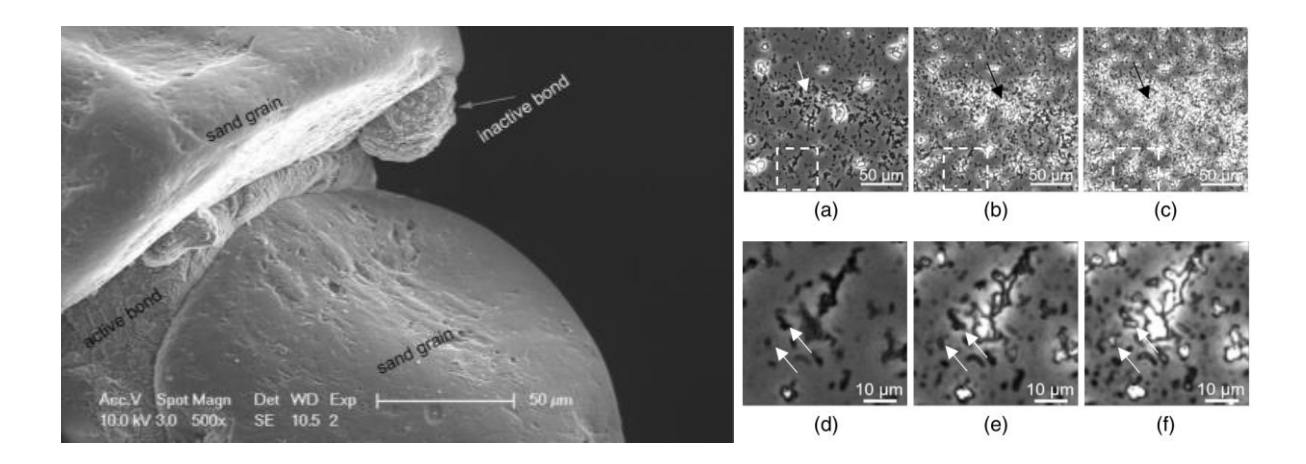


Figure 3.1 – (left) SEM image showing an active calcite bond which bridges two grains of sand and an inactive calcite bond (Terzis & Laloui, 2018) and (right) Microscope images showing the precipitation of irregularly shaped CaCO₃ crystals and the fixation of bacterial cells during the precipitation process. (Wang et al., 2019).

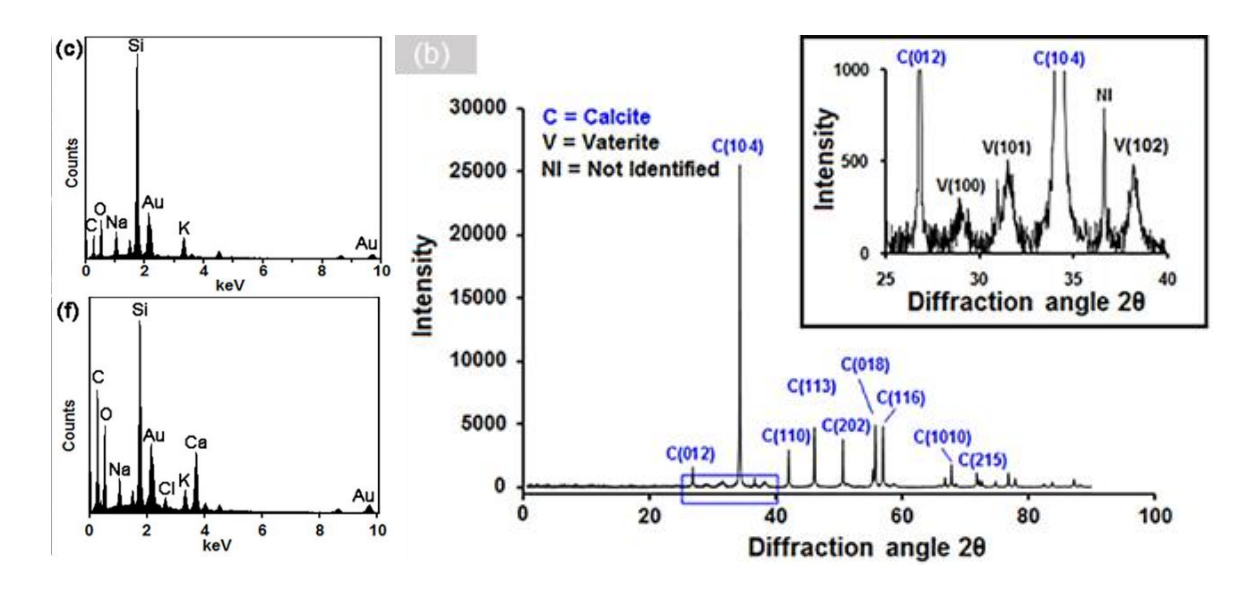


Figure 3.2 – (left, top) EDS spectra collected on *S. pasteurii* control cells and (left, bottom) *S. pasteurii* cells clearly showing presence of crystalline deposits on the cell-wall showing presence of Ca and (right) XRD plot indicates the formation of calcite and vaterite polymorphs (Ghosh et al., 2019).

The biocement precipitation clogs soil pores in the soil, which can be monitored instead of detecting the mineral presence. Pore clogging can be monitored by comparing pore sizes and void ratios before, during, and after the treatment, and can be done through Mercury Intrusion Porosimetry (MIP). This technique is employed on a 1x1x1 cm³ sample to obtain the pore size distribution. By comparing the distribution of a treated sample to that of an untreated one, the effects of biocementation can be detected.

Quantifying the calcium carbonate content (CCC) serves as strategy for monitoring the production of biocement. CCC can be determined through either direct or indirect methods. In the direct approach, a soil sample, typically around 5 g, is required (Choi et al., 2017). The washing method adapted from Portuguese standard NP-E196-1996 (1966) (Borges et al. 2020) and according with American standard (D 4373, 1996) (Choi et al., 2016; Terzis

et al., 2016) stands out due to its simplicity and effectiveness. Indirect measurements, on the other hand, rely on estimating the concentration of ions retained inside the soil, considering chemical analysis. They are not explored further as they are unsuitable for geotechnical applications, being expensive, lab-based, and not easily deployable in the field. This prevents engineering contractors from obtaining real-time data to inform treatment design.

Biocementation technique enhances the mechanical and the hydraulic proprieties of the soil. Quantifying these improvements during and after the treatment provides a tool for monitoring the effects of biocement. Mechanical and hydraulic characteristics can be measured through geotechnical laboratory standard tests conducted on soil samples. These tests include (i) triaxial tests, (ii) unconfined compression tests, (iii) direct shear tests, (iv) oedometer tests, (v) indirect tensile tests, and (vi) the permeability tests. These assessments can be carried out on samples prepared on laboratory. Figure 3.3 presents an example of the a study for different feeding solution dosages and frequencies relating unconfined compression strength with calcium carbonate precipitation (Al Qabany & Soga, 2013).

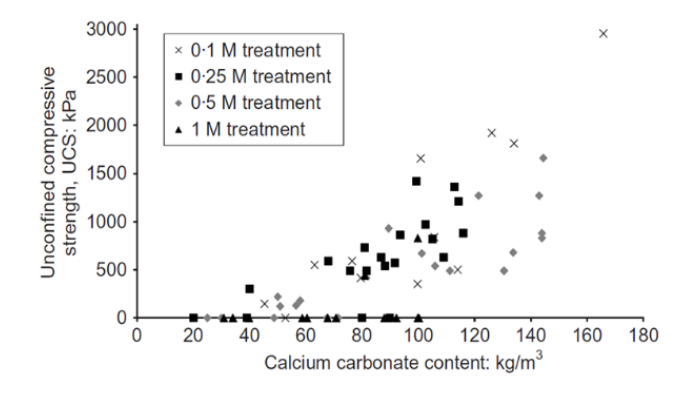


Figure 3.3 – Unconfined compression strength plotted against calcite precipitation for different treatments (Al Qabany & Soga, 2013)

Several monitoring techniques have been developed or adjusted for laboratory-scale biocemented test samples, like the ones presented before. *In situ* monitoring can be complemented with laboratory tests on collected samples. The selection of sampling locations can be informed by *in situ* data, aiding in understanding the homogeneity of the biocementation treatment. As biocementation treatment is still emerging on side in geotechnical engineering, *in situ* monitoring strategies are limited. However, traditional strategies can be adapted for this purpose, e.g., geophysical tests.

Geophysical tests serve as a quantitative monitoring strategy, requiring calibration for the specific study. These non-destructive tests have significant potential for repetitive *in situ* application and allow to analyse large volumes, compatible with civil engineering scale. Among the most widely used geophysical methods are the measurement of seismic wave velocity and electrical resistivity. Seismic waves velocities are related to geomaterials density, making them a valuable tool for monitoring treatment progress. On the other hand, electrical resistivity can detect the high salinity of ions in the treatment solution, as illustrated in Figure 3.4 for

an *in situ* example. Geophysical prospection tests have been employed as a monitoring tool in laboratory samples (Saneiyan et al., 2018; Y. Wu et al., 2011), large scale model tests (van Paassen et al., 2010) and *in situ* treatments (van Paassen, 2011).

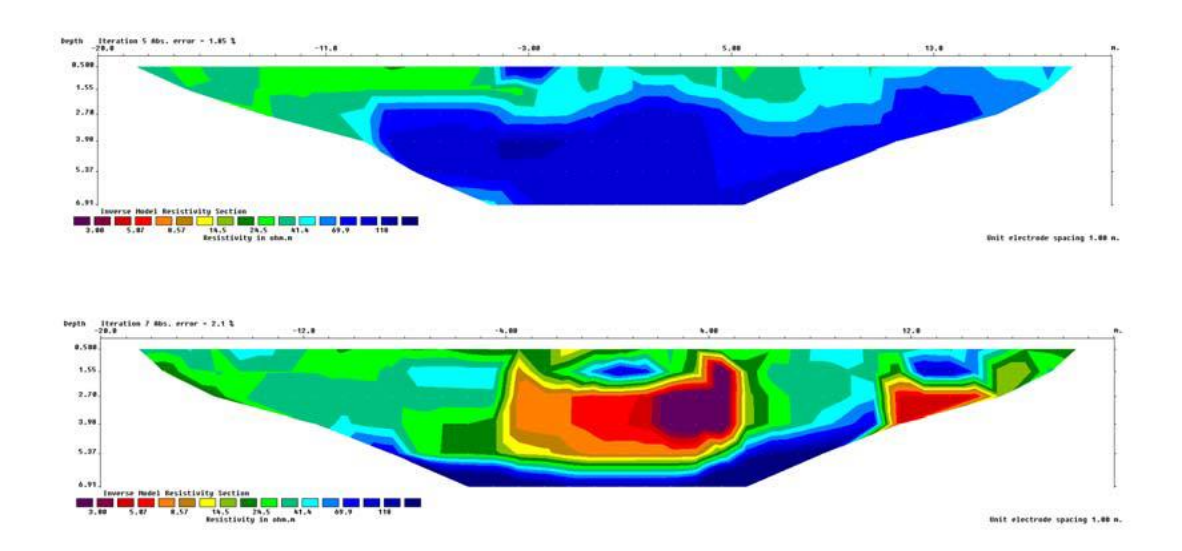


Figure 3.4 – The geoelectrical resistivity measurements before (top) and during (bottom) treatment indicate the approximate area, which is affected by biogrouting. (van Paassen, 2011)

Soil and liquid sample monitoring are complementary and conducted at distinct stages of the treatment. Soil sample monitoring evaluates changes in physical properties, such as the ones already described. In contrast, liquid sample monitoring focuses on the biological and chemical properties of biocementation agents, detecting and quantifying the presence of enzymes, microorganisms, chemical reagents, and resulting products.

Throughout the biocementation treatment, optical density, measured at a wavelength of 600 nm (OD $_{600}$), is typically measured with a spectrophotometer and can serve as an indicator of biomass concentration (Harkes et al., 2010). This a standard method to estimate the number of cells in a fluidic sample, because the cells in suspension interfere with light dispersion through the medium.

Analyses conducted on effluent samples contribute to the monitoring of the treatment. The Nessler method enables the measurement of ammonium (NH_4^+) in the effluent solution, allowing for the estimation of hydrolysed urea and the concentration of carbonate (CO_3^{2-}) within the soil (Whiffin et al., 2007). Inductively coupled plasma optical emission spectroscopy (ICP-OES) is an analytical technique employed to measure the concentration of calcium (Ca^{2+}), as it makes it possible to estimate the remaining concentration in soil available for reaction (Terzis et al., 2016).

Urease activity measures the quantity of urea hydrolysed per unit of time. The urea hydrolysed can be determined by a conductivity method under standard conditions and using Equation (3.1) (Harkes et al., 2010; Whiffin, 2004). Electrical conductivity increases proportionally with the increase of ions products of the urea hydrolysis reaction (Equation (1.1), Chapter 1, section 3.1). This monitoring method is performed on a sample of just the ureotelic agent, because the presence of ions from feeding solution interferes with the measurements.

Urease hydrolysed
$$(mM) = Conductivity (mS) \times 11.11$$
 $(R^2 = 0.9988)$ (3.1)

Monitoring urease concentration is useful because the urease enzyme is responsible for the hydrolysis of urea. Urease concentration in the inflow fluid is known in enzyme induced calcite precipitation (EICP) treatment, however urease can be flushed out of the soil when the treatment fluid is flowing or if further injections are programmed due to the difficulty to fix the total of enzyme introduced. In microbially induced calcite precipitation (MICP), bacteria have more capacity to adhere to soil particles than enzyme, because they are larger and have cell membranes. Monitoring the amount of enzyme produced by bacteria is a hard task because it is intracellular (produce inside the bacterial cells) and mixed with other enzymes and bacteria are producing continuously urease enzyme at unknown concentrations. Nevertheless, a monitoring strategy can be measuring the concentration of urease, and this can be determined using classical approaches for detection of analytes such as high-performance liquid chromatography and gas chromatography. Nevertheless, these methods are usually accompanied by an extensive processing time, trained personnel requirements and high costs (Albuquerque, 2017). Chromatography is a laboratory technique used to separate and analyse complex mixtures of substances, separating their individual components, including the analyte, which is the substance or chemical constituent to be analysed from an analytical point of view.

Developing a biosensor able to determine the urease concentration can be a crucial step to develop this monitoring strategy. Biosensor-based devices have advantages such as high sensitivity and selectivity to their target, rapid processing period, user-friendliness, easy to implement, and being cost-beneficial (Salek-Maghsoudi et al., 2018). This idea has been under detailed study in the past by the research group (Albuquerque, 2017; Ferreira Cardoso, 2015; Valentim, 2016) and is the focus of this chapter. The background will be described in detail in the next section.

3 Biosensor to detect urease

3.1 Biosensor principle

A biosensor is capable of detecting an analyte (substance or chemical constituent interesting from an analytical point of view) in a sample. As illustrated in Figure 3.5, their working principle combines a biological sensing element and a physicochemical detector that enables sensing of molecular interactions between the biocomponent and the desired analyte. Finally, a transducer or a detector element transforms the signal resulting from the interaction of the analyte with the biological entity into a signal that can be measured and quantified. The biological sample can be, for example, sample body fluids, food samples, cell cultures and environmental samples and the analytes can be nucleic acids, natural products, antibodies, enzymes, cell receptors, organelles, microorganisms, tissues, etc., so biosensors are very versatile. Transducers in biosensors may be optical, electrochemical, micromechanical, piezoelectric, magnetic or thermometric, that will produce either discrete or continuous electronic signals proportional to the quantity of analyte present in a sample (Dixit, 2016).

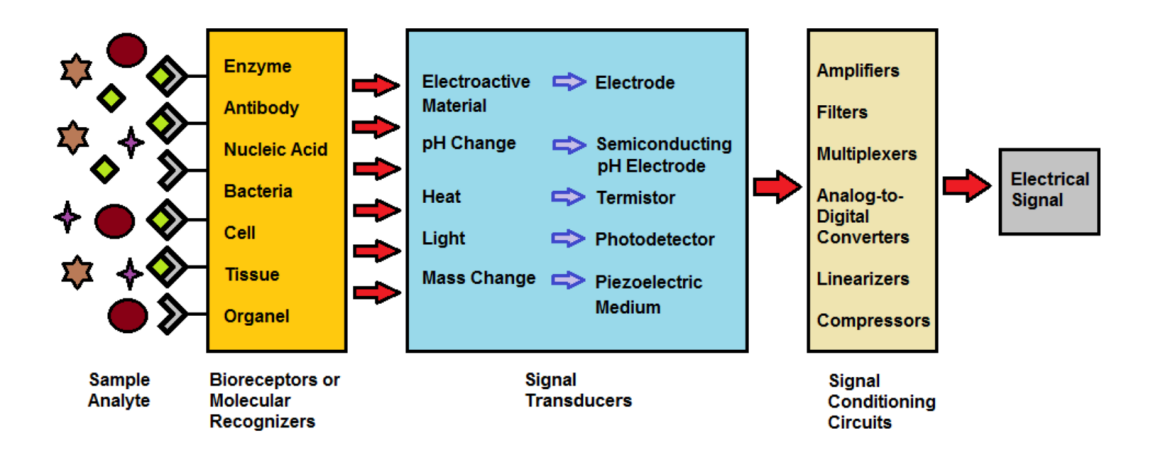


Figure 3.5 - Biosensor operating principle: main subsystems (Vargas-Bernal et al., 2012)

3.2 Lab-on-a-chip

3.2.1 Overview

The Lab-on-a-chip (LoC) consists on a device able to integrate one or several laboratory functions on a single integrated circuit (commonly called a "chip") of only millimetres to a few square centimetres to achieve automation (Volpatti & Yetisen, 2014). The main advantage is low fluid volumes consumption (less waste, lower reagents costs and less required sample volumes for diagnostics), which on geotechnical engineering works scale consists of a disadvantage in terms of the representativeness of the samples collected and analysed.

The LoC device adopted in this study is not fully automated, however the research group has been pursuing automation as a goal. It consists of a magnetoresistive platform, a print circuit board where biochips with magnetoresistive sensors are connected and a U-shaped microfluidic channel. The sensors are functionalized, then the microfluidic channel drives fluids to the sensors while the *Biochip Platform Interface V3.2* software acquires the signal transduced by the magnetoresistive platform.

3.2.2 Magnetoresistive platform

The magnetoresistive chip based read-out platform (MR platform) was developed in *Instituto de Engenharia de Sistemas e Computadores Microsistemas e Nanotecnologias* (INESC MN) (Germano et al., 2009) and acts as an interface to transform the detection into an electrical signal shown on the Biochip Platform Interface software develop by INESC MN and *Instituto de Engenharia de Sistemas e Computadores: Investigação e Desenvolvimento* (INESC ID) (Figure 3.6).



Figure 3.6 – Magnetoresistive chip based read-out platform

The MR platform is composed by 4 main components shown in Figure 3.7: 1) battery, for power supply and portability; 2) control and acquisition board, where the data is collected from the MR-sensor and transmitted to the user computer; 3) inductor to generate an external magnetic field and 4) port and a support for the biochip moted on a printed circuit bord (PCB) in which biology takes place (Valentim, 2016).

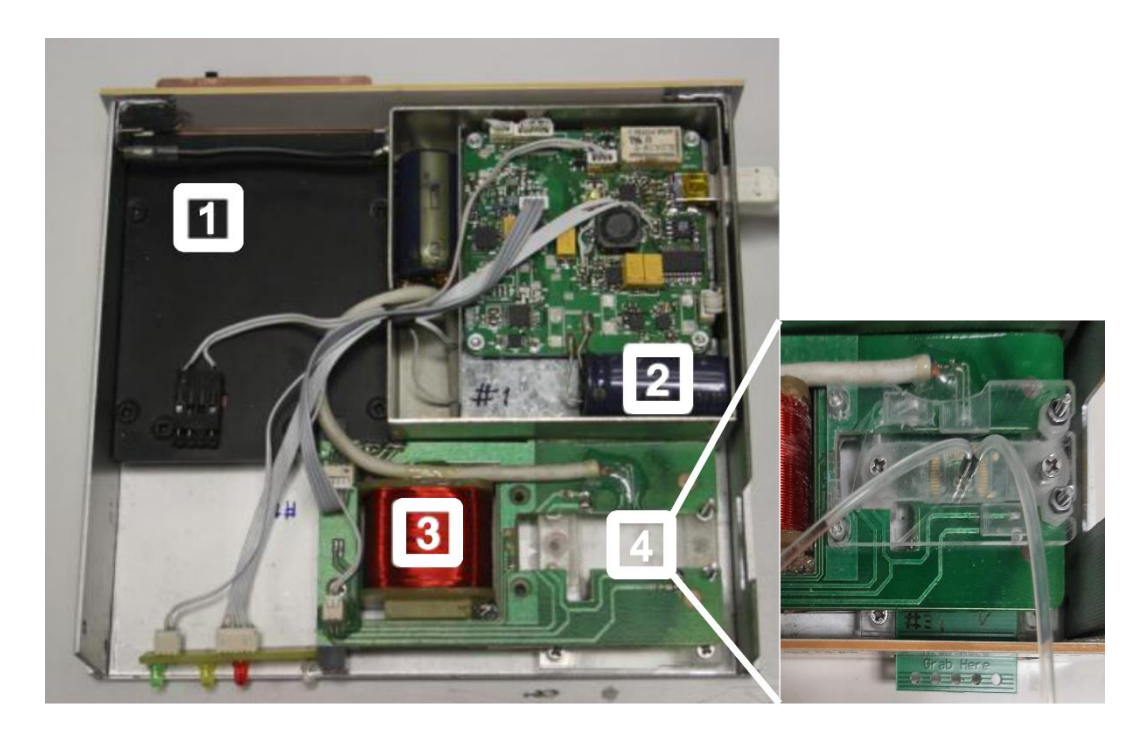


Figure 3.7 – Components of the biochip platform: (1) power supply/battery; (2) control and acquisition board; (3) inductor and (4) biochip port and support.

The MR platform, as illustrated in Figure 3.8, can detect variations in the resistance of MR sensors when an external magnetic field is applied, so it detects the biorecognition. First the analyte is immobilized on the biochip surface (Figure 3.8 a). The biorecognition assay starts with the introduction of the recognizer (Figure 3.8 b) previously labelled with a magnetic particle (Figure 3.8 c). The magnetic nanoparticles (MNPs) are superparamagnetic, which means that they have zero magnetization when a magnetic field is not applied, becoming uniformly magnetized over an applied field. This magnetic specificity prevents agglomeration of nanoparticles and any interference, making them suitable for biological applications (Demas & Lowery, 2011).

These particles are coated with dextran and streptavidin-modified, presenting about 1000 binding sites for biotin present in the recognizer. If the analyte and the recognizer are complementary, the binding occurs (Figure 3.8 d). A washing step removes all the entities which were not recognized. Finally, an external magnetic field is applied to magnetize the particles (Figure 3.8 e). The fringe field created by the immobilized magnetic nanoparticle (MNP) is detected by the MR sensor (Figure 3.8 f). The sensor's electrical resistance variation is proportional to the number of biomolecular recognition events (Germano et al., 2009). This is due to the ability of these superparamagnetic particles.

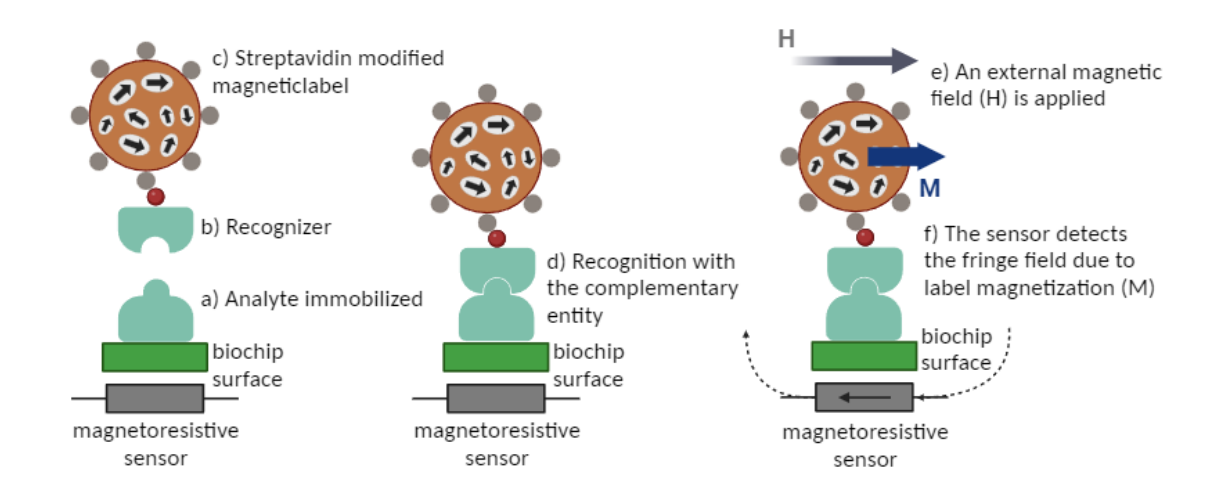


Figure 3.8 – Biorecognition steps on the magnetoresistive biosensor (Adapted from Germano et al. (2009)).

Electronic platforms offer several advantages, including the capability for real-time signal processing, the utilization of standard communication technologies that reduces the development time, and the providing of a user-friendly graphical interface on a computer for complete control over the measurement procedure. Experiments conducted using this platform have been documented in the literature and have demonstrated advantages over tests conducted in open chambers. These advantages include enhanced assay reproducibility and a reduction in the time required for magnetically labelled target molecules to reach the surface, about a 60% decrease (Freitas et al., 2012).

3.2.3 Biochip

The biochips were microfabricated in a cleanroom at INESC MN, where each MR sensor consists of two spin-valve (two magnetic layers separated by a non-magnetic spacer) with dimensions 46.6 x 2.6 μ m². The sensors were microfabricated with the stack Si/Al₂O₃ 100/Ta 1.5/NiFe 2.8 /CoFe 2.8 /Cu 2.7 /CoFe 3.3 /MnIr 7.5 /Ta 5 (thicknesses in nm). In the end of the microfabrication process, the sensors were coated with a gold film layer (Cr 5nm /Au 40nm) for biological immobilization purposes. The spin-valve sensors used were characterized, showing a minimum resistance of 730-850 Ω and a magnetoresistance of ~5.5 %. Each chip has a total of 31 sensors, with 1 of them serving as reference, and the remaining 30 sensors are divided into two rows, each containing 15 sensors. Figure 3.9 (a) presents a biochip diced and mounted in a PBC properly, Figure 3.9 (b) presents an AutoCAD design of the biochip (6.3 X 7.4 mm) and Figure 3.9 (c) a sequence of magnified microscopes pictures of the biochip (a previous version of the biochip described). It is visible the two rows containing 15 sensors each, which are further divided into three groups of 5. Several biochips were microfabricated in a silicon wafer, then each one was diced and mounted in a PBC properly.

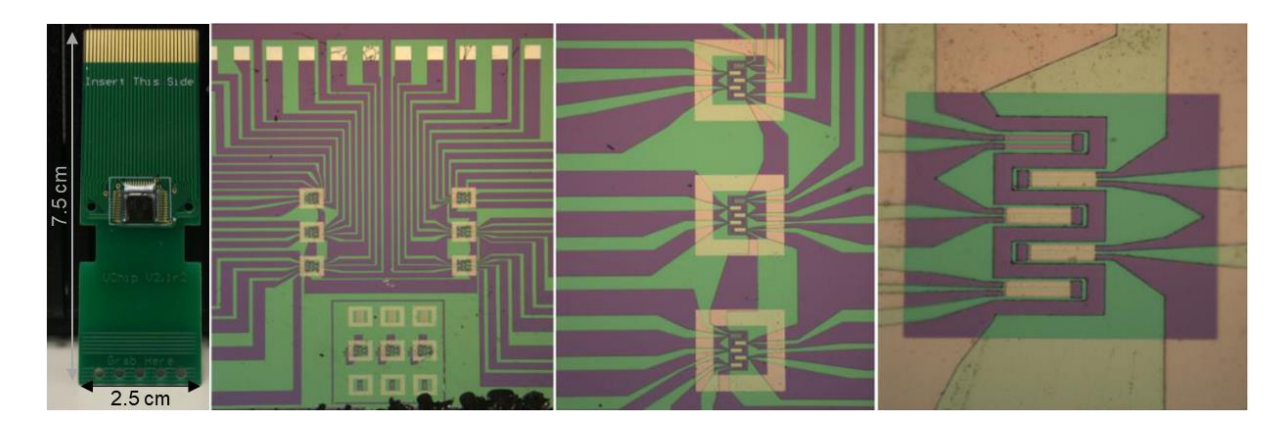


Figure 3.9 – Biochip (6.3 X 7.4 mm) mounted on a PCB next to three microscope pictures (40X, 160X and 800X magnifications) of the fabricated piece (Valentim, 2016).

3.2.4 Microfluidics

Placing the microfluidic system on top of the biochip is essential, as it helps guide the solutions over the sensors. The microfluidic is a U-shaped channel in polydimethylsiloxane (PDMS), which was designed in INESC MN to be placed on top of the biochip. The microchannel was designed to create a secure seal with the biochip, preventing any leakage and facilitating the inflow and outflow of solutions over the sensors during signal acquisition.

Valentim (2016) developed a new equipment to produce U-shaped channels, enabling the fabrication of a larger quantity of channels simultaneously while reducing the number of defective ones. The innovative design also leads to more effective channels. The key innovation of this system is that the bond between the PDMS cube and the biochip is temporary. After the assay, it can be removed without damaging the biochip, allowing for its reuse of biochip and PDMS cube. Figure 3.10 presents a scheme and a photo of the PDMS U-channel aligned on the biochip.

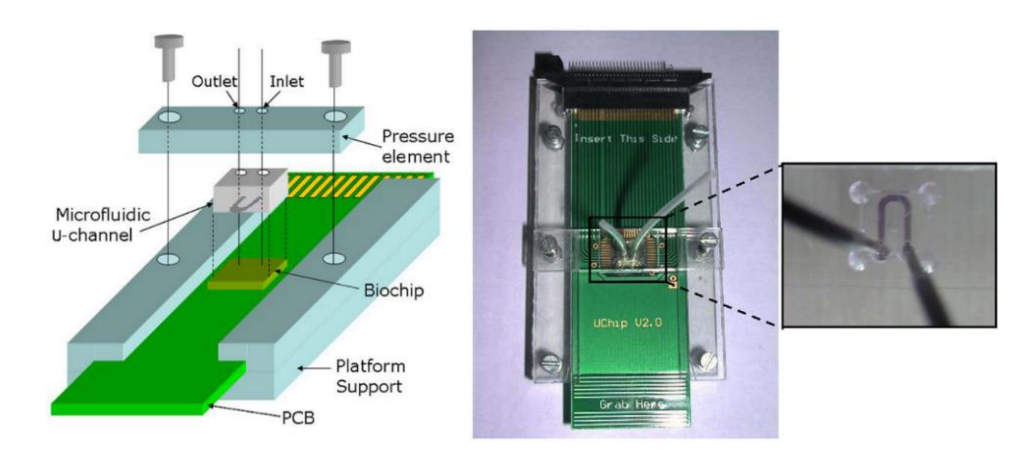


Figure 3.10 – (left) Schematic representation of the microfluidic platform components showing how the alignment and sealing of the channel is achieved and (right) photo of pressure platform including the PCB aligned with the platform support and with the PDMS U-channel, in detail the PDMS element with the U-Shaped channel filled with coloured fluid (Martins et al., 2010)

3.3 Immunoassays

An immunoassay is a biochemical test that measures the presence or concentration of a molecule in a solution using an antibody. The molecule detected by the immunoassay is often referred to as an analyte and is the target or the antigen. This molecule is a protein in many cases. Immunoassays rely on the ability of an antibody to recognize and bind a specific molecule in what might be a complex mixture of molecules. The immunoassay is a fundamental tool on the detection of urease using the biosensor strategy within the LoC.

The direct immunoassay performed on the LoC presented is an adaptation of direct ELISA (enzyme-linked immunosorbent assay) where an antigen must be immobilized on a solid surface and then conjugated with a detection antibody that is linked to a molecule which labels the antigen (Figure 3.11). In a conventional ELISA, this label is commonly an enzyme which changes colour in the presence of a substrate. In this work, a magnetic nanoparticle conjugated to an antibody via streptavidin-biotin interaction acts as a label.

Sandwich immunoassay is also inspired in conventional Sandwich ELISA however the difference between Direct and Sandwich immunoassays is the use of an extra antibody. As Figure 3.11 shows on Sandwich immunoassay, a capture antibody adsorbs to the surface and captures the target, which is the antigen labelled.

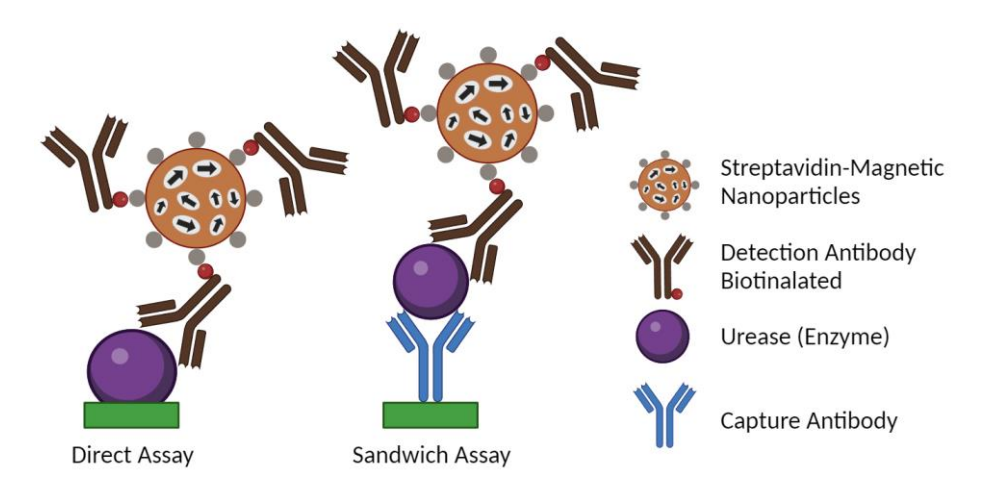


Figure 3.11 – Scheme of direct and sandwich immunoassays to detect urease.

3.4 Detecting urease (background)

Prior to utilizing biochips for urease detection, biochemical processes were initially optimized on gold pads. These gold-coated silicon pieces, with a thin gold film (500 Å), were obtained by cutting them from a silicon wafer. They come in the size of 5 x 7 mm 2 for single, double, or quadruple spots. The double and quadruple spotting methods ensure consistent washing and timing conditions for parallel tests, facilitating comparisons between different assays.

Gold pads serve as preliminary substrates that mimic the surface of sensors on the biochip. An important distinction is that gold pad assays provide qualitative results, presenting either a visual signal or none (Figure 3.12). However, with the use of image analysis software, it is possible to quantify the signal. This simplicity makes

these assays solely influenced on biological and chemical interactions, excluding issues related to the MR platform when desired results are not achieved.

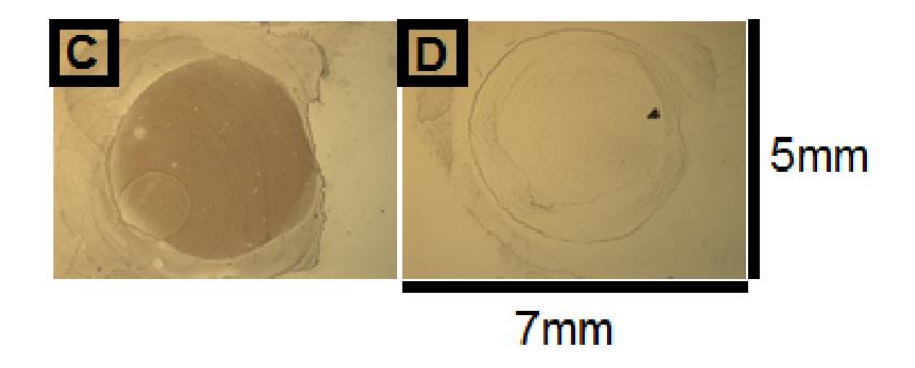


Figure 3.12 - Gold pads assays with signal (left) and without (right) (Ferreira Cardoso, 2015).

Ferreira Cardoso (2015), as the pioneering research in urease detection for use with the MR platform, focused primarily on gold pad assays. This research defined the key reagents for the experiments, including the crosslinker (Sulfo-LC-SPDP), which promotes a steadier bond on gold by the first layer of antibodies. Additionally, Bovine Serum Albumin (BSA) was selected as a blocking agent. Ferreira Cardoso (2015) research focused on competitive and sandwich immunoassays as potential detection strategies. The sandwich immunoassay was proven to be more effective and calibration curves were obtained as function of concentration of urease *C. ensiformis* (Jack bean) on gold pads assays.

Valentim (2016) conducted tests using both direct and sandwich immunoassays as detection strategies on gold pads and the dice biochips. The direct immunoassay method was implemented on the MR platform, successfully achieving a calibration curve within the range of 10 to 30 mg/mL of urease *C. ensiformis* (Jack bean) concentration.

Albuquerque (2017) compared direct and sandwich immunoassays as detection methods urease *C. ensiformis* (Jack bean). No visual difference was observed between the two methods. Although in the negative controls, where no urease was used, some particles were still observed to be attached to the surface, though the difference between the control and bioactive substrate was clearly notable. Finally, calibration curve for quantifying urease using the direct immunoassay method was established within the urease concentration range of 0.5 to 70 mg/mL (Figure 3.13). However, this approach is not ideal for complex samples, containing other proteins other than urease (e.g., fluid from soil samples) as it can lead to greater non-specific adsorption to the sensor surface, reducing the specific binding of urease and consequently increasing the possibility of false negatives. This assay protocol serves as a valuable starting point for defining the sandwich immunoassay protocol.

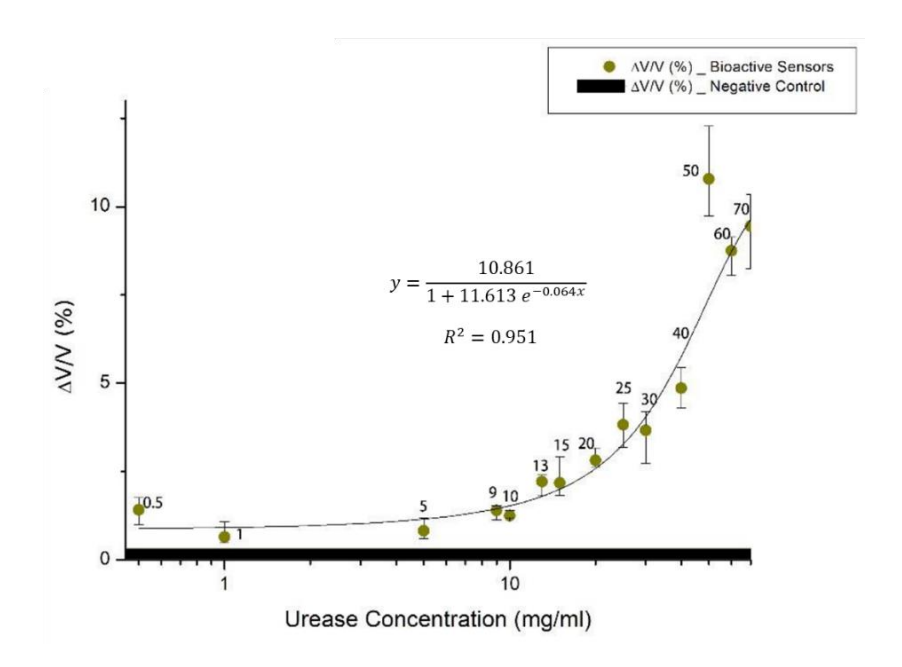


Figure 3.13 – Calibration curve for urease quantification using the MR platform and performing a direct immunoassay (Albuquerque, 2017).

In Albuquerque (2017) research, efforts were made to extract and isolate urease from *S. pasteurii* using complex microbiology techniques. A biosensor functionalized with *S. pasteurii* urease, employing the sandwich immunoassay detection method, was tested on the platform, but no signal was observed. Further experiments suggested that some sort of inhibition is occurring on urease that is caused by other protein present in the solution.

4 Materials and methods

4.1 Reagents

In this work all reagents used in the biochemical tests were of analytical grade and the water deionized. The buffers used were a phosphate buffer 0.1 M pH 7.4 (PB), and a phosphate buffer 0.1 M pH 7.4 Tween 20 0.02% (v/v) (PB Tween20). PB was prepared with Sodium Phosphate Dibasic at 0.07541 M and Sodium Phosphate Monobasic at 0.02459 M, being pH adjusted with Sodium hydroxide. PB Tween20 was prepared with Tween 20 at 0.02% (v/v) in PB 0.1 M pH 7.4 buffer.

Three types of antibodies were used for the immunoassays performed in this work. The first is Anti-*Canavalia ensiformis* urease rabbit polyclonal antibody biotin-conjugated from Rockland, which was prepared at 10, 20, 50 and 70 mg/mL in PB 0.1 M pH 7.4. This is the one that binds on the label, the magnetic nano particles (MNP).

The other two are called the capture antibodies and were used on the biochip and prepared at 50, 100 and 200 mg/mL in PB 0.1 M pH 7.4.

The anti-Canavalia ensiformis urease rabbit polyclonal antibody is specific to the antigen (urease), in this work it is called the positive antibody. The other, the anti-Escherichia coli antibody was used for control, as it is

non-specific to urease and is not supposed to detected urease. In this work it is called the negative antibody. Both are from Abcam.

The reagents used on the immunoassay were a crosslinker, a blocker and the analyte urease enzyme. They are: Sulfo-LC-SPDP (Sulfosuccinimidyl 6-(3'-[2 pyridyldithio]-propionamide) hexanoate) from ThermoFisher Scientific at 2 mg/mL, Bovine Serum Albumin (BSA) 5% (w/v) from fisher scientific at 50 mg/mL and enzyme *Canavalia ensiformis* (Jack bean) from Sigma-Aldrich at various concentrations between 0 and 40 mg/mL were prepared in PB 0.1 M pH 7.4, respectively.

The magnetic nanoparticles (MNP) were used as label in the assay. Nano meter sized superparamagnetic particles (250 nm, Nanomag-D) 75-80% (w/w) magnetite from Micromod were coated with dextran and streptavidin-modified, presenting about 1000 binding sites for biotin and a stock concentration of 10 mg/mL in PB Tween20.

On the biocement tests, the urease solutions were prepared in the same way as for the biosensor at 10, 20 and 30 mg/mL. It was used urease *C. ensiformis* (Jack bean) from Sigma-Aldrich (~ 1 U/mg) in PB 0.1 M pH 7.4 (PB), to keep the pH stable during the storage of collected samples overnight at - 4°C. The feeding solution was prepared using urea and calcium chloride (source of calcium) from PanReac AppliChem, each at 0.5 M in distilled water.

4.2 Equipment

A magnetic concentration is an equipment to preform magnetic separation, i.e. to resuspend the MNP in different solutions. The DynaMag-2 magnet from ThermoFisher Scientific was used in this work (Figure 3.14 (left)). The scheme on Figure 3.14 (right) explains its work principle: an Eppendorf is placed on the equipment, then the MNPs are concentrated on a side of the Eppendorf, the supernatant is with a pipette collected and discarded, and, finally, the MNPs are resuspended in the new solution.

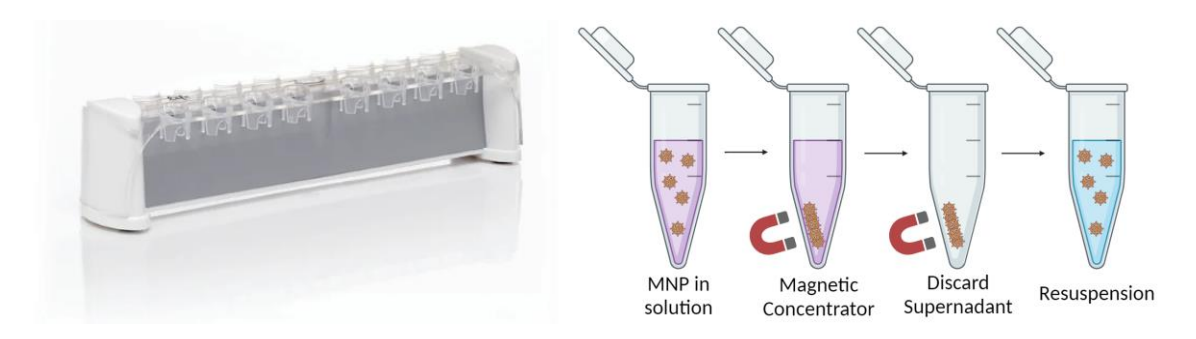


Figure 3.14 – (left) Magnetic concentration DynaMag-2 magnet from ThermoFisher Scientific and (right) magnetic separation process.

The pump used to insert the target solution on the microfluids was the NE-300 Just Infusion Syringe Pump (Figure 3.15). To clean the biochips was used the 144AX UVO cleaner from Jelight Company.



Figure 3.15 – NE-300 Just Infusion Syringe Pump.

4.3 Procedures

4.3.1 Biochip cleaning

The surface preparation of the biochip involves several steps, beginning with rinsing the chip using Isopropyl Alcohol (IPA), washing it with distilled water, and then drying with an air gun. This is followed by a 15-minute cycle in the UVO cleaner. The biosensors can be reuse, the main challenge is how to effectively remove the analytes from the biochip without damaging the spin-valves underneath the gold layers. If fewer than 5 sensors are damaged, the biochip is considered for reuse. In such cases, the surface preparation process includes rinsing the chip with Alconox detergent, then with IPA, followed by washing it with distilled water and air gun drying, and ends with a 35-minute cycle in the UVO cleaner.

4.3.2 Immunoassay procedure used for optimization

The main immunoassay procedure used for optimization in section 5 is explained here, the concentrations and amounts which were optimized are not explicit here.

The functionalization of biosensors process starts by covering all sensors of the biochip with 40 μ L of Sulfo-LC-SPDP (Figure 3.16 (a)). After 1 hour of incubation in a humid chamber at room temperature (RT), the substrates were washed with PB 0.1 M pH 7.4, to remove any unbound crosslinker molecules, and dried with an air gun. A volume of 1 μ L of capture antibody was spotted. To detect urease 15 of 30 sensors were spotted with anti-*C. ensiformis* urease rabbit polyclonal antibody and the other 15 sensors were spotted with anti-*E. coli* antibody as negative control (Figure 3.16 (b)). It is left to react for 1 hour in a humid chamber at RT and it is clean with PB 0.1 M pH 7.4. Finally, 40 μ L of BSA 5% (w/v) was spotted on the substrate and incubated at RT for 1 hour (Figure 3.16 (c)). After another cleaning step with PB 0.1 M pH 7.4, the biochip is functionalized and ready to be inserted on the MR platform (Figure 3.16 (d).

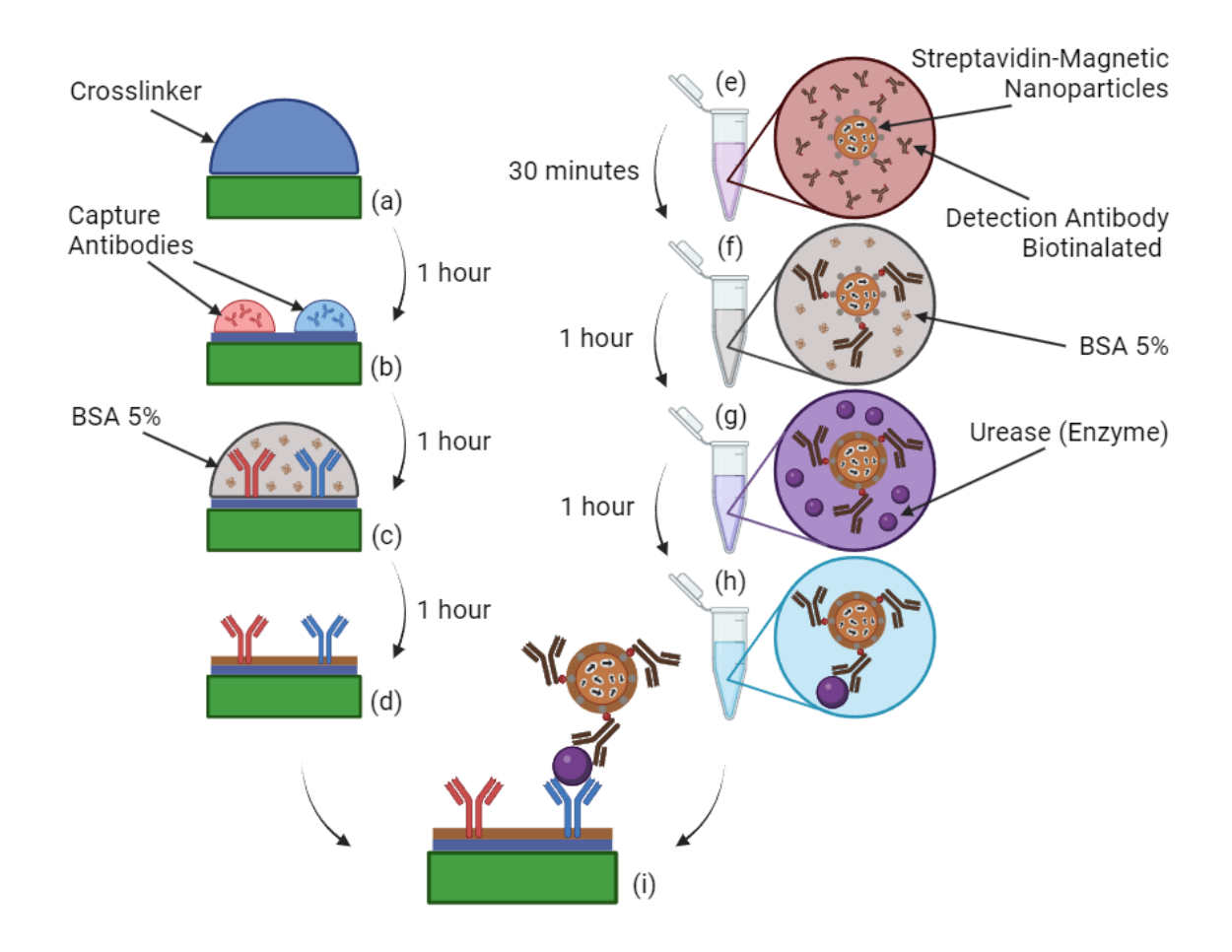


Figure 3.16 – Scheme of the immunoassay procedure.

In the meantime, the MNPs solution with the sample, or target solution, was prepared in an Eppendorf. The supernatant of 2 μ L of MNPs stock solution resuspended in 200 μ L of PB-Tween 20 was removed with the aid of a magnetic concentrator (DynaMag-2, Invitrogen). After, 50 μ L of anti-*C. ensiformis* urease rabbit polyclonal antibody biotin-conjugated solution in PB 0.1 M pH 7.4 was added (Figure 3.16 (e)). The solution is left to react for 30 minutes at RT. The supernatant of this solution was removed, resuspended in 50 μ L of PB Tween 20 and removed with the aid of a magnetic concentrator. The detention solution was resuspended in 50 μ L of BSA 5% (w/v) (Figure 3.16 (f)) and left to react for 1 hour at RT. After, the supernatant of this solution was removed, resuspended in 50 μ L of PB Tween 20 and removed with the aid of a magnetic concentrator. The detention solution was resuspended in 50 μ L of urease solution (Figure 3.16 (g)) and left to react for 1 hour at RT. Finally, the supernatant of this solution was removed, resuspended in 10 μ L of PB Tween 20 (Figure 3.16 (h)).

4.3.3 MR platform read out

After the functionalization, the biochip is inserted into the MR platform and the U-shaped microfluidic channel is placed on the biochip, which is responsible for transporting fluids over the sensing area of the chip

The MR platform is connected to a computer via a regular USB port and the *Biochip Platform Interface V3.2* software was used for data acquisition. Before starting the experiment, certain settings must be configured. Figure 3.17 shows the interface screen after the transfer curves of the biochip sensor have been read (Matrix

Transfer Curve). The observed transfer curve matches the expected pattern, indicating that the spin-valves under each gold rectangle were not damaged, and the readings for this sensor are reliable. The measurement conditions used were 1 mA DC for sensors biasing, an in-plane transverse external AC excitation magnetic field of 1.1 kA/m rms or 13.5 Oe rms (211 Hz), and a DC field of -3.2 kA/m or -40 Oe for MNP magnetization. The configured values can be observed in the top part the software displayed (Figure 3.17).

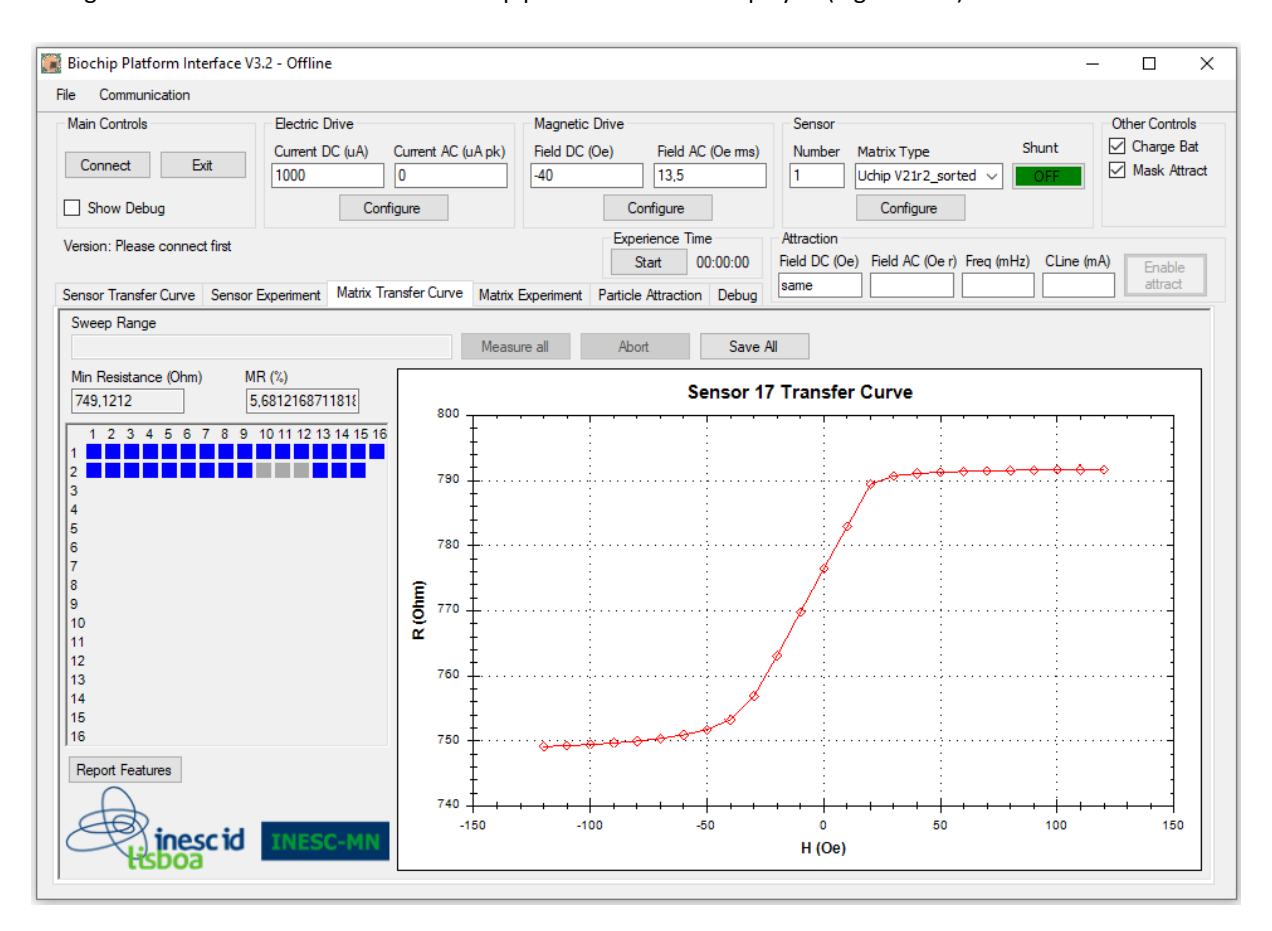


Figure 3.17 – *Biochip Platform Interface V3.2* showing graphical representation of the transfer curve corresponding to the 17th sensor of a biochip.

The experiment started by fill up the channel with PB 0.1M pH 7.4 at 50 μ L/min and check for any leakage of the channel. In the absence of leakage, the baseline of the sensors was acquired for 5 minutes (Figure 3.18 (baseline)). Then the target solution (MNPs solution) was pumped into the PDMS channel and left to settle down over the sensing area for 20 minutes (Figure 3.18 (saturation)). Finally, it was performed a washing step to remove the unbound MNPs and the binding signal was record for 5 minutes. This last step consisted of pumping PB 0.1M pH 7.4, starting with a velocity of 10 μ L/min until the channel was filled, and then the velocity was increased to 50 μ L/min (Figure 3.18 (binding)). Figure 3.19 presents a typical output, where it is identified the baseline signal and the binding signal. The signal is calculated according with Equation (3.2), where Signal % is the normalized signal detected of the sensor output, $V_{Baseline}$ is the baseline signal, $V_{Binding}$ is binding signal and ΔV is the difference between them, the voltage variation.

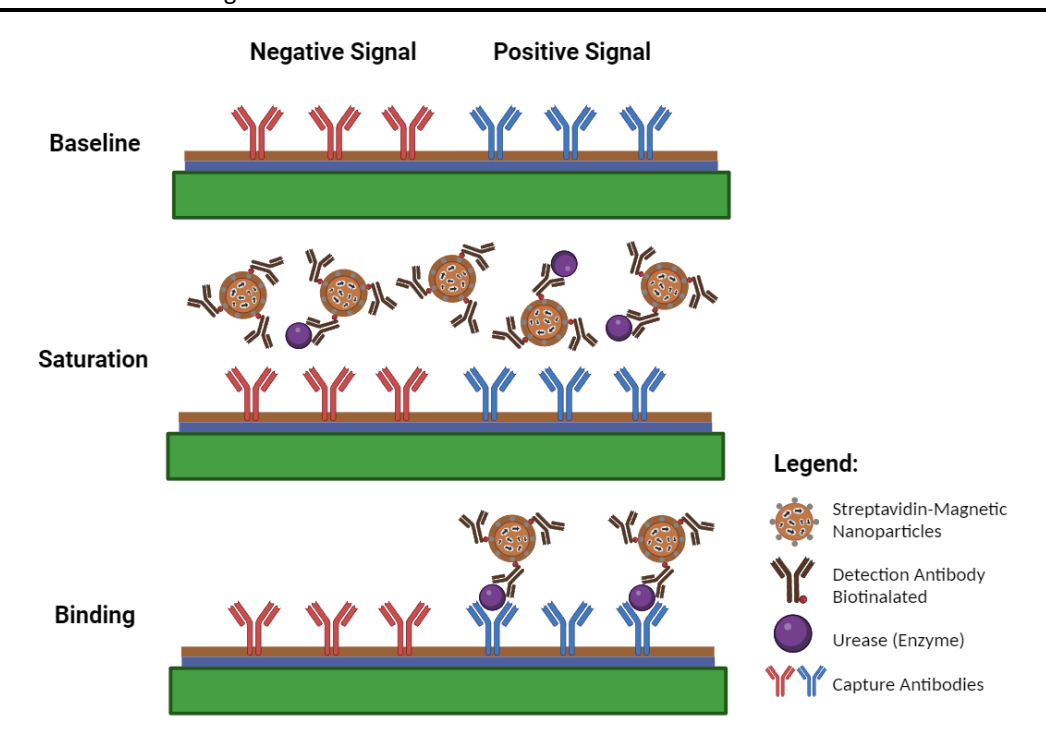


Figure 3.18 – Scheme of the measuring steps on the MR platform: baseline, saturation and binding.

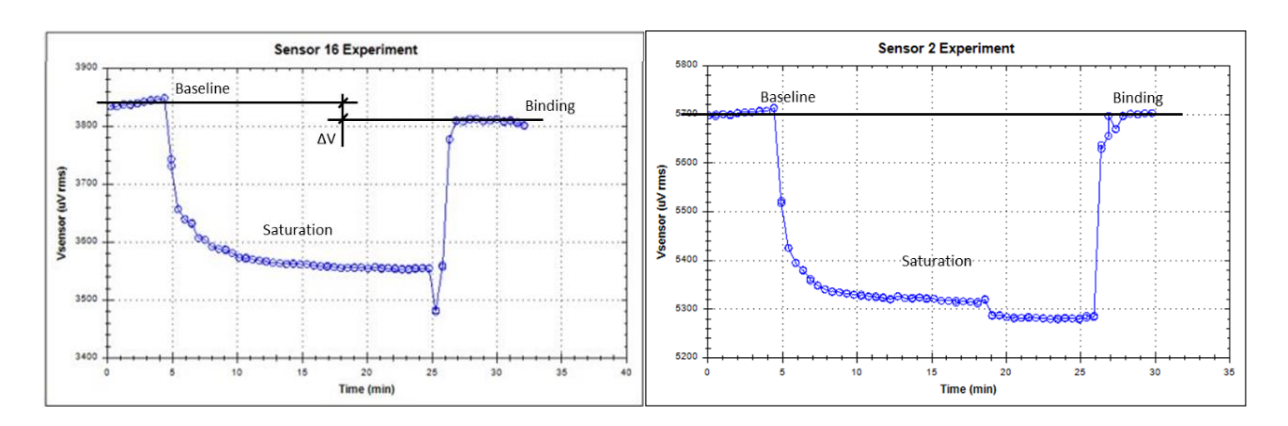


Figure 3.19 – *Biochip Platform Interface V3.2* plots outputted of a positive signal on the 16th sensor (left) and a negative signal on the 2nd sensor (right) of a biochip.

Signal % =
$$\frac{V_{Baseline} - V_{Binding}}{V_{Baseline}} \times 100 = \frac{\Delta V}{V} \times 100$$
 (3.2)

4.3.4 Calcium carbonate content

The calcium carbonate content (CCC) was determined using acid washing method adapted from Portuguese standard (NP-E196-1996, 1966). The dry mass of the sand sample was measured using an oven at 105° C for 24 hours before the test (m_1) and then the soil was placed in hydrochloric acid (HCl, 0.5 M) until the reaction was complete. Then it was washed with distilled water, filtered and dried again in an oven at 105° C for 24 hours to measure the final mass (m_2) The calcium carbonate content is the ratio between the dry mass lost after the test

(mass of biocement which is acid soluble) and the initial dry mass of the sample, calculated according to Equation (3.3).

$$CCC\% = \frac{m_1 - m_2}{m_1} \times 100 \tag{3.3}$$

5 Immunoassay optimization

5.1 Overview

To target and measure the signal of a specific analyte on the lab-on-a-chip (LoC), it is essential to optimize and define an immunoassay final protocol. This optimization process considers several key factors: (i) the range of operation; (ii) the biological and chemical cross-reactions; (iii) the portability, (iv) the easy to use for a non-expert user, (v) the presence of soil particles and (vi) the management of resources (economically).

Although there was an existing calibration curve for detecting urease enzyme from (Albuquerque et al., 2019), it proved to be unsuitable for the intended use of the biosensor as a monitoring tool due to certain unconsidered aspects, e.g., soil particles, the presence of other molecules apart from urease, and urease from other sources. Prior to the optimization process, preliminary tests were conducted, considering these factors. A sandwich assay protocol was designated as the initial basis for optimization.

To achieve the desired operational range, the concentration of the detection antibody was varied. Altering the capture antibody concentration served as a method to assess whether the assay was being executed optimally. Additionally, a new calibration curve was defined, capable of detecting urease at concentrations below 10 mg/mL. Finally, the biosensor protocol was tested in the presence of the feeding solution, which introduced some challenges.

5.2 Gold pads assays (preliminary tests)

The gold pads were used in a preliminary study to investigate several aspects of the assay, including the type of detection and the choice of blocking reagent. Both direct and sandwich assays, as well as capture and immobilization detection methods, were considered. The blocking reagents tested included a BSA 5% solution and *anti-E. coli* antibodies. Control tests without urease were conducted in parallel to validate the assay results. During the assay, a solution containing 10 mg/mL of urease was tested. The assays were performed with quadruple spotting and in duplicate to ensure the reliability of the results. Figure 3.20 illustrates a result with two visible spots representing a positive signal and no spots indicating a negative signal (control).



Figure 3.20 – Gold pad assay with a visible positive signal (the visivle two white circles on top) and no spots indicating a negative signal (the abstance of the two white circles on bottom).

This study distinguishes between two types of detection procedures based on the sequence of procedural steps using the same reagents and amounts. These methods can be simplified as capture and immobilization detection. In immobilization detection, the reagents are applied directly onto the gold pad surface sequentially, layer by layer. On the other hand, capture detection involves certain steps occurring in an Eppendorf tube. The capture detection method offers the advantage of time savings and is particularly suitable for assays involving analytes mixed with other entities, such as impurities.

Table 3.1 presents the assays performed and the results from the preliminary assays conducted on the gold pads. As expected, the direct assays with BSA 5% were successful, consistent with the findings of Albuquerque et al. (2019), validating these tests. The chosen protocol for optimization, already presented in section 4.3.2, was the sandwich assay with capture detection using BSA 5% as a blocking reagent. This protocol proved to be effective and is better suited for samples with impurities, such as those from soil, which may contain various molecules beyond just the urease enzyme.

		T	1
Assay	Detection	Bloking agent	Results
Direct	Immobilization	BSA 5%	Signal
Sandwich	Immobilization	BSA 5%	Signal
Direct	Capture	BSA 5%	Signal
Sandwich	Capture	BSA 5%	Signal
Sandwich	Immobilization	anti- <i>E. coli</i> antibody	No signal
Direct	Capture	anti- <i>E. coli</i> antibody	No signal
Sandwich	Capture	anti- <i>E. coli</i> antibody	Signal

Table 3.1 – Results of the gold pads tests.

5.3 Optimization process on MR-platform

5.3.1 Overview

The optimization process begins with the protocol adapted from Albuquerque et al. (2019) and described in section 4.3.2. Various optimization steps were subsequently tested and incorporated into the protocol's development. The Table 3.2 provides an overview of the key optimization steps to enhance the performance of the biosensor assay for detecting urease.

Table 2.2 Voy antimization	n ctanc an tha pracadur	a af tha biacancar acc	ay for dotacting urgaco
Table 3.2 – Key optimization	ii stebs oii the brocedur	e oi tile bloselisol ass	av for detecting drease.

Optimization Steps	Description		
Concentration of Detection Antibody	Varied to achieve the desired operational range.		
Capture Antibody Concentration	Altered to assess assay optimization in the economical aspect.		
Detecting Urease at Lower	Adjustments and variations made to develop a calibration curve		
Concentrations	capable of detecting urease below 10 mg/mL.		
Tosting with Fooding Solution	Biosensor protocol tested in the presence of the feeding solution,		
Testing with Feeding Solution	which introduced challenges during the testing process.		

5.3.2 Varying detection antibody concentration

The detection antibody concentration, specifically the *Anti-C. ensiformis* urease rabbit polyclonal antibody biotin-conjugated, was subjected to optimization. In this regard, concentrations of 10, 20, 50, and 70 μ g/mL were examined. The protocol that had been tested on the gold pads was then applied to the biosensor strategy using a detection antibody concentration of 10 μ g/mL. Figure 3.21 (a) presents the results obtained, which showed signal values in the zero range, indicating the need for optimization.

To enhance the sensitivity of detection, the concentration of the detection antibody was increased to 20 μ g/mL. Figure 3.21 (b) demonstrates that it became possible to detect urease concentrations between 30 and 40 mg/mL, which are concentrations outside the range considered in this work for EICP due to economic reasons. Therefore, the calibration curve defined still holds potential for improvement.

Further increasing the concentration to 50 μ g/mL, as shown in Figure 3.21 (c), revealed the capacity to detect urease within the 10 to 30 mg/mL range. These values align closer with those employed in biocementation tests, which are typically low around 3 mg/mL (Almajed et al., 2018; Rodríguez & Cardoso, 2022).

Finally, a concentration of 70 μ g/mL was tested to ascertain the feasibility of detecting urease below 10 mg/mL. Figure 3.21 (d) indicates that this concentration increment did not yield any advantage and showed signal values in the zero range.

Table 3.3 presents all results of the signal measures and the confidence interval at 95% on the MR platform for the calibration curves of the sensor varying the concentration of antibody (DAB).

Table 3.3 – Signal measures and the confidence interval at 95% on the MR platform for the calibration of the sensor varying the concentration of antibody (DAB).

Concentration	DAB 10 μg/mL		Pease DAB 10 μg/mL DAB 20 μg/mL		DAB 50 μg/mL		DAB 70 μg/mL	
(mg/mL)	Signal (%)	CI 95	Signal (%)	CI 95	Signal (%)	CI 95	Signal (%)	CI 95
0.0	0.43	±0.08	0.23	±0.06	-0.03	±0.05	-	-
1.0	-	-	-	-	-	-	0.55	±0.04
2.5	-	-	-	-	-	-	0.11	±0.08
3.0	-	-	-	-	-	-	1.56	±0.10
3.5	-	-	-	-	-	-	0.64	±0.04
5.0	0.62	±0.11	0.30	±0.06	-0.11	±0.03	-	-
6.0	-	-	-	ı	ı	ı	0.62	±0.05
10.0	0.45	±0.07	0.20	±0.04	0.12	±0.04	1	1
15.0			0.33	±0.05	0.78	±0.37	1	1
20.0	0.73	±0.11	80.0	±0.13	1.16	±0.16	-	-
25.0	0.37	±0.14	0.17	±0.05	1.70	±0.19	-	-
30.0	-	-	0.21	±0.07	3.76	±0.31	1	-
35.0	-	-	2.79	±0.09	-	-	-	1
40.0	-	-	4.74	±0.30	-	-	-	-

Average ± Confidence interval at 95%

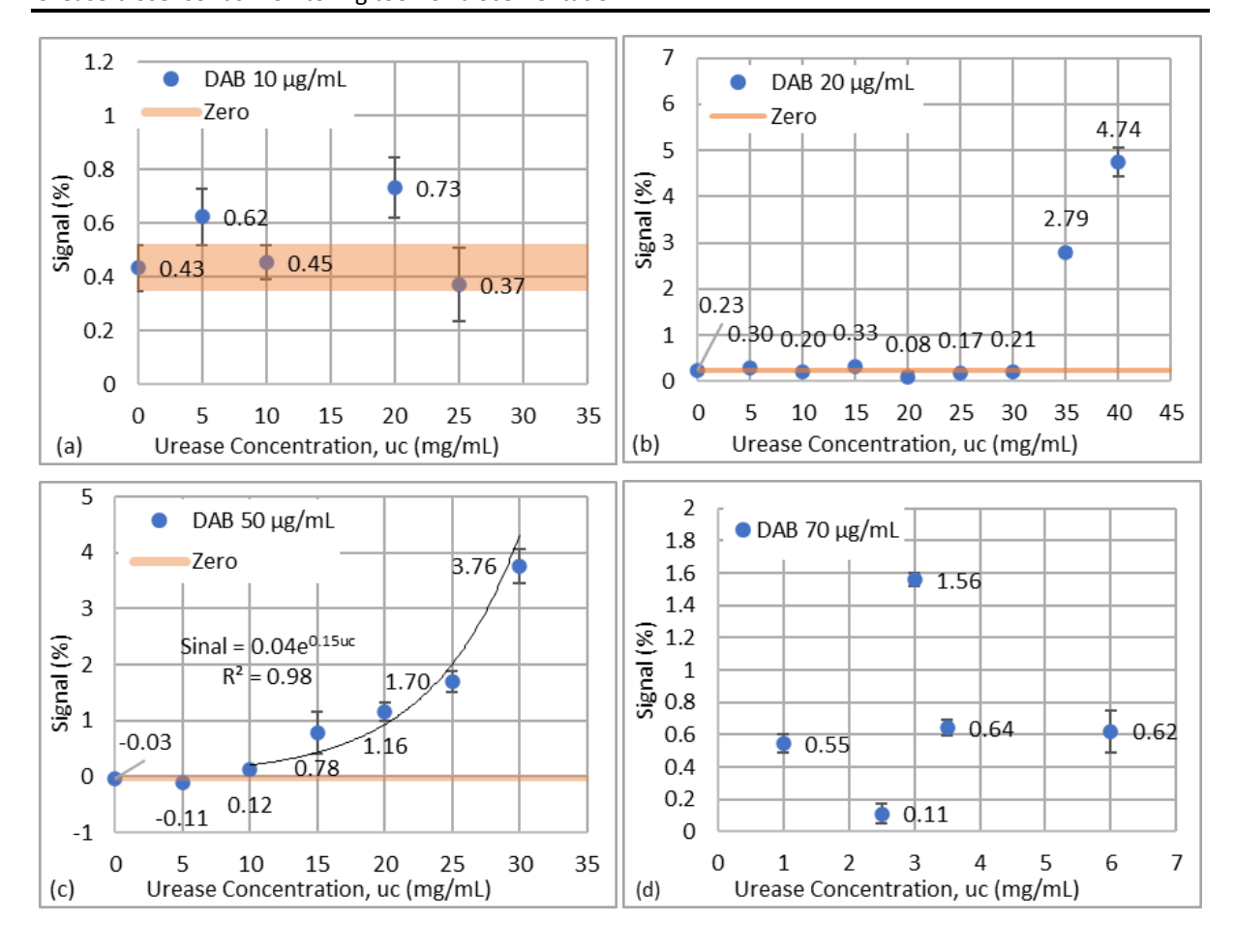


Figure 3.21 – Calibration curves of the sensor varying the concentration of antibody (DAB): (a) 10 μ g/mL; (b) 20 μ g/mL; (c) 50 μ g/mL and (d) 70 μ g/mL.

5.3.3 Varying capture antibody concentration

Concentration of the capture antibody (anti- $\it{C.ensiformis}$ urease rabbit polyclonal antibody and anti- $\it{E.coli}$ antibody) was varied to understated if it was possible to increase the signal or maintain the signal and reducing the cost per test by decreasing the capture antibody concentration. Both half and double the capture antibody concentration, 50 and 200 μ g/mL, were tested. The results of the signal and the confidence interval at 95% obtained with the capture antibody concentration of 50, 100, and 200 μ g/mL are showed in Figure 3.22. From the concentrations tested, it is possible to determine that 100 μ g/mL is the optimal concentration, as it presents the highest signal, so it was kept in the protocol.

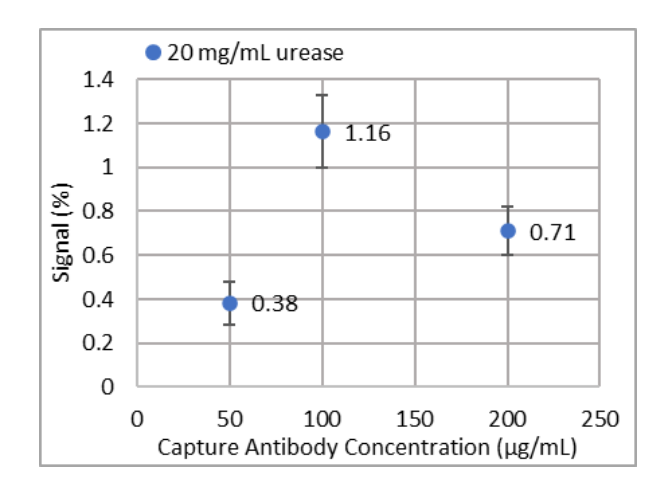


Figure 3.22 – Signal for 20 mg/mL of urease varying the capture antibody concentration.

5.3.4 Protocol for Detecting Urease at Lower Concentrations

Some variations in the protocol were tested to enable a sandwich immunoassay with capture detection to detect urease concentrations under 10 mg/mL. In this assay, the target solution was prepared using different volumes: 3 μ L of MNPs stock solution were resuspended in 300 μ L of PB Tween 20; 75 μ L of antibody biotin-conjugated and 75 μ L of BSA 5% (w/v) were used with 75 μ L of PB Tween 20 on the washing steps; and 100 μ L of analyte solution was added. Figure 3.23 presents the calibration curve, results of the signal and the confidence interval at 95% obtain in this change of protocol. In the future, the possibility of detecting at lower concentrations could make this monitoring tool more versatile.

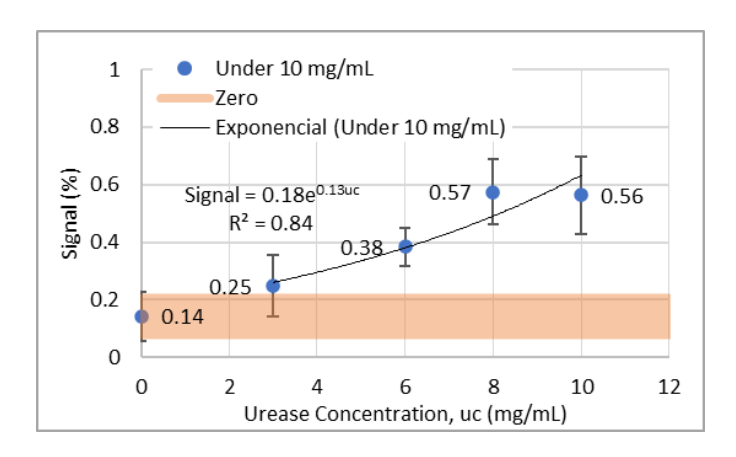


Figure 3.23 – Calibration curve to detect urease at lower concentrations between 3 and 10 mg/mL. Capture antibody at 100 μ g/mL (volume:1 μ L) and detection antibody at 50 μ g/mL (volume:75 μ L).

5.3.5 Feeding solution test

Some clusters were observed in the target solution when testing urease solutions in the feeding solution (urea and calcium chloride) instead of in PB 0.1 M pH 7.4. These clusters indicate the occurrence of undesired chemical cross-reactions with a component of the feeding solution. To identify the problematic reagent, immunoassays were conducted for each component of the feeding solution: CaCl₂ at 0.5 M in PB 0.1 M pH 7.4, urea at 0.5 M in

PB 0.1 M pH 7.4, and the distilled water used in the preparation of the feeding solution. Figure 3.24 illustrates the preparation of target solutions just before the supernatant of the sample solution was taken.

This examination revealed that calcium chloride was the source of the issue, because the clusters were only found on this sample. Indeed, a cross-reaction between PB 0.1 M pH 7.4 and the calcium from the feeding solution was identified. Equation (3.4) demonstrates the formation of calcium phosphate (Ca₃(PO₄)₂), which is insoluble in water (7.7 g/L of water according with PubChem). The Ca₃(PO₄)₂ particles interfere with MNPs, invalidating the performed assay.

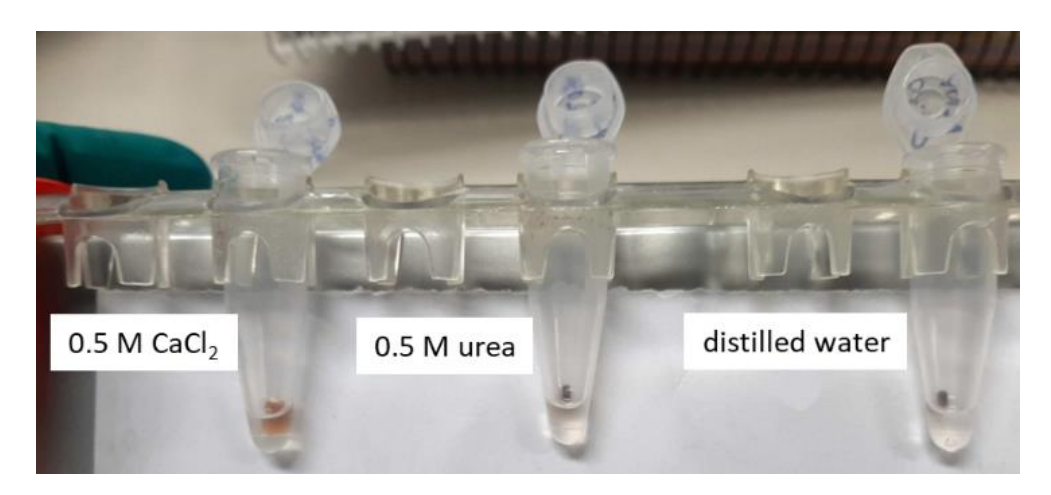


Figure 3.24 – Target solutions being prepared right before of taking the supernatant of sample solution step for the samples of the feeding solution components.

$$3CaCl_2 + 2Na_3Po_4 \rightarrow Ca_3(PO_4)_2 + 6NaCl$$
 (3.4)

Tris buffer 0.1 M pH 7.2 was tested as an alternative buffer solution to optimize a new calibration curve, however without success. In the presence of analytes without urease, the tris buffer resulted in an unusually high signal, indicating an unexpected interaction with other reagents. As a result, this buffer 0.1 M pH 7.2 is not a viable substitute for PB 0.1 M pH 7.4.

Opting for enzymes over bacteria was essential due to the need for pre-treatment in the case of bacteria. Although pre-treatment was attempted, it proved unsuccessful because the feeding solution was found to influence the results. Moreover, the more extensive preparation required for bacteria compromised portability, ultimately leading to the decision to discontinue further investigation in that direction.

5.4 Calibration curve and final procedure

After optimizing the immunoassays procedures, two protocols were selected, and two calibration curves were defined: curve CC10-30 and curve CCunder10. Table 3.4 presents the parameters of the calibration curves optimized.

Only CC10-30 was tested as a monitoring tool in this thesis because it detects the highest levels of enzyme. It was assumed that the amount of enzyme retained by the soil could be small, and therefore, the amount present in the outflow fluid was large.

Figure 3.25 illustrates the curves, where a function was fitted to the data presented in Figure 3.21 (c) (section 0) and from Figure 3.23 (section 5.3.4), left and right respectively.

Calibration curve name	CC10-30	CCunder10
Equation fitted	$S = 0.04e^{0.15uc}$	$S = 0.18e^{0.13uc}$
Coefficient of determination	$R^2 = 0.98$	$R^2 = 0.84$
Equation estimation of urease concentration	$uc = 6.51\ln(S) + 20.48$	$uc = 7.69 \ln(S) + 13.19$
Detention range	10 to 30 mg/mL	3 to 10 mg/mL
Blank measurement	- 0.03 ± 0.05 %	0.14 ± 0.04 %
Zero under	0.02 %	0.18 %

Table 3.4 – Parameter of the calibration curves: CC10-30 and CCunder10.

S – signal (%); uc – urease concentration (mg/mL)

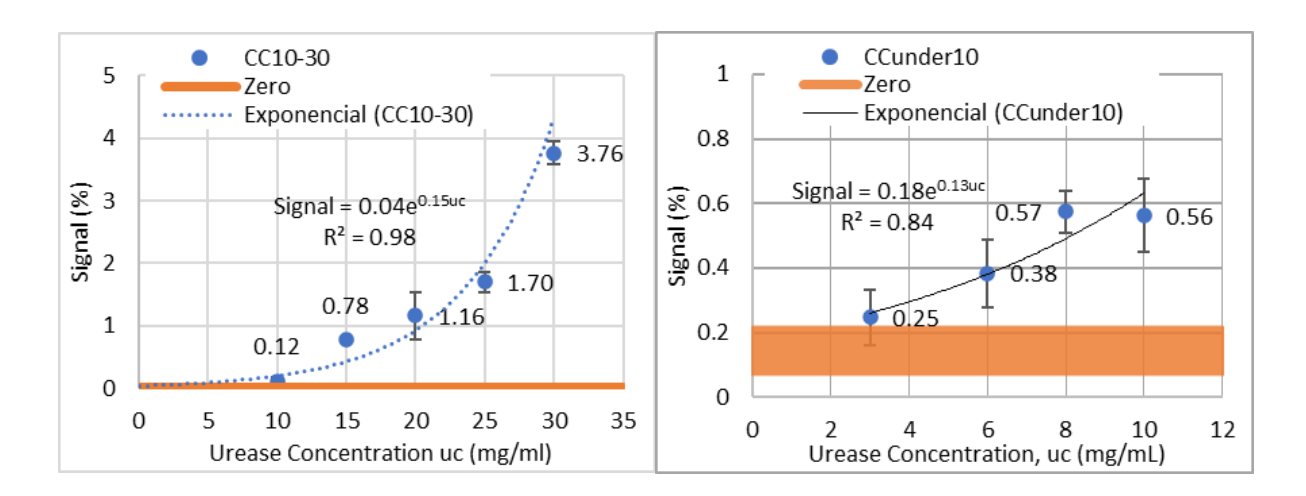


Figure 3.25 – Calibration curves of the sensor using the magnetoresistive platform: CC10-30 (left) and CCunder10 (right)

The final protocol corresponding to these calibration curves is presented here, specifically for the calibration curve CC10-30. The slight modifications for the calibration curve CCunder10 are included within parentheses.

Biochip preparation:

- 1. Cover all sensors with 40 μ L of sulfo-LC-SPDP linker at 2 mg/mL and incubate in a humid chamber at room temperature (RT) for 1 hour.
- 2. Wash the substrates with PB 0.1 M pH 7.4 and dry the biochip with an air gun.
- 3. Spot a group of 15 sensors with 1 μ L of antibody at 100 μ g/mL of anti-*C. ensiformis* urease rabbit polyclonal antibody (positive signal).

- 4. Spot the other group of 15 sensors with 1 μ L of antibody at 100 μ g/mL of anti-*E. coli* antibody as a control (negative signal).
- 5. Incubate in a humid chamber at room temperature (RT) for 1 hour.
- 6. Wash the biochip with PB 0.1 M pH 7.4.
- 7. Spot 40 μ L of BSA 5% (w/v) on the substrate and incubate in a humid chamber at RT for 1 hour.
- 8. Wash the biochip with PB 0.1 M pH 7.4.

Preparation of target solution with outflow sample:

- 1. Resuspend 2 μ L (3 μ L) of MNPs stock solution in 200 μ L (300 μ L) of PB-Tween 20 and remove the supernatant with a magnetic concentrator.
- 2. Add 50 μ L (75 μ L) of antibody solution at 50 μ g/mL in PB 0.1 M pH 7.4 and leave it to react for 30 minutes at RT.
- 3. Remove the supernatant, resuspend in 50 μ L (75 μ L) of PB Tween 20, and repeat the removal with the magnetic concentrator.
- Resuspend the MNPs solution in 50 μL (75 μL) of BSA 5% (w/v) and leave it to react for 1 hour at RT.
- 5. Remove the supernatant, resuspend in 50 μ L (75 μ L) of PB Tween 20, and repeat the removal with the magnetic concentrator.
- 6. Resuspend the MNPs solution in 50 μ L (100 μ L) of the outflow sample filtered on a #0.2 μ m filter and leave it to react for 1 hour at RT.
- 7. Remove the supernatant and resuspend in 10 μ L of PB Tween 20.

On the MR-platform:

- 1. Insert the biochip into the platform.
- 2. Place the U-shaped microfluidic channel on the biochip, responsible for fluid transport.
- 3. Fill the channel with PB 0.1M pH 7.4 at 50 μ L/min to check for leaks.
- 4. If no leaks are observed, acquire a baseline of the sensors for 5 minutes.
- 5. Pump the target solution into the U-channel and let it settle over the sensing area for 20 minutes.
- 6. Perform a washing step to remove unbound MNPs, pumping PB 0.1M pH 7.4 at 10 μ L/min initially and then increasing the velocity to 50 μ L/min when the channel is filled with PB 0.1M pH 7.4.
- 7. Record the binding signal for 5 minutes.
- 8. Analyse the output signal calculating the normalized signal detected.

6 Using the biosensor as monitoring tool

6.1 Overview

The main goal of the biosensor is to be use as a monitoring tool in biocementation works by finding relations between the measurement of urease outflow and the biocement treatment. On this part of the work, the immunoassay optimized for the calibration curve CC10-30 was tested on samples collected from the soil outflow.

The data presented has already been published in the paper by Borges et al. (2023), presented in the 8th International Symposium on Deformation Characteristics of Geomaterials (IS-PORTO 2023).

6.2 Methods used for preparing and testing soil samples

The soil tested is a silty sand (APAS 30) with uniform grading size distribution (D_{50} =0.3mm, C_c =0.94, C_u =3 .18 and G_s = 2.70). The samples were prepared with the final dry volumetric weight of 15 kN/m³, which corresponds to void ratio of 0.78. The set-up used consists of a cylindrical plastic mould (Figure 3.26), with 2.5 cm diameter and 2.0 cm height, over a plastic grid with 5 mm of height and filter paper, to allow the drainage of the treatment fluids and prevent particles from dragging throw the specimen bottom, respectively. The sample volume was 8.8 cm³ and a void volume of V_v =4.3 cm³. The solutions were irrigated in the soil on the top of the sample (inflow), using a pipette to distribute drops homogeneously in the entire area and left on the top of the sample infiltrating just by gravity.

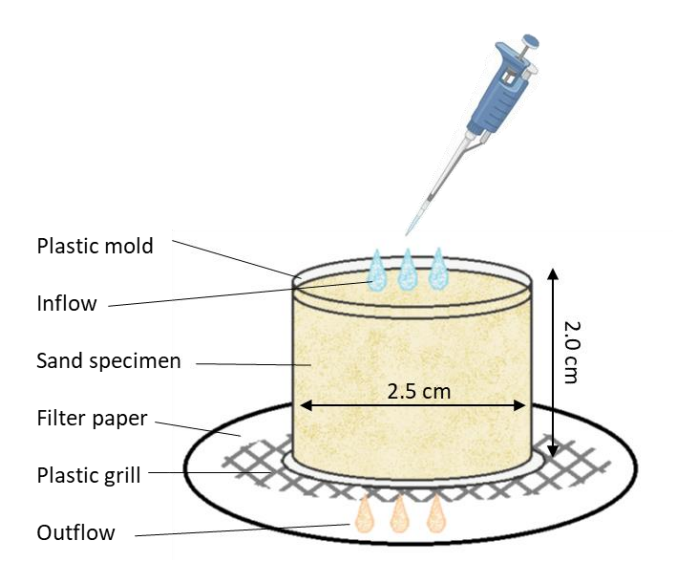


Figure 3.26 – Set-up to prepare biocemented treated soil samples.

The total volumes used were multiples of the void volume (V_v). The specimens were saturated with distilled water, then they were injected with 1 V_v of US and 4 V_v of FS, they were left overnight at room temperature, and then they were washed with 2 V_v of distilled water from the top of the specimen. In total, 9 samples were prepared and saturated with different fluids: 1 with distilled water (dH2O), 2 with feeding solution and no urease (USOFS), 2 with urease solution at 10 mg/mL (US10FS), 2 with urease solution at 20 mg/mL (US20FS) and 2 with urease solution at 30 mg/mL (US30FS). Table 2.3 presents the biocementation treatment protocols on sand samples and tests performed.

Table 3.5 – Biocementation treatment protocols on sand samples and tests performed.

Sample	Bioce	ementation treatmen	t protocol	Tests pe	rformed
		Urease	Feeding solution	Urease measure	ссс
dH2O (1)	1V _√ (4.3 mL)	-	-	-	1 per sample
US0FS (2)	1V _v (4.3 mL)	-	4V _v (17.2 mL)	-	1 per sample
US10FS (2)	1V _v (4.3 mL)	$1V_v$ at 10 mg/mL (4.3 mL)	4V _v (17.2 mL)	2 per sample	1 per sample
US20FS (2)	1V _v (4.3 mL)	$1V_v$ at 20 mg/mL (4.3 mL)	4V _v (17.2 mL)	2 per sample	1 per sample
US30FS (2)	1V _v (4.3 mL)	$1V_v$ at 30 mg/mL (4.3 mL)	4V _v (17.2 mL)	2 per sample	1 per sample

The collection of liquid samples (outflow or analyte) after passing through the soil to measure the urease concentration was made at the bottom of the samples in the space left by the grid. The collection was done with the intention to collect only US after passing through the soil, so the collection was made after the injection of the US and before that of FS. To avoid cross-contamination the grid was cleaned before the collection. The collection of the outflow in the bottom was made right after adding some drops of FS on the top of the soil. These outflow samples were kept at 4 °C overnight and filtered using a $\#0.2~\mu m$ filter before being used in the immunoassay. In total were performed four measurements per type of sample, two on each sample. This number of measurements is to consider an outlier or a measurement issue, in such hight sensitive assay is common.

6.3 Results

When analysing the outflow from the soil samples using the biosensor protocol, no cross-reaction was observed between the outflow and the immunoassay reagents. Given the sensitivity of this assay, which involves biological components and nanoparticles and was conducted with non-autoclaved sand samples, the likelihood of cross-reaction was significant. Figure 3.27 illustrates the relationship between the urease concentration in the inflow and the urease concentration in the outflow, as measured by the biosensor protocol and the proposed calibration curve. The dashed line represents an impossible scenario where the outflow's urease concentration is higher than that of the inflow. Interestingly, sample US10FS displayed a signal below the established zero point, which was considered as undetectable.

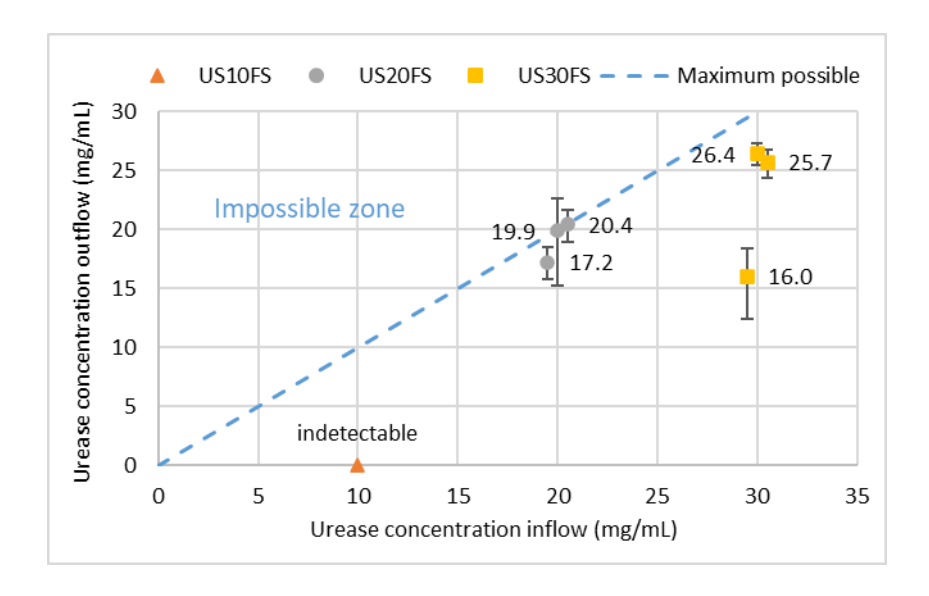


Figure 3.27 – Relationship between the urease concentration in the inflow and the urease concentration in the outflow.

Figure 3.28 illustrates the calcium carbonate content across all nine soil specimens treated using the EIPC technique. The blue dashed line represents the calcium carbonate level in the dH2O sample, establishing a reference for the treated samples. The results show that all treated samples exhibit higher calcium carbonate content, indicating biocement formation. Even in the sample treated solely with the feeding solution (USOFS), biocement is present, attributed to indigenous bacteria in the non-sterilized soil. Notably, no clear correlation between the quantity of added enzyme and the amount of calcium carbonate precipitated is evident.

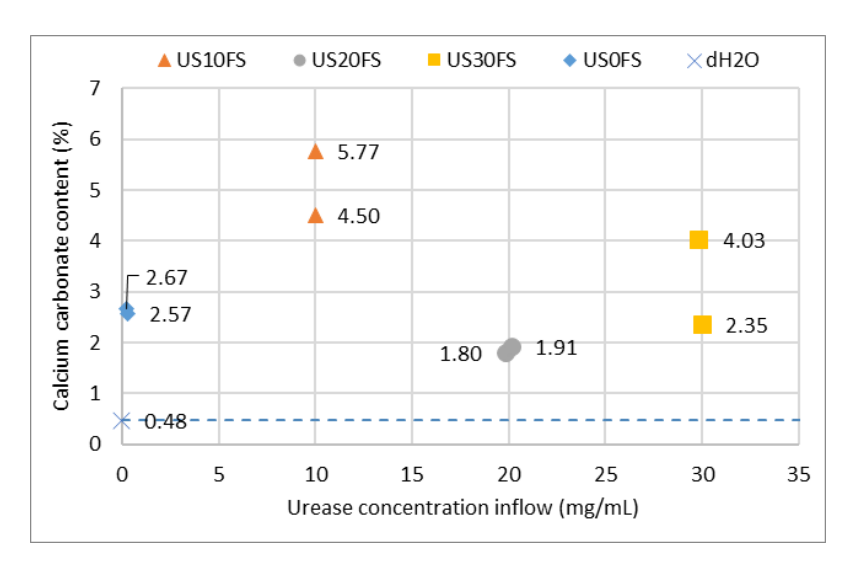


Figure 3.28 – Calcium carbonate content vs urease concentration of the inflow.

6.4 Discussion

The biosensor measured the urease concentration of the outflow solution (uc_{outflow}), indicating the quantity not retained by the soil. By comparing this with the known urease concentration of urease solutions prepared

(uc_{inflow}) added to the soil specimens, it is possible to calculate the amount left inside the specimen (uc_{inside}) using Equation (3.5).

$$uc_{inside} = uc_{inflow} - uc_{outflow}$$
 (3.5)

The data from calcium content tests performed on soil samples and urease concentration measurements obtained from the biosensor the measurements from the biosensor (considering the urease concentration fixed by the soil, i.e., urease inside the soil, computed using Equation (3.5)) are in Table 3.6. The results for the soil samples to which enzyme was added are plotted in Figure 3.29, revealing a notable correlation between the enzyme amount fixed by the soil and the e amount of calcium carbonate precipitated.

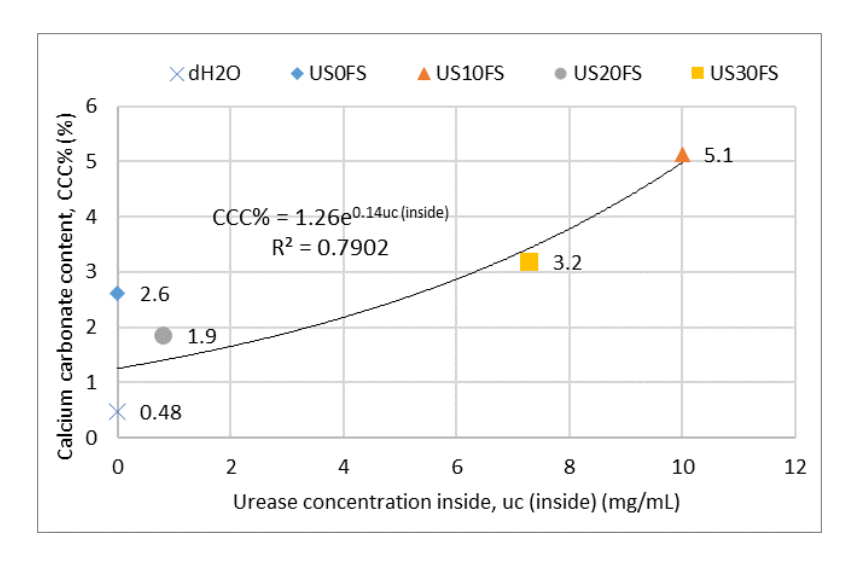


Figure 3.29 – Calcium carbonate content plotted vs urease concentration fixed by the soil (inside the soil).

Table 3.6 – Calcium carbonate content and urease concentration inside the sand samples.

	Calcium carbonate content (%)	Urease concentration inside (mg/mL)
dH2O	0.5*	not measured
USOFS	2.7 2.6 2.6 *	not measured
US10FS	5.8 4.5	10
	5.1*	10.0*
US20FS	1.8 1.9	2.8 0.1 0.0
	1.9*	0.8*
US30FS	4 2.4	14 3.6 4.3
	3.2*	7.3*

^{*}Average

As Figure 3.29 illustrates, there is a clear increase in calcium carbonate content as the urease concentration fixed inside the specimen increases, and this relationship can be adjusted with an exponential function (Equation (3.6)). Although there is some error, this correlation is better than the one found when the urease added was considered (Figure 3.28). The reason for this improvement is that only the urease inside the soil can contribute to calcium carbonate produced inside of it. Consequently, Equation (3.6) which relies on the urease concentration inside the sample in mg/mL (ucinside) determined by the biosensor, can effectively estimate the calcium carbonate content (CCC) in percentage.

$$CCC (\%) = 1.26 e^{0.14 \, u_{Cinside}} \, (mg/mL)$$
 (3.6)

Although this equation is specific to this work, a new curve can be easily fitted using data from different soils or treatment protocols with the calibration curve defined for the biosensor. This strategy of monitoring can be initially developed in the laboratory and later applied *in situ* as a non-destructive test. However, considering the smaller sample size required for the biosensor, it is essential to establish sampling protocols that ensure the samples collected are representative of the larger volumes of treated soil.

7 Costs analysis

Considering the procedure used on calibration curve CC10-30 on this cost analysis, it was assumed that the following reagents, including anti-*C. ensiformis* urease rabbit polyclonal antibody biotin-conjugated, anti-*C. ensiformis* urease rabbit polyclonal antibody, anti-*E. coli* antibody, Sulfo-LC-SPDP linker, Bovine Serum Albumin, and magnetic nanoparticles, were considered for cost assessment. The costs of PB 0.1 M pH 7.4, PB Tween20, isopropanol, Alcanox, and distilled water were not considered, as these reagent costs are negligible. The reagent prices considered have accounted for taxes and shipping to INESC MN in Lisbon, Portugal, in October 2023, from the brands and sellers presented in Table 3.7.

It was assumed that six measurements were made per day, considering an 8-hour workday. However, it is important to note that the workforce required to perform the assay is not included in this cost analysis. This assumption was made because some solutions need to be freshly prepared daily in larger quantities than necessary for the number of assays, resulting in waste, which is counted in this cost analysis. Larger quantities of solutions are necessary due to the small quantities that must be weighed and pipetted.

Additionally, in the cost calculations, for the materials one silicon wafer was considered, which corresponds to 300 PCBs with a biochip packed in each, all produced in INESC MN. It was also assumed that each of these biochips was used four times. Any other materials' costs, such pipette tips, Eppendorf tubes and paper towels, were considered negligible. All the equipment used in the assay was considered rent-free without any cost associated with maintenance, including the magnetic concentration, the syringe pump, the UVO cleaner and the MR-platform.

Table 3.7 presents the costs for each reagent and material considered with all the assumptions described and the total cost of 28.11 €/assay for six measurements made per day was estomated.

Table 3.7 – Costs analysis for the optimized sandwich immunoassay to detect urease.

	Name	Brand (Seller)	Price	Price/assay (6 assays/day)
	Anti-C. ensiformis urease rabbit polyclonal antibody biotin-conjugated	Rockland (Provided by Tebubio)	18.26 €/assay	18.26 €
Reagents	Anti- <i>C. ensiformis</i> urease rabbit polyclonal antibody	Abcam (Provided by Abcam)	0.11 €/assay	0.11€
	Anti- <i>E. coli</i> antibody	Abcam (Provided by Abcam)	0.12 €/assay	0.12€
	Sulfo-LC-SPDP linker	ThermoFisher Scientific (Provided by Alfagene)	39.06 €/day (25 assays/day max.)	6.51€
	Bovine Serum Albumin	Fisher scientific (Provided by Quimigen)	0.52 €/day (11 assays/day max.)	0.09€
	Magnetic nanoparticles	Micromod (Provided by Micormod)	0.36 €/assay	0.36€
	Total price	of reagents	18.85 €/assay 39.58 €/day	25.44 €
Materials	Biochip on PCB Produced in (Used 4x) INESC MN		10.67 €/unit 2.67 €/assay	2.67€
	(0000 1.7)		Total:	28.11 €

These costs can decrease with scale-up, as reagents and materials become more cost-effective in bulk purchases. The immunoassay's cost-efficiency will improve as production scales up, especially when LoC achieves full autonomy.

8 Discussion

The main limitations of this monitoring tool are due to several factors, including (i) the impurities on the collected samples, (ii) the significant disparity in scale between the small size of the liquid samples collected for the biosensor (in the order of microliters) and the large scale of the *in situ* ground treatment (in the order of cubic meters) and (iii) the heterogeneity of the treatment.

In the future, the biosensor aims to become a versatile monitoring tool for biocementation treatment, detecting various enzyme sources, including from bacteria or purified urease. It will work without restrictions related to the ions and components present in the feeding solution, which, in the case of bacteria, besides urea and calcium chloride ($CaCl_2$), includes ammonium chloride (NH_4Cl), sodium bicarbonate ($NaHCO_3$), yeast extract and ammonium sulphate (NH_4). Even when this operating with these impurities and variables, it should be tested case by case sample without urease to understand if there are any cross-reaction with a soil's components.

The components of the pore solution in the soils depends on soil minerals and on ecosystem which habitats the soil. Then the biosensor will detect and quantify urease without limitations.

Once this goal is achieved, a sample collection campaign representative of all treated soil can be made. A minimum of four measurements is proposed in each collection area, as was carried out in this work, to account for the disparity in scale volumes.

The selection of collection areas should be made on the designed project, it can vary based on predefined grids, injector positions, other monitoring tools, or soil characterization conducted before treatment. Conducting a collection campaign using a uniform grid is the simplest approach, but it does not consider the heterogeneity of both the biocementation treatment and the soil.

Biocementation treatments are applied to soil through various methods, with injector-based applications being one of the most common. Injectors deliver the treatment solution in a bulbous shape. In this application method, a higher concentration of urease is typically found closer to the injectors. Mapping the collection areas based on the positions of the injections provides valuable insights into the distribution of urease among different injectors. This information contributes to the optimization of injector positions by allowing adjustments or modifications such as repositioning injectors or adding/reducing them as needed.

The most valuable monitoring strategy involves the combination of multiple monitoring tools. Selecting collection areas based on the results of different tests enhances the quality of information. For instance, coupling geoelectrical resistivity testing, as shown in Figure 3.4 (section 2), can help define collection areas based on the measured electrical resistivity range, which is related to fluid dissipation. This integrated approach provides a more comprehensive understanding of the biocementation treatment.

To consider the heterogeneity of the soil is advised to use the initial characterization of the soil to map the collection areas, for example void ratio, grading size distribution and hydraulic permeability affects the fluid dissipation. This mapping approach allows for the pre-design phase mapping of collection areas, exclusively based on information from the untreated ground. This can offer a significant advantage.

9 Final considerations

9.1 Conclusion

In this chapter, a biosensor was optimized and then it was used as a monitoring tool for biocementation technique in a small soil sample treated by EICP.

Concerning the biosensor, the protocol to detect purified urease from *Canavalia ensiformis* was optimized, using a magnetoresistive platform to perform sandwich immunoassay, the one more adequate for samples collect on soil. The curves were named CC10-30 and CCunder10. The calibration curve CC10-30 is described by the equation $uc = 6.51 \ln(S) + 20.48$, where $R^2 = 0.98$. This equation is valid within the range of 10 to 30 mg/mL of urease, with a zero value of 0.02%. The calibration curve CCunder10 is described by the equation $uc = 7.69 \ln(S) + 10.000$

13.19, where $R^2 = 0.84$. This equation is valid within the range of 3 to 10 mg/mL of urease, with a zero value of 0.18%. The limitations with bacteria and feeding solution were reported.

Sand samples were treated with the EICP technique and the outflow fluids were collected to detect urease using the biosensor. The calcium carbonate content of all the biocemented sand specimens were also measured. Using the data from the sensor it was possible to estimate the urease concentration fixed inside the sample, i.e., the urease that was not washed when the feeding solution was added. Data found allowed to understand that the amount of enzyme fixed was smaller than that added to the soil, which suggests the need to investigate ways to fix the enzyme and improve the efficiency of the treatment. The information about the amount of enzyme fixed in the soil was related with that measured in the soil samples to define a relationship between the urease concentration inside the sample and the calcium carbonate content precipitated. This relationship can be used in the future to predict the amount of biocement in a sand sample treated with the EICP technique in similar conditions. Relationship such as the one found can be determined in the laboratory for other types of soils or treatment protocols using the same biosensor protocol and its calibration curve.

The biosensor optimized has strong potential to be used as a monitoring tool during the biocementation treatment, which will allow to estimate the effects of the treatment and therefore help designing biocementation treatment for different engineering geotechnical solutions.

9.2 Future studies

This study developed the research of the biosensor to detected urease enzyme. However, for optimization, it is suggested to: (i) investigate different ranges, e.g., below 3 mg/mL of urease; (ii) optimise the calibration curve CCunder10 for a higher R² value, (iii) explore a different buffer which is compatible with feeding solution components and immunoassay reagents and (iv) investigate methods for detecting urease from bacteria.

Regarding the investigation on soil samples, this analysis sets the stage for numerous additional experiments that can be conducted. It is suggested to: (i) investigate different soils; (ii) explore other treatment protocols, e.g., different quantities of solutions and urease concentrations; (iii) correlate the detected urease with other soil parameters, such as mechanical and hydraulic properties achieved with biocementation; and (iv) investigate outflows containing urease from bacteria or feeding solution, provided they are not limitations for the biosensor.

Chapter 4

Biocementation chamber and hydro-mechanical characterization of EICP treated samples

1 General overview

The development of a new chamber to apply biocementation treatment in soil samples, inspired in an infiltration column, is detailed in this chapter. Small cylindrical sand samples were treated with enzyme induced calcite precipitation (EICP) to achieve a homogeneous distribution of biocement. This chamber allowed permeability measurements after treatment, besides the extraction of intact specimens to be mounted in a triaxial chamber for strength measurement. Complementary oedometer tests were conducted on biocemented samples to fully assess the hydro-mechanical behaviour of the biocemented treated samples.

Section 2 starts with a literature review focusing on the existing procedures for preparing standard cylindrical biocemented samples. Subsequently, it explores into the challenge of achieving a homogeneous distribution of biocement across two topics: characterizing heterogeneity and attaining homogeneity. Finally, a detailed analysis of the research group's biocementation chamber is presented, highlighting the need for improvements.

Section 3 provides a literature review on the effects of biocementation on the hydro-mechanical behaviour of soils. It summarizes the main experimental results regarding unconfined compression strength, permeability, and resistance against liquefaction, while exploring the definition of shear strength and compressibility parameters.

Section 4 presents the characterization of the soil used to prepare all samples tested in this chapter, reagents and solutions, and main procedures to prepare sand samples.

Section 5 focuses on the newly designed biocementation chamber. It details the set-up developed and the improvements compared to the previous version, the procedure for preparing sand samples directly in the chamber, the treatment protocols applied using the set-up aiming to achieve homogeneity, and the innovative method for assembling biocemented samples on the triaxial equipment.

Section 6 presents the testing procedures conducted on biocemented samples. It begins with a summary of the protocols subjected to triaxial tests, oedometer tests, permeability tests, determination of calcium carbonate content and SEM observation. Following this overview, each test procedure is detailed in depth.

Section 7 analyses the results of calcium carbonate content determination and SEM observation. These tests were specifically chosen to investigate the distribution of biocementation in the sample, examining the top, middle, and bottom sections of the sample, by this manner confirming the homogeneity.

Section 8 presents the results of the triaxial tests, oedometer tests, and permeability tests, providing the hydromechanical characterization of the biocemented sand.

Section 9 provides a discussion relating the results found in different tests, comparing them with the literature results and proposing a hypothesis to justify the achieved results.

Section 10 presents the final considerations, where the main outputs from the chapter are highlighted and future studies are suggested.

2 Sample preparation for laboratory tests

2.1 Cylindrical standard samples preparation

Various procedures for the preparation of samples with a uniform distribution of biocement in volume have been explored in the existing literature. The most usual way to treat soils through biocementation to prepare samples for laboratorial testing is by using infiltration columns (Cheng & Cord-Ruwisch, 2012; Safdar et al., 2022; Yin et al., 2021).

One common method involves using a plastic or a metallic mould placed on a levelled and rigid surface (Cheng et al., 2013). To allow an easy extraction of the sample it is common to pre-cut the mould laterally. The specimen is then prepared and treated directly inside the mould, which have the advantage of simplicity in terms of materials and methods. The challenge lies in demoulding an intact cylindrical specimen, and the literature reveals two typical approaches to this obstacle: choosing a soil with some fine material or achieving a high level of biocementation.

The fact that sandy soils are the elected for this treatment make the extraction more difficult, even those containing fine material, especially when the percentage of biocement is not large enough to provide enough strength (cohesion). Opting for a soil with some fine material, which can maintain its shape without additional treatment, guarantees that the outcome can sustain its shape regardless of the level of biocementation achieved (Rezende et al., 2022).

An usual alternative is to achieve a high level of biocementation (Terzis & Laloui, 2019a). However, this method presents several disadvantages. The entire volume of the samples must reach a high level of biocementation, which is challenging due to the difficulty of achieving homogeneity. There is the risk of introduce perturbations during demoulding, even breaking the sample, and this approach does not permit the study of low levels of biocementation.

Several authors are conducting triaxial tests on samples cored from a larger volume where biocement techniques were applied (Wu et al., 2021). Typically, this involves a box containing the treated soil (Filet et al., 2012; van Paassen et al., 2009). However, this method of sample preparation has shown several disadvantages, including the requirement for larger quantities of soil and reagents. Additionally, coring is only feasible in highly biocemented samples, making it impossible to study lightly biocemented samples, because core extraction leads to disaggregation. Coring without breaking the sample can also be a challenging aspect of this approach. Despite these difficulties, it is advantageous for studying the volumetric aspects of the treatment, such as homogeneity.

Freezing samples is an option used to study saturated granular soils, which can be applied in biocemented soil. This technique requires technical expertise, and freezing can potentially damage some biocement. After the treatment, the samples are frozen in the rigid cylindrical moulds in order to facilitate easy installation onto the triaxial apparatus (Gao et al., 2019).

Several authors have used the triaxial chamber as a biocementation chamber. Initially, an untreated sample is prepared using the two-part split former with a vacuum attachment process. Following this, confining stress is applied, and finally, the biocementation treatment is carried out using tubes and taps connected to the interior of the sample (Cabalar et al., 2018; Feng & Montoya, 2017; Lin et al., 2016). The main disadvantage is that the triaxial equipment can be damaged by chemical attack or become clogged by biocement, and it is an expensive piece of equipment.

2.2 Characterization of samples homogeneity

The procedures for specimen preparation aim to create biocemented specimens with standard dimensions. The main challenge lies on ensuring uniformity in the special distribution of calcite. Addressing this challenge requires studying the heterogeneity of calcium carbonate precipitation.

Considering large treated volumes in field-scale tests, the heterogeneity can be studied unidimensionally in depth (Xiao et al., 2023) or spatially in the three dimensions (van Paassen et al., 2009). Van Paassen et al. (2009) applied biocementation treatment to a sand within a large-scale sand box (100 m³) over a 5 m distance using injection and extraction wells. The study focused on the distribution of calcium carbonate content in the treated volume, being found the spatial variability presented in Figure 4.1.

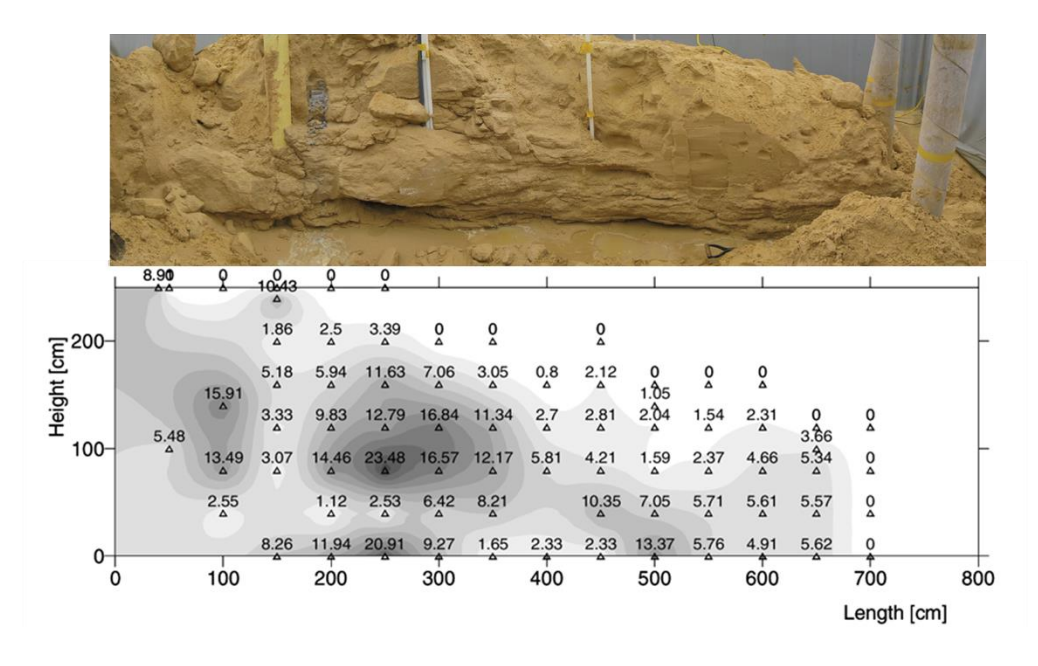


Figure 4.1 – Cross-section along longitudinal centre line through the centre injection well of the large scale

BioGrout experiment showing CaCO₃ content (%) (van Paassen et al., 2009).

X-Ray micro-computed tomography is a technique where the 3D microstructural properties of a sand sample can be characterized. The tomography aids studying the heterogeneity in a millimetric scale. Figure 4.2 presents a processed image of a biocemented sand sample analysed with this technique (Roy et al., 2023).

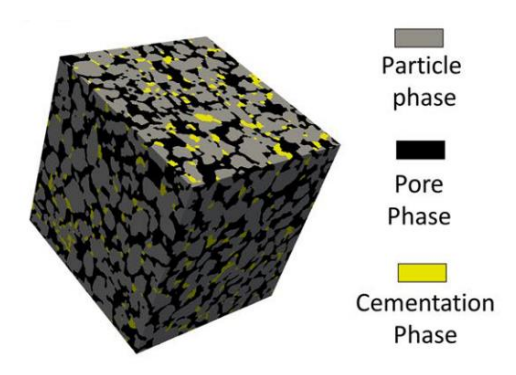


Figure 4.2 – Image of tomography on a biocemented sand sample (Roy et al., 2023)

Understanding this variation is crucial for considering its applications. Two different paths can be taken, adjusting the applications using the benefits of heterogeneity or search for strategies for achieving a homogeneous distribution of biocement.

The most common heterogeneity found in literature is the concentration of biocement near the injection points, or the formation of a superficial cover on samples, when the treatment is applied gravity. This superficial cover can be adapted to stable superficially a slope (Borges et al., 2020; Borges & Cardoso, 2023; Cardoso, Oliveira, et al., 2023). On the other hand, a delay of urea hydrolysis prevents clogging and enables a relatively uniform MICP treatment (Cheng et al., 2019).

2.3 Background from the group (Biocementation chamber)

A steel chamber to treat standard cylindrical samples was development in the past by the research group and is described by Centeno Dias et al. (2020). Figure 4.3 presents the set-up and several details. The chamber was developed to allow preparing and treating samples with biocementation, allowing to inject the treatment solutions with relatively high controlled pressure.

This steel chamber consists of a cylindrical mould with a diameter of 7.2 cm and a height of 14.0 cm. It is divided into two equal halves for easy demoulding (Figure 4.3 (b)). These halves fit into horizontal lids at the top and base (Figure 4.3 (c)), confining the tube and partially sealing it (Figure 4.3 (d)). Fluid circulation within the tube is achieved through lateral and central inlets. Internally, a perforated central tube allows for treatment injection, simulating an injector, being this the main difference of this set-up when compared with others. Alternatively, fluid injected on the top or bottom can flow within the specimen, similar to an infiltration column, which is the most standard treatment method.

While this set-up showcased some innovation, it also presented limitations that inspired the development of the set-up in this work. The identified limitations to be addressed include: (i) the size of the samples, requiring large volumes of treating solutions; (ii) leakage at the joints of the mould halves and with the top and bottom pieces

when injecting with some pressure; (iii) the need of an interface chamber for the solution, leading to the wastage of treating solution, challenging refilling, and introducing errors, often caused by bubbles, in the injected volumes; (iv) corrosion caused by chloride present in the feeding solution; and (v) difficulty in cleaning the lateral inlet/outlet.

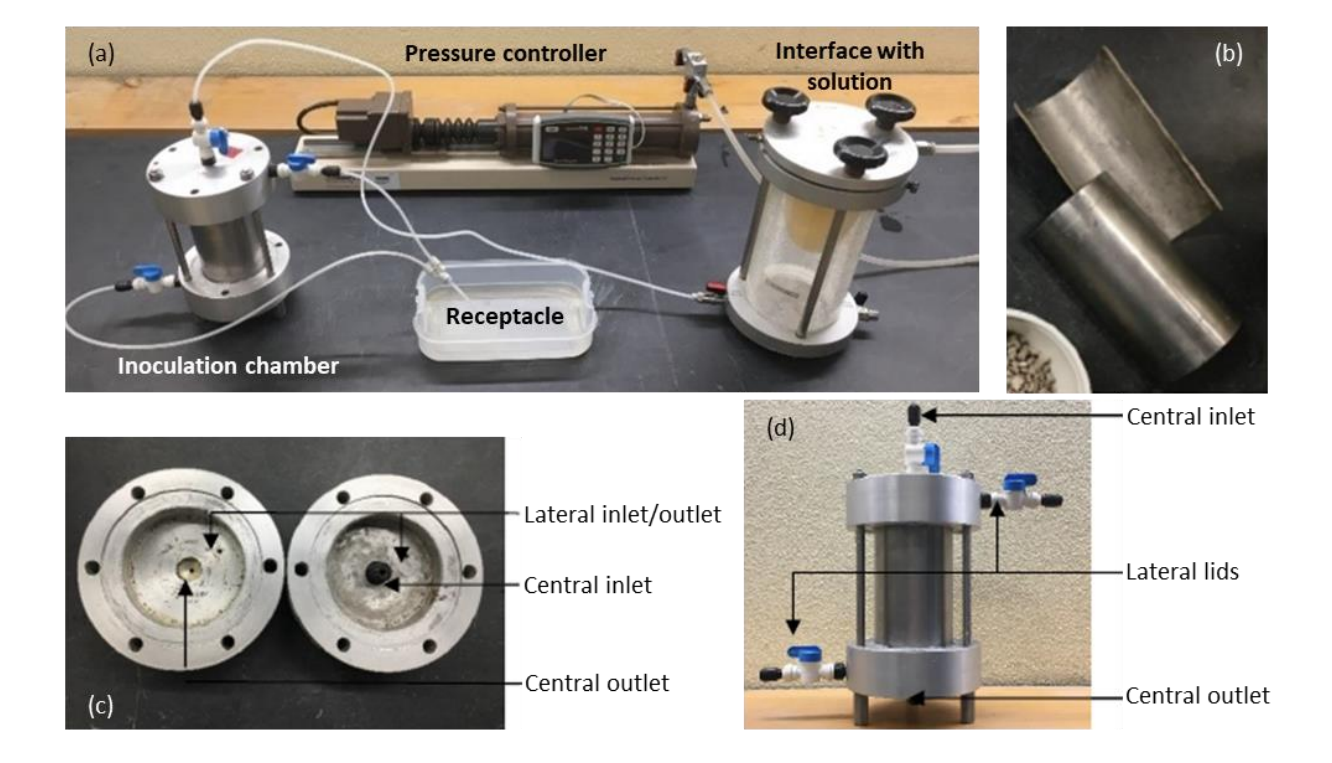


Figure 4.3 – Steel chamber: (a) set-up; (b) mould; (c) top and bottom pieces; and (d) steel chamber attached (adapted from Centeno Dias et al. (2020)).

3 Experimental results from biocementation literature review

3.1 Hydro-mechanical behaviour

The hydro-mechanical properties usually change with biocementation. As a general result, several authors reported an increment on unconfined compression strength (UCS) and a decrement on permeability with the increment of carbonate calcium content. Figure 4.4 (left) presents the data of several studies on UCS (Al Qabany & Soga, 2013; Bing, 2015; Cheng, 2012; Cheng et al., 2017; Cui et al., 2017; Darby et al., 2019; Gomez & DeJong, 2017; Ivanov, 2010; Mahawish et al., 2018; Martinez et al., 2013; Mujah et al., 2019; Stabnikov et al., 2013; Terzis & Laloui, 2019a; van Paassen, 2009; Whiffin et al., 2007; Yasuhara et al., 2012) and Figure 4.4 (right) the normalized permeability (DeJong et al., 2014; Feng & Montoya, 2016; Gomez et al., 2018; Gomez & DeJong, 2017; Lin et al., 2016; Martinez et al., 2013; Montoya et al., 2014; Montoya & DeJong, 2015; O'Donnell et al., 2018; Weil et al., 2012).

The wide range of scatter results in UCS and permeability measurements can be attributed to various factors associated with the biocementation treatment. These include the percentage of carbonate present, the

distribution of CaCO₃ crystals within the porous medium, and the adhesion of these crystals to particles (Yu et al., 2021). Additionally, the degree of saturation, which was not detailed in some studies, also significantly affects UCS results. Similarly, permeability is impacted by factors such as the initial grain size distribution and grain shape.

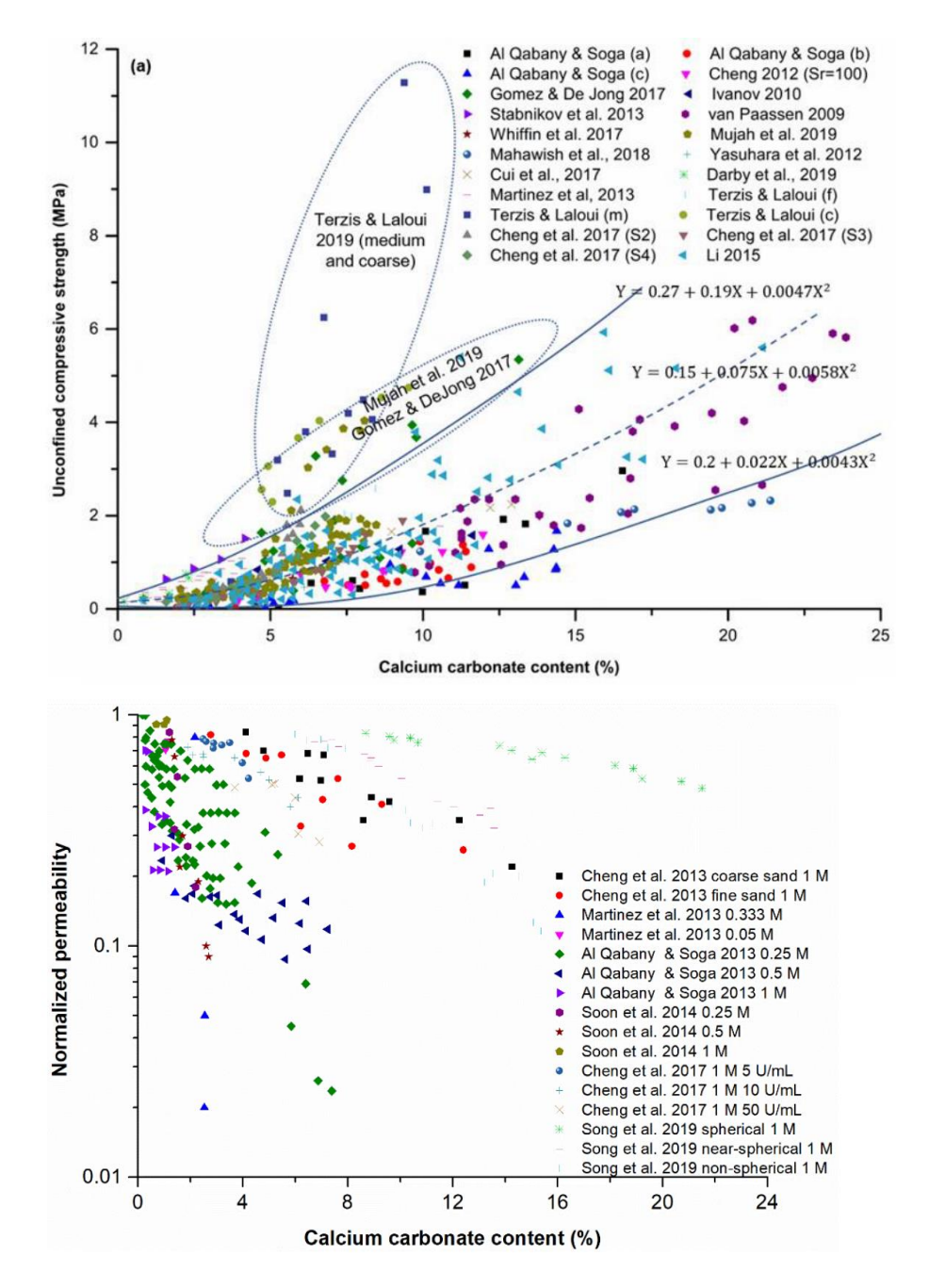


Figure 4.4 – Relationship between unconfined compression strength (top) and normalized permeability (bottom) with calcium carbonate content from several studies (Yu et al., 2021).

Biocementation treatment has the potential to serve as a ground improvement technique aimed at mitigating liquefaction and foundation settlements triggered by earthquakes (Montoya et al., 2012).

3.2 Shear Strength

The triaxial tests serve as a valuable method for understanding the behaviour of soils and establishing constitutive laws. Typically, test results are represented in the Mohr-Coulomb coordinate system of normal and shear stresses $[\sigma, \tau]$, allowing the derivation of key parameters such as the friction angle (ϕ) and cohesion (c). The same parameters can be obtained from loading paths plotted in the coordinate system average and deviator stresses [p,q], where the slope of the failure criterion (critical state line) identified as M and is related to the friction angle at critical stage.

Yu et al. (2021) compiled various triaxial results from multiple studies, as presented in Figure 4.5. These results were measured on to consolidated drained triaxial tests performed on MICP treated speciemns. The cohesion (left) and the friction angle ratio, the quotient between the biocemented and the reference, (right) of the treated specimens was plotted in Figure 4.5 as a function of formed calcium carbonate content (Bing, 2015; Cheng et al., 2013; Cui et al., 2017, 2021; Feng & Montoya, 2016; Filet et al., 2020; Gowthaman et al., 2020; Lin, 2016; Terzis & Laloui, 2019a; Wu et al., 2021). The outcomes indicate a rise in cohesion proportional to calcite content, revealing a correlated trend. However, the regression coefficient is relatively low. A similar analysis was attempted for friction angles, but the scatter is more significant, indicating a lack of correlation between these two parameters. Notably, some researchers, such as Feng and Montoya (2016) and Cui et al. (2021), observed a decrease in friction angle with increased calcite content, while others predominantly noted an increase.

This study identified lack of information regarding the failure criteria, assumptions used to interpret the results and the degree of saturation during the shear. Additionally, some findings were derived from a single confining stress, a practice not considered ideal in triaxial testing. Testing at only one confining stress level may not provide a complete understanding of how the material responds across a range of stress states, potentially leading to incomplete or biased conclusions about its behaviour and properties. Mathematically, at least two measurements are needed to determine the friction angle, and three measurements are conventionally taken to calculate a coefficient of determination and therefore account with experimental error.

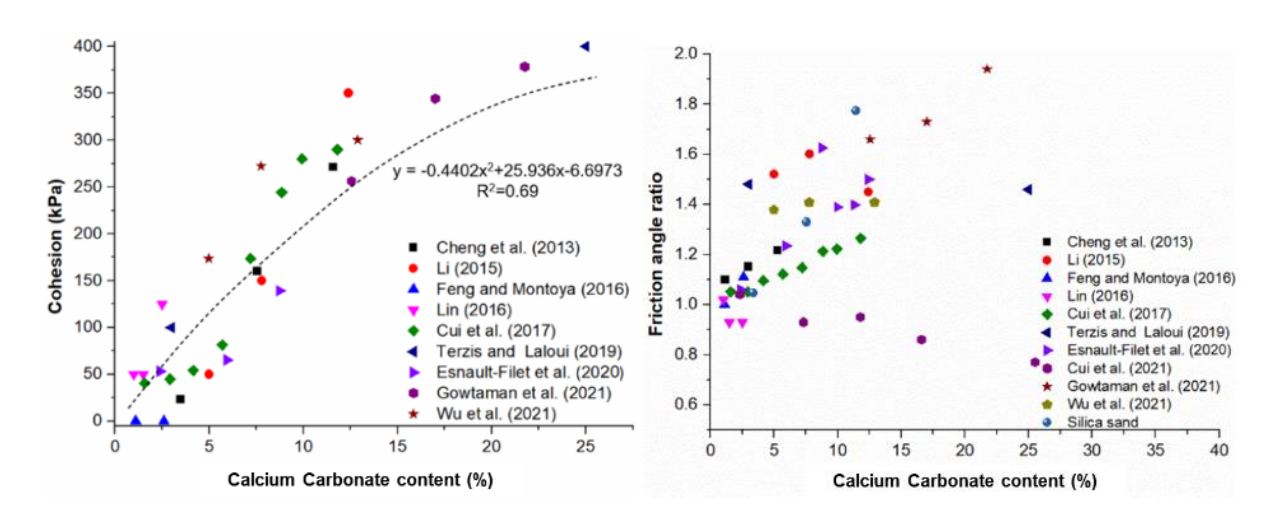


Figure 4.5 – Synthesis of consolidated drained triaxial test: (top) cohesion (kPa) and (bottom) friction angle ratio as a function of formed calcium carbonate content (%) (adapted from Yu et al. (2021))

The biocement alters the shape of soils particle, which also related with soil parameters. The shape of the sand grain influences the friction angle, it decreases with smoothen of sand grains (Xiao et al., 2019).

3.3 Compressibility

Oedometer tests are essential to complete the mechanical characterization of fine-grained soils, as they add information about the compressibility and the degree of overconsolidation. Commonly, test outcomes are represented in the axial strain (logarithmic scale) and void ratio domain $[\log(\sigma_a), e]$, allowing the derivation of parameters like the compressibility index (C_c), swelling index (C_s) and the yield stress (σ_y') with the Casagrande method (D2435-96, 1996).

In the bibliography, it is stated that biocementation treatment increases stiffness, leading to a reduction in C_c and C_s (Arboleda-Monsalve et al., 2019; Lin et al., 2016). However, the opposite, i.e. an increase in C_c and C_s of treated samples, is also reported (Calheiros, 2022; Cardoso et al., 2018; Lee et al., 2013). Calheiros (2022) explained this increase in compressibility resulted from the rupture of bonds formed by the precipitated biocement. It is a mechanism of rupture in a particulate medium, which will be more abrupt the more unstable the arrangement of particles and the higher the initial void ratio in the assembly.

4 Materials and sample preparation

4.1 Soil characterization

The soil tested is a silty sand with a uniform grading size distribution (D_{50} =0.3mm, C_c =0.94, C_u =3 .18 and G_s = 2.70) (Figure 4.6). The sand, as indicated by the mineralogical analysis in the annex, is predominantly composed of quartz.

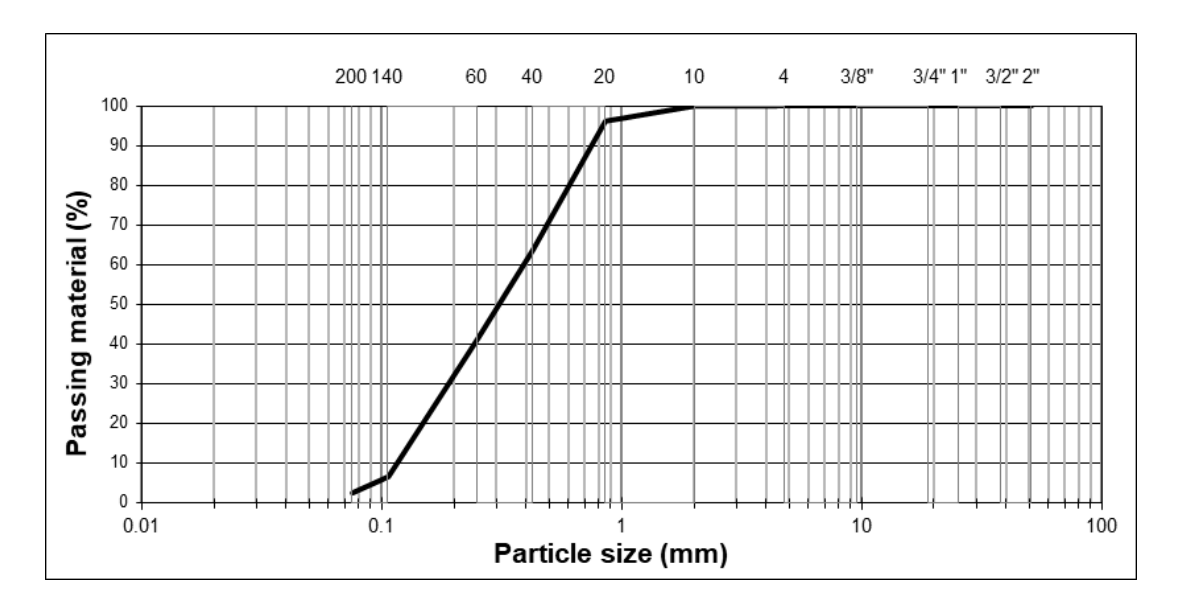


Figure 4.6 – Gain size distribution of the sand.

4.2 Treatment solutions

The treatment solution was prepared with urease from *C. ensiformis* (Jack bean), obtained from Sigma-Aldrich (~ 1 U/mg) at a concentration of 10 mg/mL, along with urea and calcium chloride (as a calcium source) from PanReac AppliChem, each at a concentration of 0.5 M in distilled water. The solution was prepared at room temperature, and without urease, which was added to the solution right before injecting it into the sand samples. This was done to prevent the immediate initiation of the hydrolysis reaction when urease and urea come into contact.

The control solutions consisted of distilled water and feeding solution. The feeding solution was similar to the treating solution but lacked urease. It comprised urea and calcium chloride at a concentration of 0.5 M in distilled water. In this work, all reagents used were analytical grade.

4.3 Standard sample preparation procedures

In this work all samples were prepared with the final dry volumetric weight of 15 kN/m³, which corresponds to void ratio of 0.78.

The untreated sand samples were assembled on the triaxial chamber as it is the common practice for a non-cohesive specimen, with a two-part split former with vacuum attachment on cylindrical mould with 7 cm diameter and 14 cm height.

The oedometer samples were directly prepared in the stainless steel rings with 7 cm diameter and 2 cm height, placed on an impermeable surface to mimic the treatment protocol conditions in the biocementation chamber, (Section 5.3), as closely as possible. The solutions were irrigated into the soil on the top of the sample (inflow) using a pipette to distribute drops homogeneously across the entire area. The solution was left on the top of the sample to infiltrate just by gravity. No distinction was made between top and bottom injection, and this limitation was considered negligible due to the reduced height, approximately 4 times less than the biocementation chamber. After irrigation, the samples were covered to prevent evaporation. In the end of the treatment, the prepared samples were transferred to a porous stone to be installed on the oedometer apparatus.

5 Biocementation chamber developed

5.1 Set-up

A new set-up was developed for this work and presented in Figure 4.7. It consists of four components: (i) a chamber, (ii) a peristaltic pump, (iii) a receptacle to collect the outflow fluids, and (iv) a piping system.

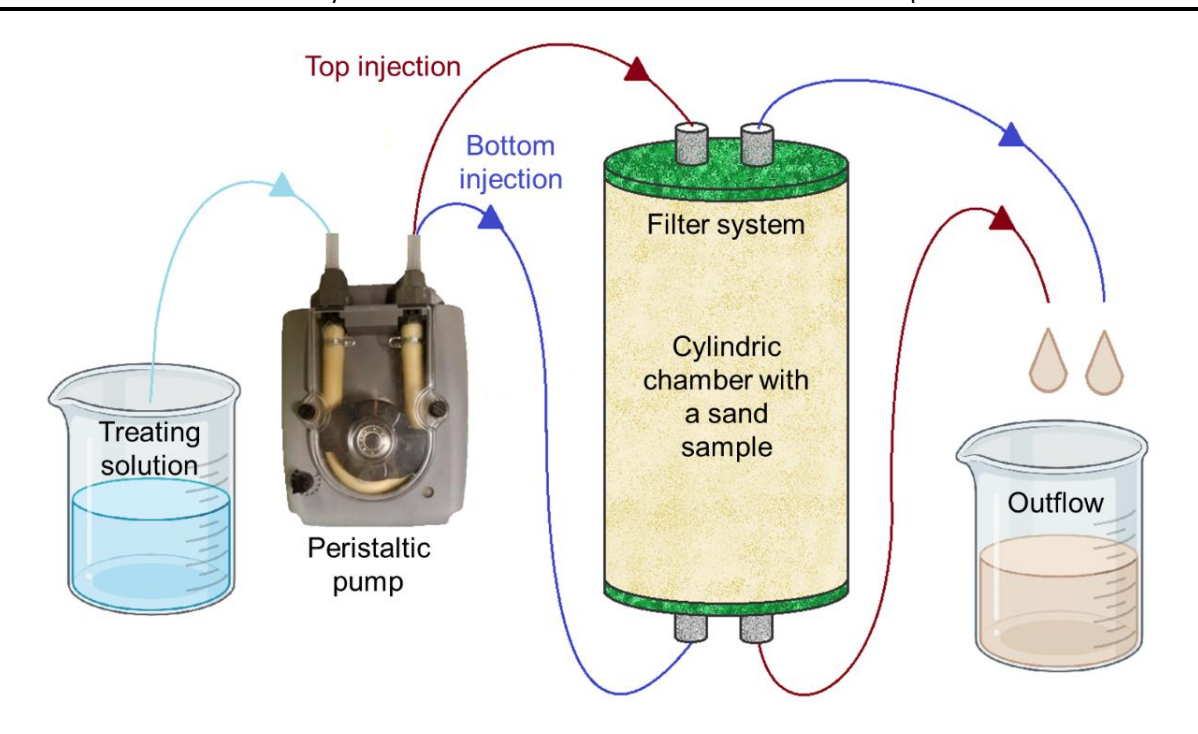


Figure 4.7 – Scheme of the set-up with the biocementation chamber

The chamber is the main component is where the sand sample is placed and treated with the biocementation technique. It is made of transparent acrylic, this material was chosen to allow the visualization of the sample. It comprises a mould, a top and a bottom lid, and three risers. The mould consists of an acrylic tube with the inner diameter of 36 mm and a hight of 100 mm. Both the top and bottom lids share the same design, consisting of a circular acrylic plate with a 10 mm thickness and a circular indent with an O-ring where the mould is compressed to ensure watertightness. Each lid is equipped with two brass inlets/outlets that can be connected to the piping system or closed with an appropriate lid. These valves can be easily attached, detached, and cleaned. The three risers connect the two lids, compressing the O-rings onto the mould. They also serve as pedestal, elevating the bottom lids and making them more accessible to collect fluids or manage pipes.

The peristaltic pump is used to maintain a constant flow and it is in direct contact with the solutions, which is easily accessible and cleanable.

The receptacle serves to collect the outflow fluids, which can be gathered for analysis or appropriately discarded based on the nature of the fluid.

The piping system is composed by flexible tubes of polyurethane 98, which connect all the components and conduct the fluids.



Figure 4.8 – Biocementation chamber top (left) and side (right) views.

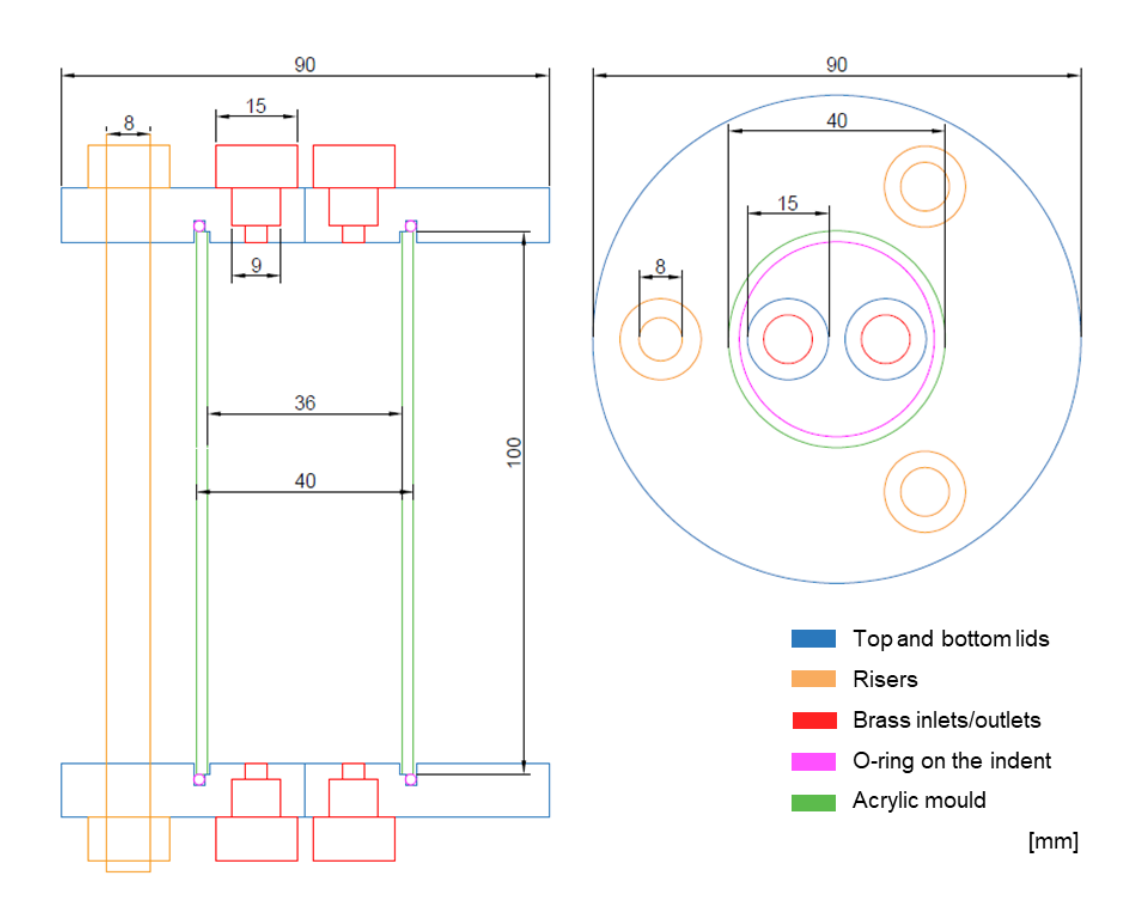


Figure 4.9 – AutoCAD scheme of the biocementation chamber.

The new set-up was designed with the purpose of addressing the issues of the previous arrangement. With this goal in mind, the new set-up introduces the following advancements:

- The specimen volume was significantly reduced, decreasing about five times the volume of fluids and sand.
- The set-up enables injection under pressure, up to 350 kPa, effectively resolving the leakage problem.
- The use of a peristaltic pump eliminates the need for an interface. The interface chamber, with a larger volume than the intended injection volume, was less cost-effective. Moreover, it was challenging to refill, potentially introducing errors, often caused by bubbles, in the injected volumes.
- The set-up is non-metallic to prevent corrosion in contact with chloride originating from the feeding solution.
- The inlets/outlets are smaller and without curves, making them accessible for cleaning in case of clogging.
- The assembly of the sample was optimized to allow for demoulding with reduced perturbations.
- The set-up provides the possibility to observe the samples during the treatment.

5.2 Sand sample preparation

The samples were cylindrical with 36 mm diameter and 84 mm height, resulting in a void volume of V_v =38 cm³. The samples were prepared directly in the chamber of the set-up, which inner walls were covered by an acetate sheet to simplify their removal at the end of the treatment. This acetate sheet was coated with a thin layer of petroleum jelly (Vaseline) to adhere to the mould and latter act as a release agent. The solid mass of sand (m_s =129.7 g) was weighed on a scale and placed inside the mould using a uniform procedure (maintaining the sand fall high) to ensure a homogeneous void ratio in the sample. On the top and bottom, a highly permeable geotextile (Figure 4.10) was placed between two filter papers to allow to the homogeneous distribution of the treatment samples and to prevent particles from passing through the specimen bottom, respectively.



Figure 4.10 – Geotextile.

5.3 Treatment protocols using the set-up developed

The main goal of the biocementation chamber was to prepared samples with a homogeneous distribution of biocement. Several protocol variations were tested with this in mind, changing several parameters: (i) the duration of the treatment cycle, (ii) the number of cycles, (iii) the injection direction, and (iv) the initial state, with or without pre-saturation. They allowed to understand their influence on the biocement distribution. This preliminary study helped selecting the protocols for triaxial tests.

The treatment involves injecting multiple volumes of the treatment solution, equal to the void volume (V_v) , into either the top or the bottom of the sample at a slow flow rate. A flow rate of 1 L per 3 hours (equivalent to 333 mL/h) was selected based on initial experiments using coloured water. These experiments revealed that the colour uniformly saturated the visible sand sample, the subsequent washing step effectively removed all visible colouration, and the pressure applied did not cause tearing of the filter paper.

One injection is referred to as a treatment cycle. Each cycle concludes with the start of a new cycle, or with the final washing step using distilled water to complete the treatment. The duration of each cycle can vary in terms of days \pm 1 hour. Each sample may be pre-saturated or unsaturated (dry) before the treatment. Table 4.1 details several specifications and Table 4.2 the timeline of the protocols of biocementation treatment performed using the biocementation chamber.

Table 4.1 – Protocols of biocementation treatment performed using the biocementation chamber.

Protocol	Number of cycles	Duration of the cycle	Injection direction	Initial state	Comments
1EU12B	1	12 days ± 1h	Bottom	Dry	Triaxial
1EU2T	1	2 days ± 1h	Тор	Dry	Triaxial
1EU2B	1	2 days ± 1h	Bottom	Dry	
2ES1T/B	2	1 day ± 1h	Bottom/Top	Saturated	
2EU1T/B	2	1 day ± 1h	Bottom/Top	Dry	
1EU1T	1	1 day ± 1h	Тор	Dry	
2EU1T	2	1 day ± 1h	Тор	Dry	
3EU1T	3	1 day ± 1h	Тор	Dry	
FU2T	1	2 days ± 1h	Тор	Dry	Control
H2O	0	-	Тор	Dry	Control

Table 4.2 – Timeline of the protocols of biocementation treatment performed using the biocementation chamber.

				Treatme	ent days			
Protocol	0	1	2	3	4	•••	12	13
1EU12B		TS inj ↓						dH2O
1EU2T		TS inj ↓		dH2O				
1EU2B		TS inj ↑		dH2O				
2ES1T/B	dH2O	TS inj ↓	TS inj ↑	dH2O				
2EU1T/B		TS inj ↓	TS inj ↑	dH2O				
1EU1T		TS inj ↓	dH2O					
2EU1T		TS inj ↓	TS inj ↓	dH2O				
3EU1T		TS inj ↓	TS inj ↓	TS inj ↓	dH2O			
FU2T		FS inj ↓		dH2O				
H2O	dH2O							
TC: :] _				luan	 l		
TS inj ↓	Treating solution injected from top			dH2O	Distilled w	<i>r</i> ater		
TS inj ↑	Treating solution injected from bottom				Unsaturat	ed (dry) san	nple	
FS inj ↓	Feeding so	olution injed	cted from to	р		Day witho	ut injection	

Table 4.3 presents the protocols used to compare and understand the impact of the protocol variations on the homogeneity of biocement and distribution on the sample.

Table 4.3 – Protocols used to investigate the homogeneity of biocement in the treated samples.

Protocols compared	Study motivation		
1EU12B and 1EU2B	Influence of the duration of the cycle		
1EU1T, 2EU1T and 3EU1T	Impact of the number of cycles		
1EU2T and 1EU2B (1EU12B)	Direction of injection		
2ES1T/B and 2EU1T/B	Influence of the initial pre-saturation		
FU2T and H2O	Control samples with feeding solution and with distilled water.		

5.4 Sample extraction from the new chamber for triaxial tests

An innovative procedure was adopted to extract the treated samples from the new chamber into the triaxial chamber with minimal perturbations. This approach was necessary to address the challenge of insufficient amount of biocement precipitated, and ensured a well-prepared sample for the triaxial test, minimizing disturbances and maintaining the integrity of the treated sand samples throughout the process.

The sample preparation for the triaxial test was adapted from the conventional method for non-cohesive specimens using a two-part split former with a vacuum attachment.

In this modified procedure, an acrylic cylindric stick was used to gently push the sample out of the acrylic mould, to a half-cylinder PVC shape base (Figure 4.11 (left)). The acetate was then carefully removed, utilizing the half-cylinder shape to facilitate this step. The specimen was rolled and remoulded as needed, always respecting the position of the portion of soil that came off during the process.



Figure 4.11 – Demoulded sample after biocementation treatment (left) and (right) sample on the triaxial equipment (right)

Following the initial demoulding, the sample was pushed into the membrane using the acrylic cylindric stick, aided by a membrane stretcher. The vacuum was released horizontally, allowing the membrane to maintain the sample's shape for subsequent steps. Then, the sample was placed in the triaxial chamber, carefully placing the bottom and top O-rings. The vacuum pump was connected into the base inlet of the chamber. Finally, the top tube was attached to the sample's top, closing the air circuit (Figure 4.11 (right)). With the vacuum pump engaged, the procedure continued as in a remoulded sample.

6 Tests on biocemented samples

6.1 Overview

The biocementation samples prepared in the chamber underwent several tests. The protocols 1EU12B, 1EU1T, and H2O (control) received more extensive characterization. In the new biocementation chamber, the tests followed a specific order. Initially, the permeability test was conducted on the chamber before demoulding. Subsequently, the sample was demoulded, and the triaxial test was performed. Finally, the sample was sectioned into three parts, and small samples were collected for the determination of calcium carbonate content (CCC) distribution in length and for observation under scanning electron microscopy (SEM). Table 4.4 provides a summary of tests on biocementation samples for each protocol.

Table 4.4 – Tests performed in each protocol of biocementation treatment performed using the biocementation chamber.

	Tests on biocemented samples								
Protocol	Triaxial test	Oedometer test	Permeability test	CCC	SEM				
1EU12B	✓	√ *	✓	√	✓				
1EU2T	✓	√ *	✓	√	✓				
1EU2B	*	*	*	√	*				
2ES1T/B	×	×	✓	✓	×				
2EU1T/B	*	*	✓	√	*				
1EU1T	×	×	✓	✓	×				
2EU1T	*	×	✓	✓	*				
3EU1T	*	×	✓	√	×				
FU2T	×	×	✓	✓	√				
H2O	√ **	√*	✓	-	✓				

^{*} specimens prepared directly on the odometer ring ($\emptyset = 7 \ cm, h = 2 \ cm$)

^{**} specimens prepared with two-part split former with vacuum attachment ($\emptyset=7~cm,h=14~cm$)

6.2 Triaxial test

The untreated sample (H2O) triaxial tested were performed for confinement stresses around of 100 kPa, 150 kPa and 250 kPa (not 200 kPa due to a technical issue).

1EU12B and 1EU2T protocols samples were prepared on the biocementation chamber. The triaxial tested were performed for confinement stresses around of 100 kPa, 150 kPa and 200 kPa. The samples were prepared with the same protocol, but same differences can be noticed due to the nature of the biocementation treatment, as there is some variability although it was intended to be minimized.

All triaxial tests were performed saturated with a B value of the Skempton's expression over 0.98, this was achieved by increasing the chamber and the back pressures, for around a week and keeping their difference lower then the confinement stress value. The stain rate applied was 0.5 mm/min. The consolidated undrained triaxial tests were performed following ASTM Standard D4767-95 (1988).

6.3 Oedometer test

The oedometer tests where performance according with ASTM Standard D2435-96 (1996). The samples tested were 1EU12 and 1EU2 in which the biocementation treatment was applied to be identical to that adopted for samples 1EU12B and 1EU2T, respectively, and H2O to be the control protocol. The stresses steps were 0 kPa, 12.3 kPa, 49.0 kPa, 98.1 kPa, 196.2 kPa, 392.4 kPa, 784.7 kPa, 1569.4 kPa, 392.4 kPa, 12.3 kPa and 0 kPa.

6.4 Permeability test

A permeability test is used in geotechnical engineering to assess the saturated permeability of soils, which is the soil's ability to allow water to flow through it. The test is typically conducted in a permeameter, although in this work the test was adapted to be conducted on the biocementation chamber after the treatment, Figure 4.12 presents a scheme of the set-up when measuring the permeability. The inlets and outlets ports were used for introducing and controlling the flow of water. The transparency of the chamber allows for easy observation of the water level, because a saturated soil sample is essential for the test. The other inlet and outlet ports served as connectors for piezometers.

To initiate the test, a constant flow of water was introduced into the chamber through the inlet and determined on the outlet. The initiation of the constant water flow marked the beginning of the test. The permeability was computed using the definition of flow and Darcy's law (Equations (4.1) and (4.2), respectively, where q is the flow, v is the velocity, A is the cross area, k is the permeability, Δh is the loss of water head and L is the length of water pathway.

$$q = vA \tag{4.1}$$

$$q = vA$$

$$v = ki = k\frac{\Delta h}{I}$$
(4.1)
(4.2)

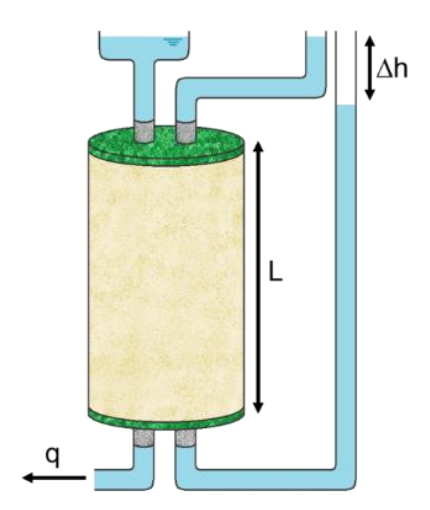


Figure 4.12 – Scheme of constant water height permeability test performed in the new biocementation chamber.

6.5 Calcium carbonate content (CCC)

The calcium carbonate content (CCC) was determined using acid washing method adapted from Portuguese standard (NP-E196-1996, 1966). The dry mass of the sand sample was measured using an oven at 105° C for 24 hours before the test (m_1) and then the soil was placed in hydrochloric acid (HCl, 0.5 M) until the reaction was complete. Then it was washed with distilled water, filtered and dried again in an oven at 105° C for 24 hours to measure the final mass (m_2) The calcium carbonate content is the ratio between the dry mass lost after the test (mass of biocement which is acid soluble) and the initial dry mass of the sample, calculated according to Equation (4.3).

$$CCC\% = \frac{m_1 - m_2}{m_1} \times 100 \tag{4.3}$$

To evaluate the CCC distribution, the determination was made is three positions of the sample: (i) top; (ii) middle and (iii) bottom. Figure 4.13 presents a scheme of this of the three equal parts of division.



Figure 4.13 – Sample division for calcium carbonate content determination.

6.6 Scanning electron microscopy (SEM)

The images captured through scanning electron microscopy (SEM) provide direct information about the presence of calcium carbonate minerals when visible. SEM associated with the technique of energy-dispersive X-ray spectroscopy (EDS) allows for the identification of chemical elements, such as calcium, carbon, and oxygen.

7 Homogeneity of biocement distribution

7.1 Calcium carbonate content (CCC)

Table 4.5 presents the calcium carbonate content (CCC) obtained from the washing test performed on samples treated on the biocementation chamber. Figure 4.14 presents the relationship between the calcium carbonate content and the position of the sample (Top, Middle and Bottom) found for each treatment protocol (Table 4.3 and Table 4.4). It is possible to understand that the CCC precipitated is low and therefore the sand samples were lightly biocemented. This figure also shows the average and standard deviation, which help to understand the homogeneity.

Comparing CCC found for the 2ES1T/B and 2EU1T/B protocols, it becomes apparent that initial saturation contributes to reach a more homogeneous distribution. A comparison between the 1EU2B and 1EU2T protocols indicates that injection through the top enhances homogeneity, as 1EU2B displays higher values of CCC at the bottom, potentially considered an outlier. The comparison of 1EU12B and 1EU2T protocols also suggests that the injection from the top contributes to homogeneity, even though the cycles had different durations.

For protocols 1EU1T, 2EU1T, and 3EU1T, an increase in CCC was anticipated with the increment in the number of cycles, though it is not evident on the results. This could be attributed to the cycle duration, because longer cycles might enhance the effectiveness of the treatment. However, this is not observed in the comparation of 1EU1T with 1EU2T protocols, where the duration of the cycle duplicate and CCC remained stable. These protocols, along with 1EU2T, exhibit higher CCC at the top, which is the injection position.

These results aid on the selection of protocols, a more homogeneous biocemented and a less were selected, 1EU2T and 1EU12B, respectively, to performance a more extensive hydro-mechanical characterization.

Table 4.5 – Calcium carbonate content (CCC) for several protocols and positions: Top, Middle and Bottom

Protocol	Bottom	Middle	Тор	Average CCC (%)
1EU12B	3.07 ± 0.84	0.90 ± 0.20	0.55 ± 0.14	1.39 ± 0.70
1EU2T	0.85 ± 0.18	1.07 ± 0.38	1.40 ± 0.17	1.11 ± 0.20
1EU2B	5.45	1.67	0.54	2.55 ± 3.33
2ES1T/B	1.33	1.00	0.89	1.07 ± 0.30
2EU1T/B	0.62	0.59	1.87	1.03 ± 0.95
1EU1T	0.90	0.90	1.54	1.11 ± 0.48
2EU1T	0.61	0.94	1.37	0.97 ± 0.49
3EU1T	0.68	0.94	1.75	1.12 ± 0.72

Average \pm Confidence interval at 95%

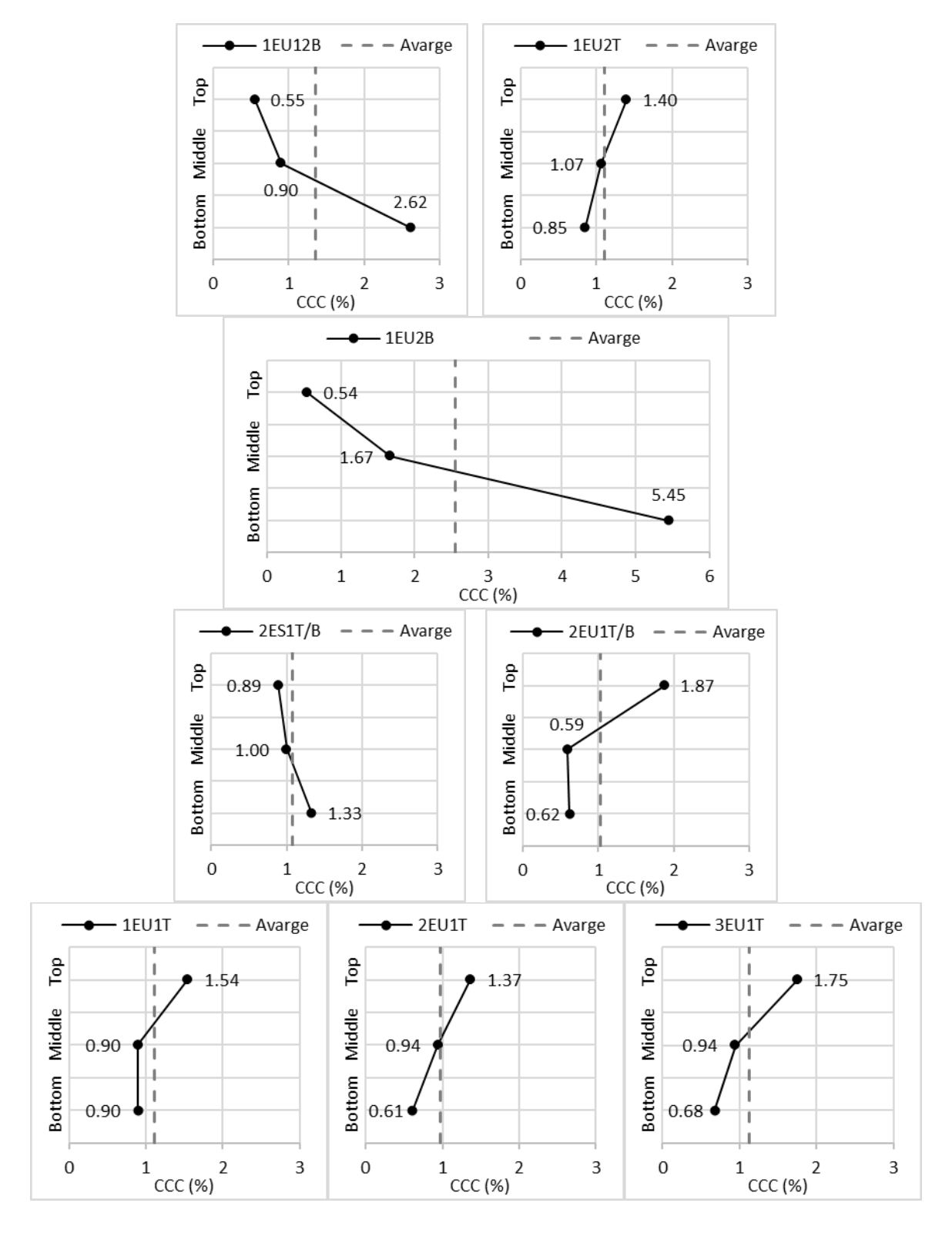


Figure 4.14 – Relationship the calcium carbonate content and between the position of the sample (Top, Middle and Bottom)

7.2 Scanning electron microscopy (SEM)

Figure 4.15, Figure 4.16 and Figure 4.17present SEM images under three different amplifications, while Figure 4.18, Figure 4.19 and Figure 4.20 present the energy-dispersive X-ray spectroscopy (EDS) results. They were obtained in small portions of soil extracted from the control samples (H2O and FU2T), and for the samples subjected to protocols 1EU12B, and 1EU2T (top, middle and bottom samples).

For the control samples H2O and FU2T, the SEM images reveal the absence of calcium carbonate crystals. It is also possible to observe that, the untreated sand grains present a rough texture with angular edges. The EDS did not detected calcium, confirming the absence of biocement.

For the protocols 1EU12B and 1EU2T, SEM images of the soil show cubic-shaped minerals in both top and bottom samples, indicating the presence of calcite minerals. This was confirmed by EDS, which detected calcium, carbon, and oxygen. The middle samples of protocols 1EU12B and 1EU2T exhibited the same type of minerals covering the grain, being the presence of calcium carbonate confirmed by EDS in the case of 1EU2T. In the case of 1EU12B the EDS did not confirm, however, given the confirmation on top and bottom of the same protocol, the similarities with 1EU2T middle section images and the fact that only a small sample is collected for SEM, this sample could not be representative of all middle section. The grains appear to be, after the precipitation of the biocement, suggesting a smoother texture compared to those observed in the untreated samples. However, this smoother texture may be a disadvantage as rounded grains may not contribute to increase friction.

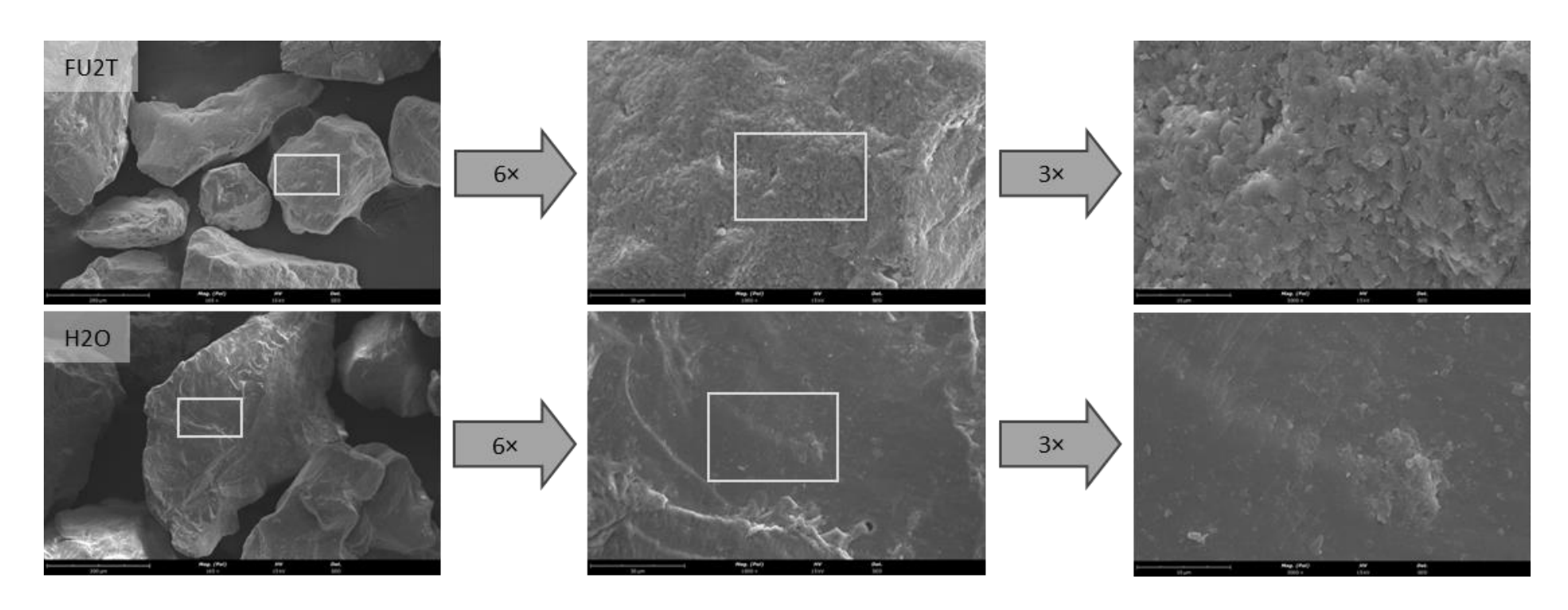


Figure 4.15 – SEM images for 3 amplifications of control protocols: FU2T (top) and H2O (bottom).

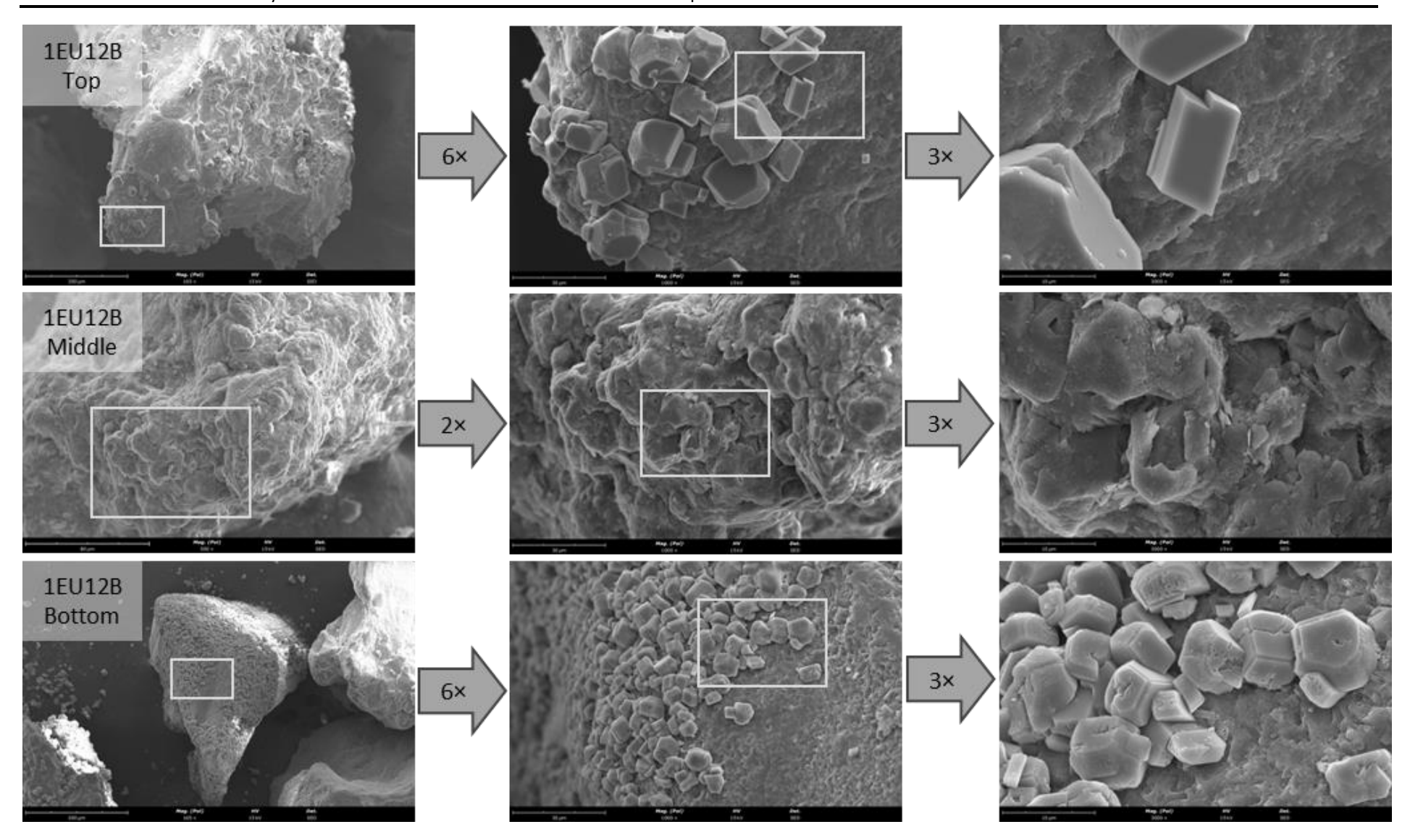


Figure 4.16 – SEM images for 3 amplifications of 1EU12B protocol: top sample (top), middle sample (centre) and bottom sample (bottom).

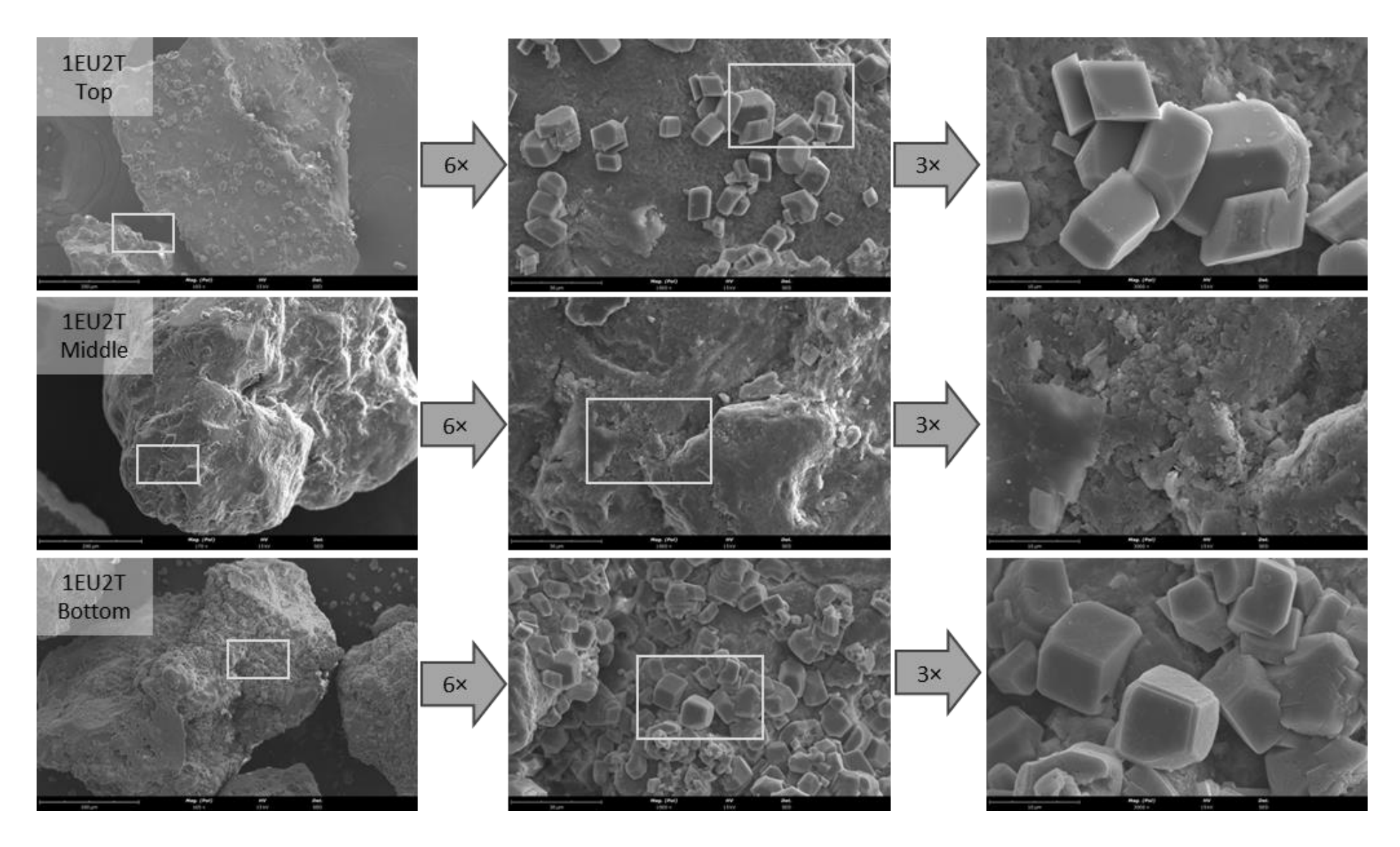


Figure 4.17 – SEM images for 3 amplifications of 1EU2T protocol: top sample (top), middle sample (centre) and bottom sample (bottom).

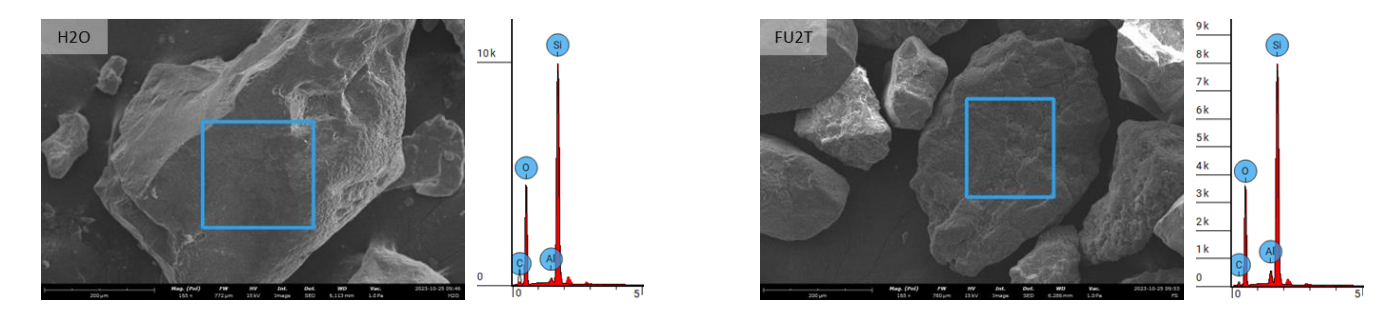


Figure 4.18 – Energy dispersive X-ray spectroscopy (EDS) results on H2O (left) and FU2T (right)

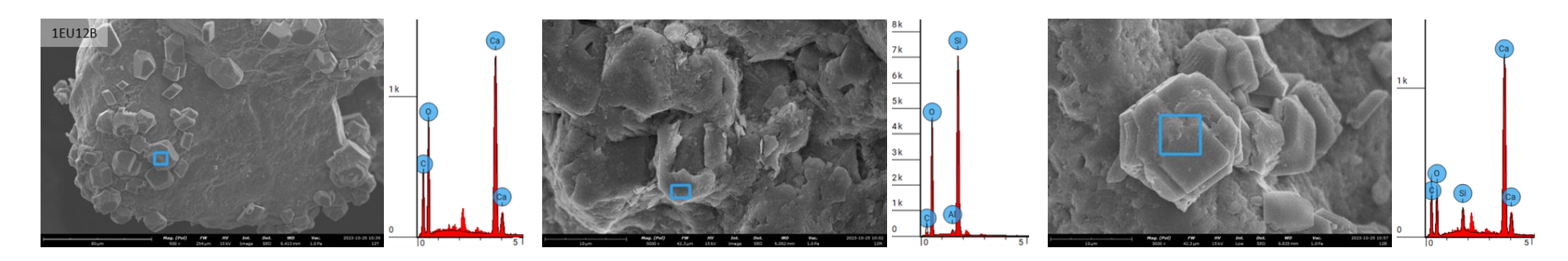


Figure 4.19 – Energy dispersive X-ray spectroscopy (EDS) results on 1EU12B sample top (left), middle (middle) and bottom (right)

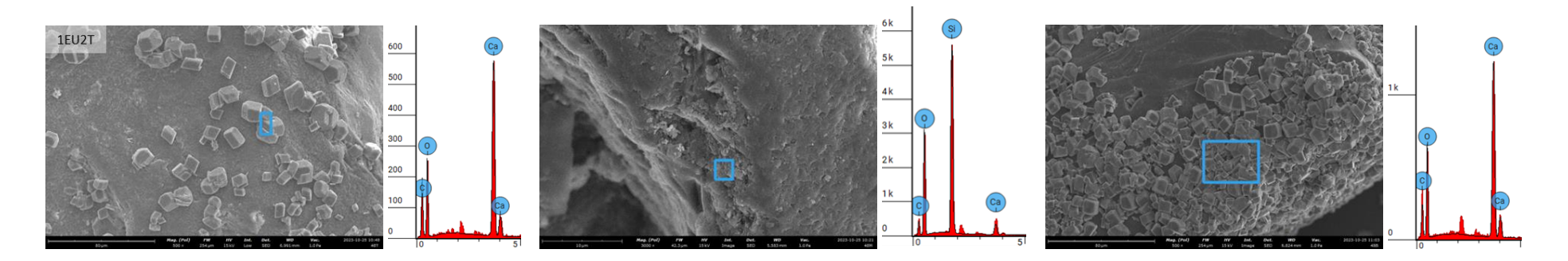


Figure 4.20 – Energy dispersive X-ray spectroscopy (EDS) results on 1EU2T sample top (left), middle (middle) and bottom (right)

8 Hydro-mechanical characterization

8.1 Triaxial test

The consolidated undrained triaxial tests were performed following ASTM Standard (D4767-95, 1988). The main results are presented in Figure 4.21, in the form of a plot deviator stress vs. axial strain, and in Figure 4.22, a plot of pore pressure vs. axial strain. The peak state was considered at the maximum deviatoric stress and the critical state when the highest axial strain reached was up to 20% (being the excess of water pressure practically constant). Table 4.6 presents the data of critical and peak states identified on the samples for the different treatment protocols and considering the confinement stresses.

All specimens exhibited a peak, except for sample with protocol 1EU2T under the confinement total stress of 158.3 kPa. The presence of a peak indicates a dense sand condition. This may be due to the initial state and not to the presence of biocement because the quantities measured in these samples were not very high.

Table 4.6 – Critical and peak states data for all protocols and confinement stresses of the triaxial tests performed.

			Critical state	e	Peak state			
Protocol	Total Stress	Deviator	Axial	Pore	Deviator	Axial	Pore	
FIOLOCOI	(kPa)	Stress	Strain	Pressure	Stress	Strain	Pressure	
		q (kPa)	ε _a (%)	∆u (kPa)	q (kPa)	ε _a (%)	Δu (kPa)	
	102.1	1869.2	20.0	-767.0	2248.0	11.3	-745.0	
1EU12B	150.6	1356.4	16.7	-597.0	1591.4	10.6	-598.0	
	204.1	1707.8	19.0	-793.0	2213.2	10.6	-759.0	
	102.7	1320.9	18.4	-563.0	1667.9	11.9	-569.0	
1EU2T	158.3*	2423.7*	20.0*	-910.0*	2426.6*	19.7*	-906.0*	
	201.3	1345.6	16.4	-577.0	1556.9	12.5	-564.0	
	101.7	1198.8	18.9	-448.0	1792.4	10.2	-628.0	
H2O	150.8	1993.9	18.6	-747.0	2296.5	14.4	-724.0	
	251.6	1255.1	18.1	-408.0	1671.9	9.9	-461.0	

^{*}Sample without a clear peak

The data analysis adopted the Critical State concept (Schofield & Wroth, 1968) was done using the known Equations (4.4) and (4.5) representing Mohr-Coulomb envelope (Critical State) and the peak envelope, respectively. In these expressions, au_c and au_p are the shear stress of critical and peak states, σ' is the normal stress, ϕ'_c and ϕ'_p are the friction angles at critical and peak states and c' is the cohesion. Cohesion is considered only for the peak state and in this case is explained by true cohesion resulting from some natural bonding in case of granular materials. However, peak can also be related to dilatancy associated to changes on particle arrangement caused by shear deformation, and on to the presence of bonds. This is the other definition of peak valid for granular soils, which is given by Equation (4.6) (Bolton, 1986), where $\phi_{\rm p}'$ is the friction angle at peak, $\phi_{\rm c}'$ is the friction angle at the critical state and ψ is the dilatancy.

$$\tau_c = \sigma' \tan \phi_c' \tag{4.4}$$

$$\tau_{c} = \sigma' \tan \phi'_{c}$$

$$\tau_{p} = c' + \sigma' \tan \phi'_{p}$$

$$\phi'_{p} = \phi'_{c} + \psi$$

$$(4.4)$$

$$(4.5)$$

$$(4.6)$$

$$\phi_p' = \phi_c' + \psi \tag{4.6}$$

Figure 4.23 presents the Mohr circles and the corresponding Mohr-Coulomb envelopes determined using the three samples for each treatment protocol. Cohesion is zero for all cases at peak stage, even when the soil was treated, because the amount of biocement precipitated was not large enough to create bonds between sand particles. This absence of cohesion is attributed to the relatively small percentage of biocement formed in the treatment protocols adopted. Therefore Equation (4.6) is the one to be used for the definition of peak angle.

The corresponding friction angles at critical and peak states are estimated and presented in Table 4.7. For the critical state the envelope was determined through linear regression. The peak state envelope was determined using the peak values, to allow finding the dilatancy angle. Although the void ratio after consolidation was not the same for all samples, a single peak envelope fitted them all acceptably.

Considering the values from Table 4.7, the friction angle at critical state has kept the same after biocementation treatment, considering the standard deviation. This was not expected and could be explained by the different procedures adopted to prepare the untreated (standard procedure) and the treated sample, using the new biocementation chamber. It is worth to note that Cui et al. (2017) and Lin (2016) have also reported a decrease in the friction angle after biocementation treatment, consistent with the observed in this work.

The dilatancy angle measured for the untreated samples (H2O protocol), 33.6° was higher than that observed for the treated samples (32.7° and 32.0° for 1EU12B and 1EU2T protocols, respectively). It can be the case that the innovative procedure adopted for sample preparation could have introduced some perturbation, however the proximity of the values indicates that disturbance may not be very relevant. In addition, it can be more likely that the samples were prepared in a relatively dense state because of dilatancy observed, and therefore the effect of the initial void ratio was dominant when compared to that of the presence of the biocement.

The friction angle ratio is the relation between the friction angle of the biocemented treated specimen (ϕ'_{bio}) and referential friction angle (ϕ'_{ref}), in this case the one of sample H2O, Equation (4.7) presents this relation. The friction angle ratio is presented on Table 4.7.

Friction angle ratio =
$$\frac{\phi'_{bio}}{\phi'_{ref}}$$
 (4.7)

Figure 4.24 presents the effective stress paths, in which the Critical State Line (CSL) is represented. CSL is represented on Equation (4.8), being its slope M_c given by Equation (4.9), where ϕ'_c is the friction angle at the critical state.

$$q = M_c p' (4.8)$$

$$M_c = \frac{6 \sin \phi_c'}{3 - \sin \phi_c'} \tag{4.9}$$

The effective stress paths presented in these plots become parallel to the CSL because liquefaction has occurred. The peak values identified allowed to plot a peak line, also passing at zero and confirming dilatancy instead of cohesion.

The comparison between the different protocols is done in

Figure 4.25, in which the relationships between deviatoric stress and pore pressure with axial strain (top/centre), and the relationships between deviatoric stress and mean effective stress (bottom) are plotted for each confinement stress applied. By observing

Figure 4.25 (bottom) comparing the effective stress paths, it is possible to understand that the biocementation treatment reduced liquefaction. This is a well-known result observed by others (Montoya et al., 2012).

Table 4.7 – Friction and dilatancy angles for the different protocols of the triaxial tests.

Protocol	Total Stress (kPa)	Friction angle at critical state (°)	Friction angle at peak state (°)	Dilatancy angle (°)	Friction angle ratio Critical	Friction angle ratio Peak	CSL slope (M _c)
1EU12B	102.1 150.6 204.1	29.1 (R ² =0.997)	34.8 31.0 32.3 32.7 ± 1.6	5.7 1.9 3.2	0.94	0.97	1.16
1EU2T	102.7 158.3* 201.3	30.6 (R ² =0.997)	33.6 32.2* 30.3 32.0 ± 1.7	4.6 3.1* 1.2	0.99	0.95	1.23
H2O	101.7 150.8 251.6	31.0 (R ² =0.999)	33.4 34.6 32.7 33.6 ± 1.0	4.4 5.5 3.6	-	-	1.24

^{*}Sample without a clear peak
Average ± Standard deviation

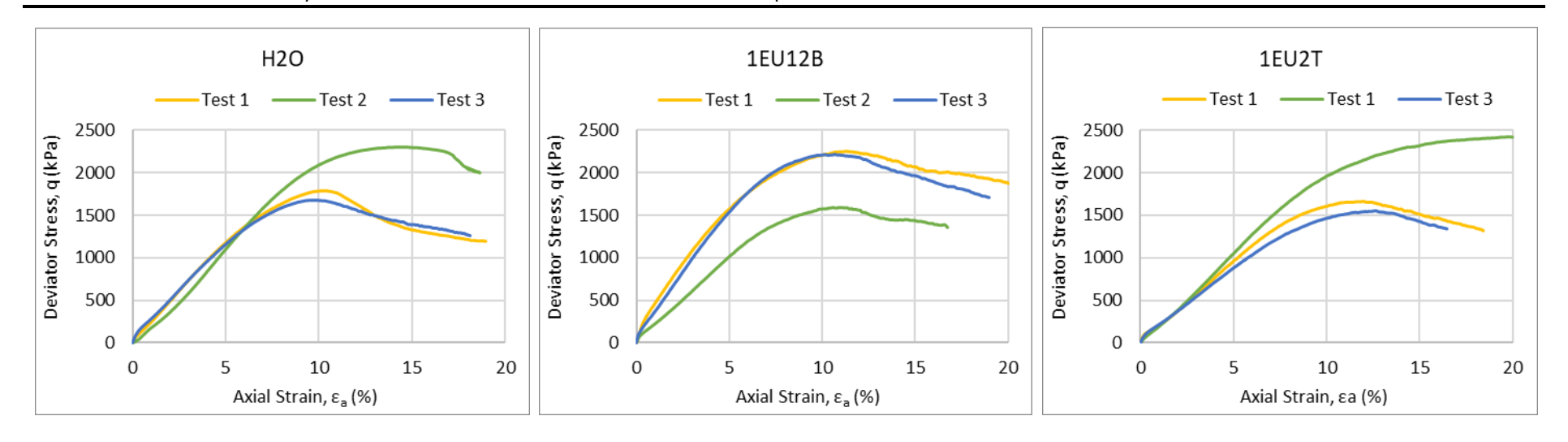


Figure 4.21 – Triaxial undrained test results: deviator stress vs. axial strain for H2O (left), 1EU2T (middle) and 1EU12B (right) protocols.

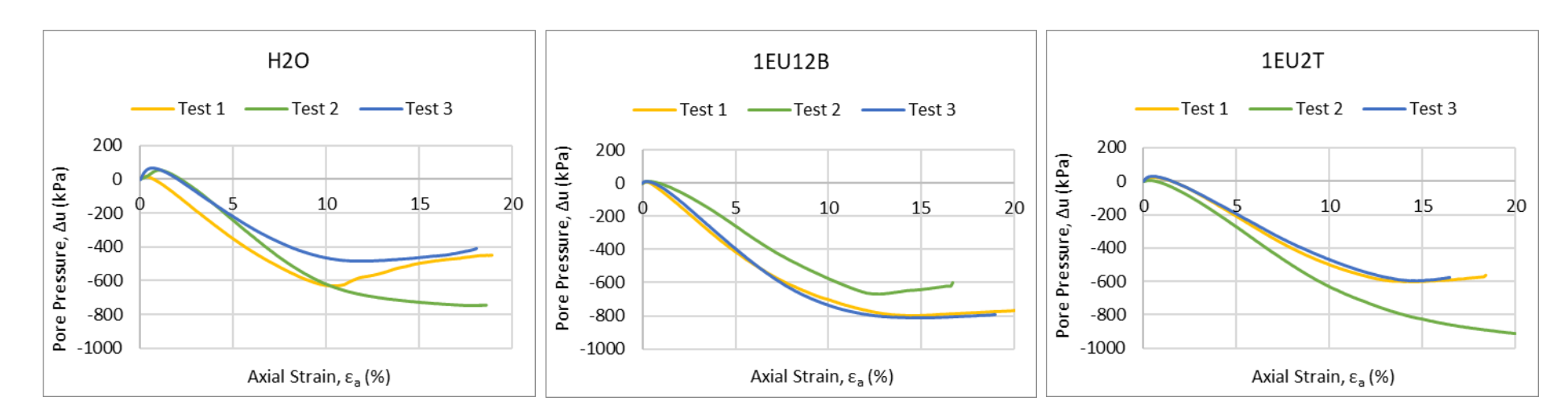


Figure 4.22 – Triaxial undrained test results: pore pressure vs. axial strain for H2O (left), 1EU2T (middle) and 1EU12B (right) protocols.

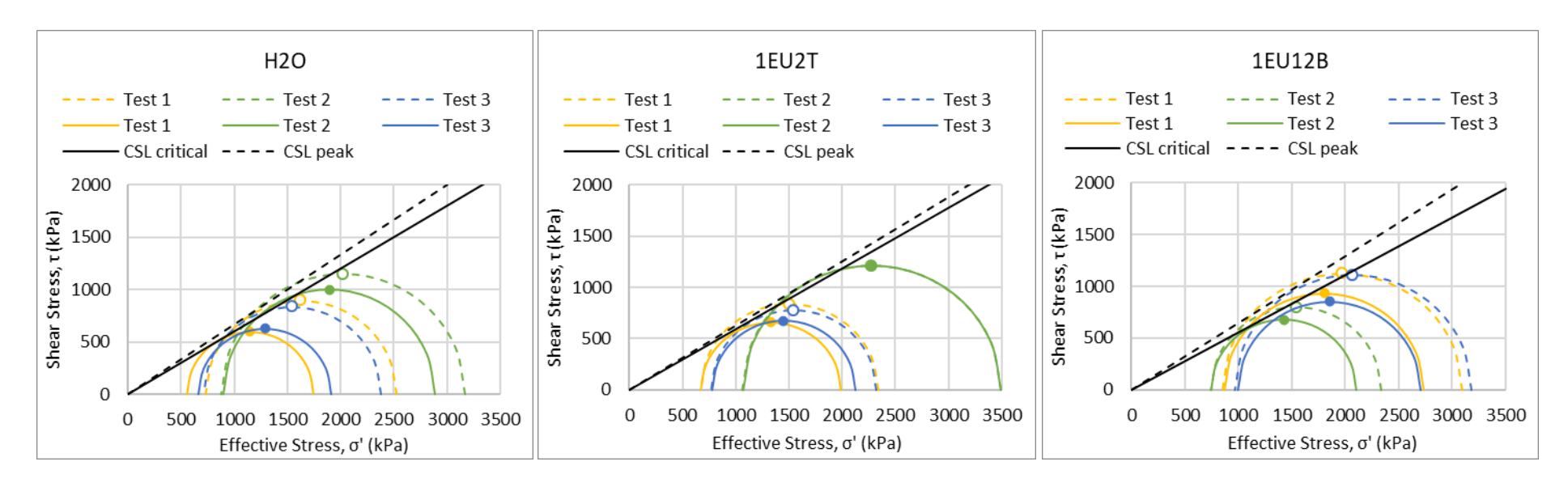


Figure 4.23 – Triaxial undrained test results: Mohr circles for peak and critical states with CSL representation for H2O (left), 1EU2T (middle) and 1EU12B (right) protocols.

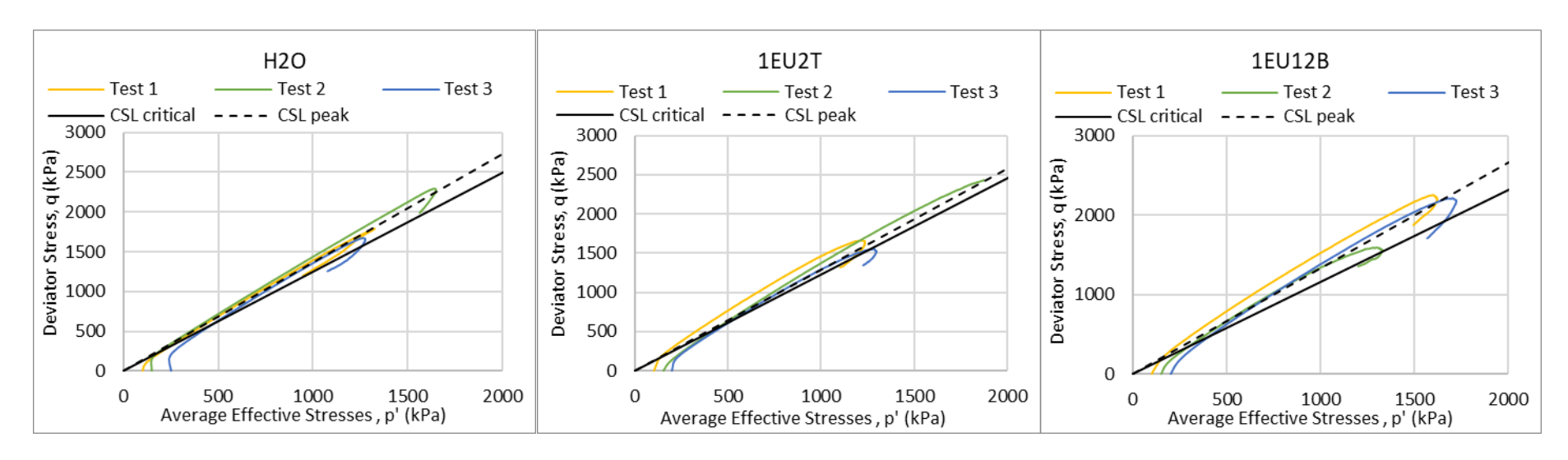


Figure 4.24 – Triaxial undrained test results: effective stress paths with CSL representation for H2O (left), 1EU2T (middle) and 1EU12B (right) protocols.

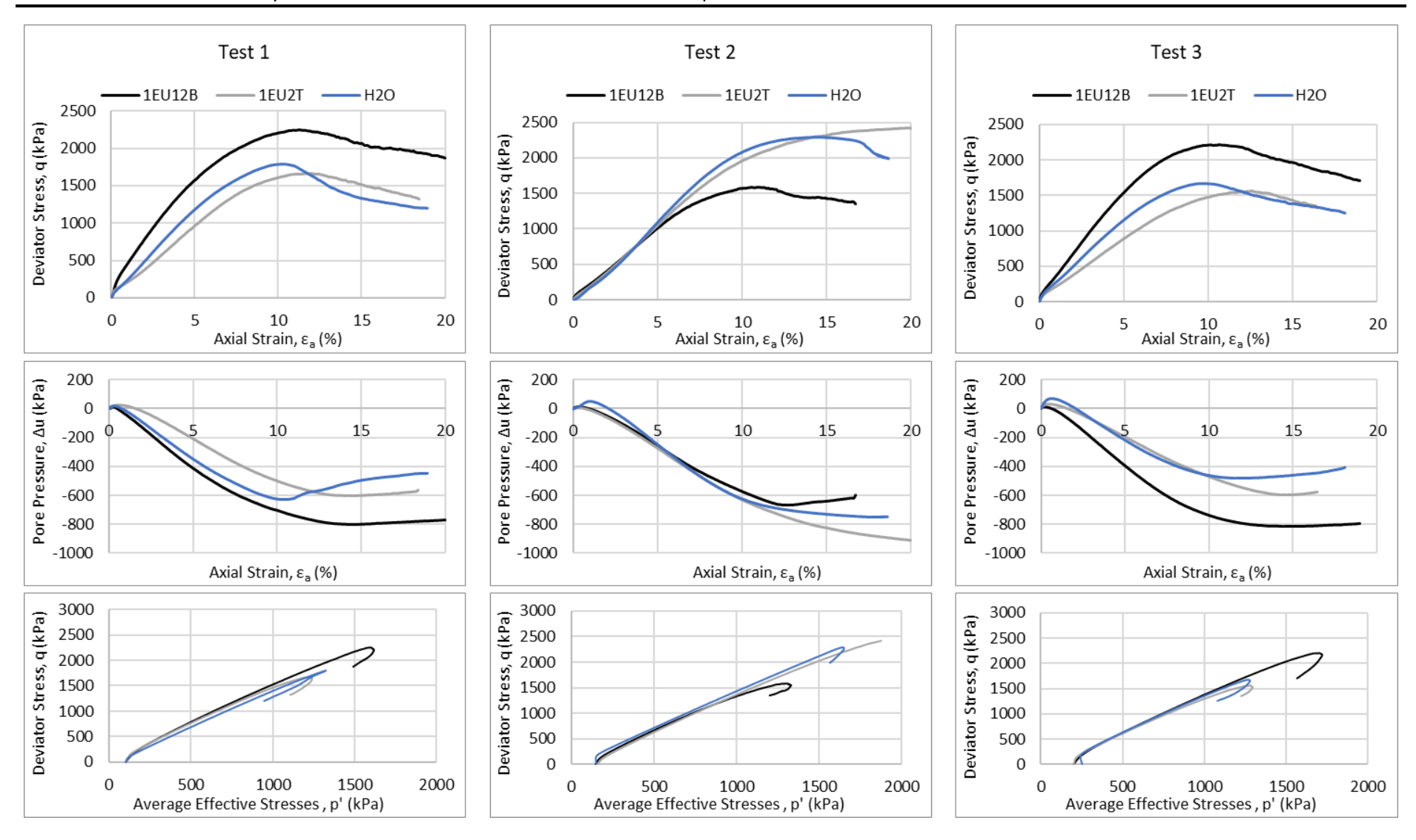


Figure 4.25 – Triaxial undrained test results: deviator stress vs. axial strain (top); pore pressure vs. axial strain (centre) and effective stress paths for confinement stresses (bottom) for the confinement stresses of 100 kPa (left), 150 kPa (centre) and 200/250 kPa (right).

8.2 Oedometer tests

Figure 4.26 presents the compressibility curves measured during the oedometer teste performed on the untreated and treated samples. The initial void ratio of all samples was 0.78. The elastoplastic compressibility index (C_c), the elastic compressibility index (C_s) and the yielding stress (σ_y') for each protocol are presented in Table 4.8. These indexes can be converted into Cam Clay compressibility parameters, as presented in Equations (4.10) e (4.11), where λ is the elastoplastic compressibility and κ is the elastic compressibility, also presented in Table 4.8. The calcium carbonate content measured after the oedometer test performance are also presented in Table 4.8.

The results from the oedometer tests reveal that the elastic compressibility index (C_s) remained relatively constant throughout the different treatment protocols, while there was an increase in the elastoplastic compressibility index (C_c) and the yield stress (σ_v') in both biocementation protocols, nearly doubling.

$$C_c = 2.3 \lambda$$
 (4.10)
 $C_s = 2.3 \kappa$ (4.11)

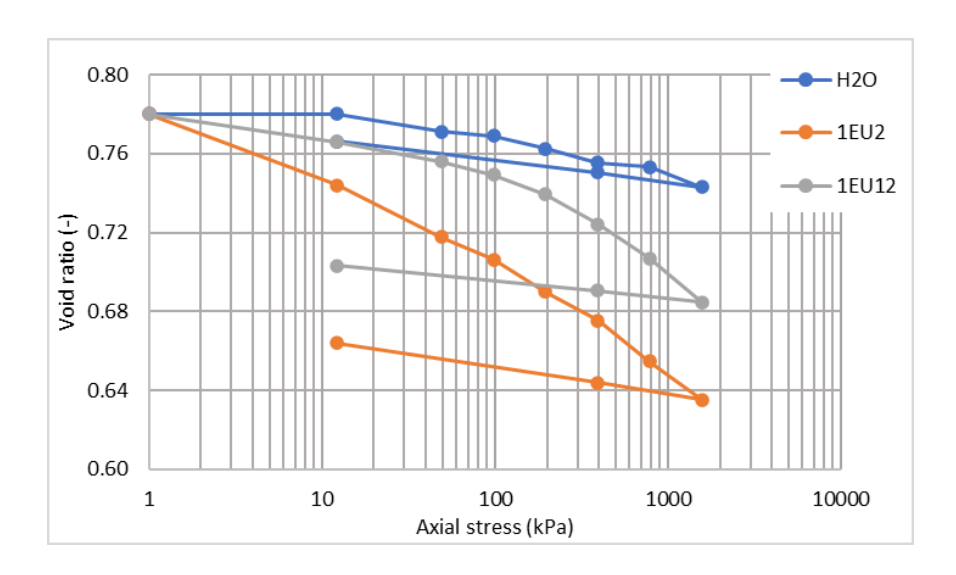


Figure 4.26 – Compressibility curves of H2O, 1EU2 and 1EU12 protocols.

Table 4.8 – Oedometer parameters for H2O, 1EU2 and 1EU12 protocols.

Protocols	H2O	1EU2	1EU12
C_c	0.034	0.064	0.074
C_s	0.012	0.014	0.010
λ	0.015	0.028	0.032
к	0.005	0.006	0.004
σ_y' (kPa)	167	362	329
CCC (%)	0.94	1.73	2.23

The fact that elastoplastic compressibility index C_c increased for the biocemented sand instead of being reduced indicates that the presence of the biocement does not contribute to increase the stiffness of the treated materials. For this reason, or no bonds were formed, or they were broken during loading. This will be discussed latter.

8.3 Permeability tests

The Table 4.9 presents the sturated permeability (Kh) values measured in the permeability tests performed on the biocementation chamber after the treatment. It is possible to understand that the permeability decreased by around an order of magnitude after the treatment. This result indicates or some clogging of soil voids, or the increment of tortuosity due to the presence of the biocement precipitated. In the comparison of protocols 1EU1T, 2EU1T, and 3EU1T, it is apparent that permeability decreases with an increase in the number of treatment cycles. This reduction in permeability was similarly observed with the increment of the duration of the treatment cycles, as seen in protocols 1EU1T, 1EU2T and 1EU12B, and will be discussed latter.

The normalized permeability is the relation between the permeability of the biocemented treated specimen $(K_{h,bio})$ and permeability for the reference case $(K_{h,ref})$, which is the one of sample H2O-Equation (4.12) presents this relation, being the values of the normalized permeabilities presented in Table 4.9.

Normalized permeability =
$$\frac{K_{h,bio}}{K_{h,ref}}$$
 (4.12)

Table 4.9 – Permeability of the biocementation samples

Protocol	Permeability (× 10 ⁻⁶ m/s)	Normalized permeability
1EU12B	0.51 ± 0.24	0.38
1EU2T	0.70 ± 0.19	0.52
1EU2B	Not measured	Not measured
2ES1T/B	1.01 ± 0.23	0.75
2EU1T/B	1.61 ± 0.22	1.19
1EU1T	1.03 ± 0.02	0.76
2EU1T	0.99 ± 0.00	0.74
3EU1T	0.72 ± 0.01	0.53
FU2T	1.88 ± 0.01	1.40
H2O	1.35 ± 0.01	1.00

Average \pm Confidence interval at 95%

9 Discussion

The main purpose of treating the soils using biocementation is to enhance their hydro-mechanical properties. Table 4.10 summarizes the outcomes of the triaxial and oedometer tests, including also the permeability and calcium carbonate content. The CCC values specific to the samples tested are specified due to the biocement distribution variation. The analysis of these results reveals that the observed variability is linked to the inherent challenges of reproducing a biological treatment. Despite employing the same protocol and conditions, variations in results persist, highlighting the intrinsic heterogeneity in a sample.

Table 4.10 – Summary of all tests for 1EU12B, 1EU2T and H2O protocols.

	Triaxial test					Oedometer test		Permeability	Calcium carbonate content				
Protocol	Total Stress (kPa)	φ' _c (°)	ϕ_p' (°)	ψ (°)	CCC middle (%)	Permeability (× 10 ⁻⁶ m/s)	Paraments outputs	CCC (%)	test (× 10 ⁻⁶ m/s)	Bottom (%)	Middle (%)	Top (%)	Average (%)
1EU12B	102.1 150.6 204.1	29.1 R ² =0.99 7	34.8 31.0 32.3 32.7 ± 1.6	5.7 1.9 3.2	0.87 0.94 1.15	0.76 - -	0.169 (λ) 0.022 (κ) 329 kPa (σ_y')	2.23	0.51 ± 0.24	3.07 ± 0.84	0.90 ± 0.20	0.55 ± 0.14	1.39 ± 0.70
1EU2T	102.7 158.3* 201.3	30.6 R ² =0.99 7	33.6 32.2* 30.3 32.0 ± 1.7	4.6 3.1 1.2	1.14 0.71* 1.67	0.70 0.51 1.53	0.148 (λ) 0.033 (κ) 362 kPa (σ_y')	1.73	0.70 ± 0.19	0.85 ± 0.18	1.07 ± 0.38	1.40 ± 0.17	1.11 ± 0.20
H2O	101.7 150.8 251.6	31.0 R ² =0.99 9	33.4 34.6 32.7 33.6 ± 1.0	4.4 5.5 3.6	-	-	0.078 (λ) 0.028 (κ) 167 kPa (σ_y')	1	1.35 ± 0.01	-	-	-	-

Average ± Santander deviation

*Sample without a clear peak

Average ± Confidence interval at 95%

The values measured for the CCC both for the permeability/triaxial tests and the oedometer tests are slightly different. Larger values were found for the oedometers than for the permeability/triaxial tests. This cannot be explained by washing caused by the permeability tests because the oedometer samples were also submerged in distilled water during the tests. Possibly it can be explained by the presence of a stiff cover of biocemented soils in the top of the oedometer samples. Nevertheless, for both type of tests the largest CCC was found for treatment protocol 1EU12B.

Starting with the analysis of the effects of the treatment on permeability, as presented in the Figure 4.27 it is obvious that normalized permeability reduces with increasing values of calcium carbonate content, being the relationship aligned with the results from other studies, for comparison. This indicates a decrease in permeability with the precipitation of biocement. This correlation, however, exhibits a low coefficient of determination, attributed to the inherent heterogeneity of the treatment.

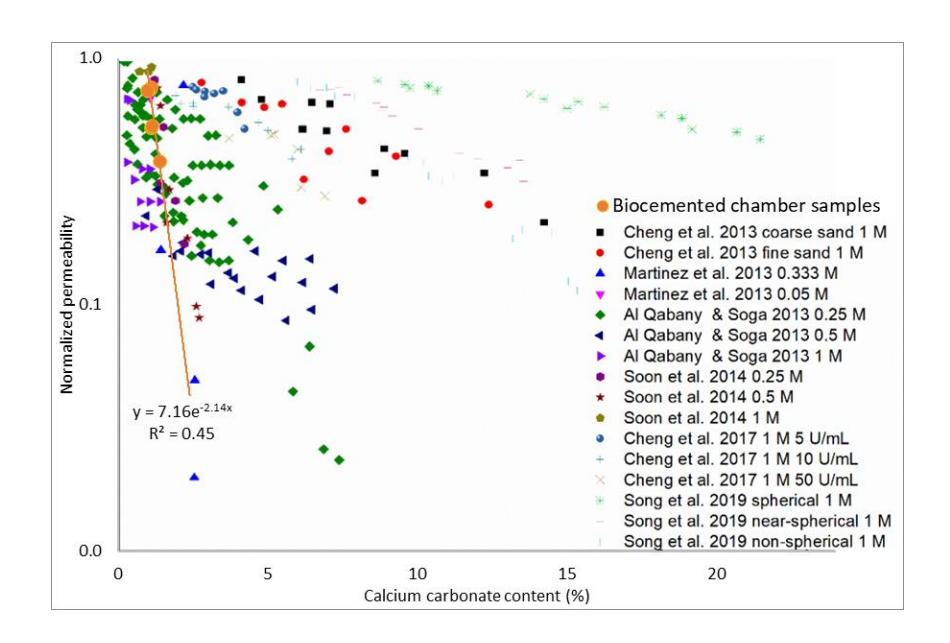


Figure 4.27 – Relationship between permeability and calcium carbonate content for treated samples on the biocementation chamber compared to other studies (adapted from Yu et al. (2021))

The results from the oedometer tests reveal that the elastic compressibility index (C_s) remained relatively constant throughout the different treatment protocols, while there was an increase in the elastoplastic compressibility index (C_c) and the yield stress (σ_y') in both biocementation protocols. This significant increment suggests a considerable enhancement in soil compressibility, contradicting some studies in the literature which suggested a reduction in compressibility and an increase in stiffness with biocementation treatment (Arboleda-Monsalve et al., 2019; Lin et al., 2016). However, it was observed the opposite in some studies (Cardoso et al., 2018; Lee et al., 2013), including a study performed on the same sand (Calheiros, 2022). This increase in compressibility can be attributed to the rupture of bonds formed by the precipitated biocement, resulting in a mechanism of rupture within the particulate medium. This mechanism is more pronounced in arrangements with higher void ratios, leading to a greater increase in compressibility.

Another possible explanation for this increment in compressibility could be the formation of a coating on the grains, a biofilm, or the biocement itself, which could decrease friction and promote their relative displacements. Furthermore, the observed reduction in friction angle in the triaxial tests supports this explanation, indicating that the treatment may have facilitated relative particle displacements and allowed for higher levels of relative density, consequently leading to higher settlements and increased compressibility. These findings underline the complex interplay between biocementation treatment and soil compressibility, highlighting the need for further research to fully understand the underlying mechanisms and optimize treatment outcomes.

Considering strength, the values of the friction angles measured are presented in Figure 4.28, depicted in relation to the calcium carbonate content and aligned with the results from other studies, for comparison. The values found are in accordance with existing data.

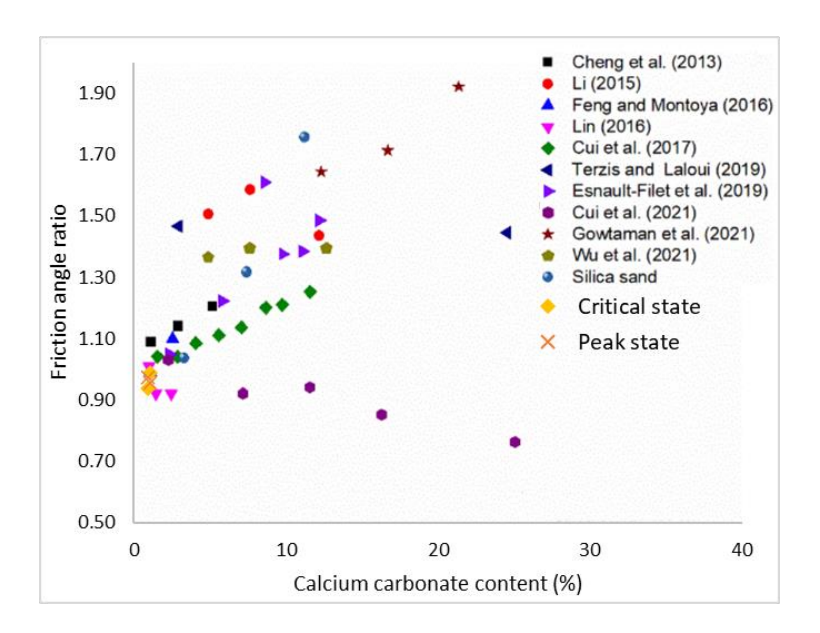


Figure 4.28 – Relationship friction angle ratio of critical and peak sates and calcium carbonate content compared to other studies (adapted from Yu et al. (2021))

Figure 4.29 illustrates the shear behaviour expected for the treated sand in comparison with that measured for the untreated one (cohesionless and with friction angle ϕ'_{sand}) in terms of the Mohr-Coulomb envelopes at critical state. This figure includes a scheme of the particles and the presence of biocement precipitated. Changes in shear strength are expected after the biocementation treatment, being explained by: (i) Hypothesis 1 - shear strength increases because friction increases caused by roughness generated by the presence of biocement inclusions in the particles surfaces (friction angle increases, $\phi'_{hyp1} > \phi'_{sand}$); (ii) Hypothesis 2 - shear strength increases because cohesion increases caused by the presence of bonds connecting the particles ($\phi'_{hyp2} = \phi'_{sand}$ and $c'_{hyp2} > c'_{sand} = 0$); (iii) Hypothesis 3 - shear strength maintains because the biocement treatment is light, and therefore friction maintains (friction angle reduces, $\phi'_{hyp3} = \phi'_{sand}$).

Hypothesis 3 is the one observed in this work. Because the soil treated is a cohesionless sand and the friction angle maintains, which was observed in the SEM images presented in Figure 4.16 and Figure 4.17, where is possible to see few biocement minerals.

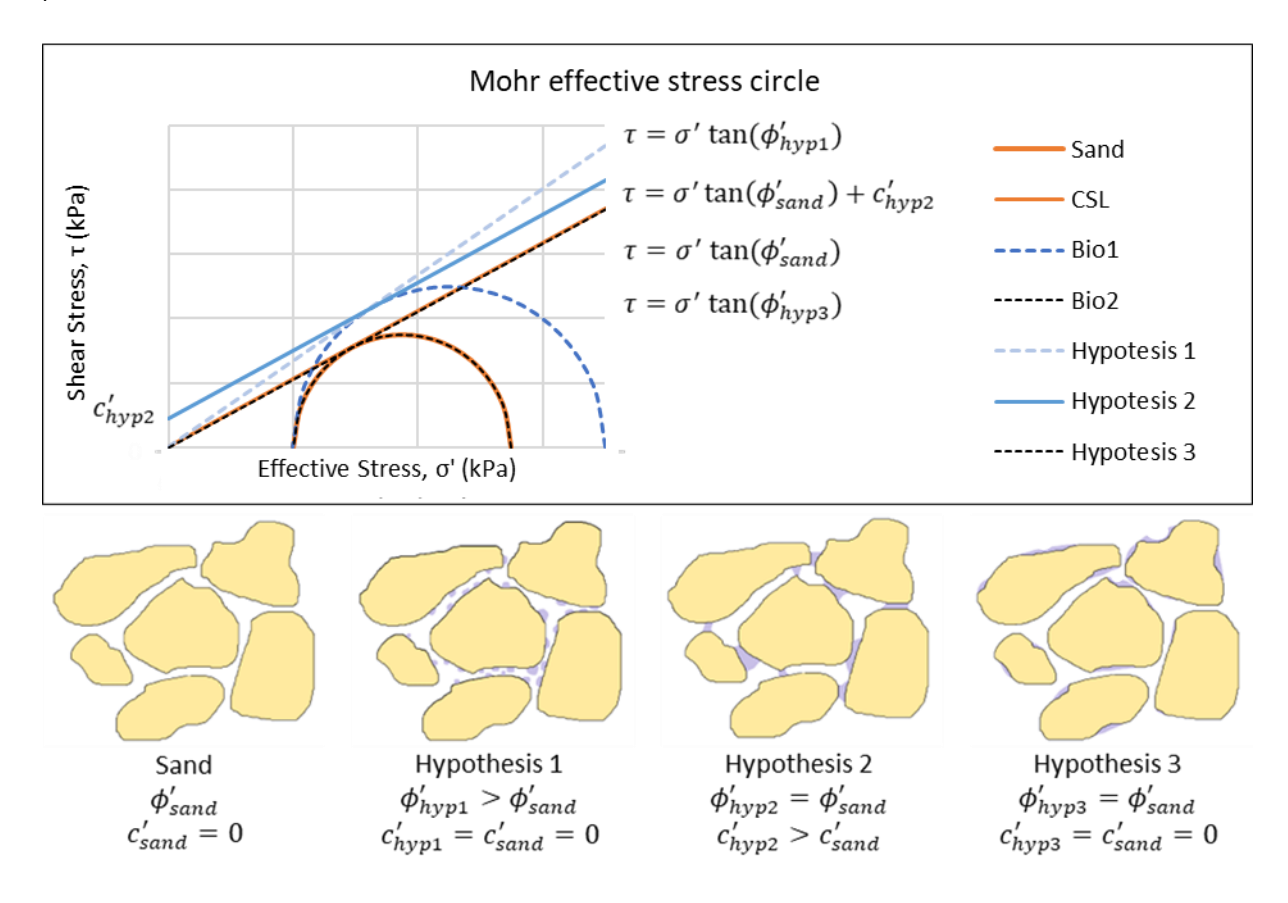


Figure 4.29 – Mohr circles for critical states with CSL representation expected for the treated sand in comparison with that measured for the untreated sand (top) and corresponding schemes of biocement (gray) distribution on sand particle (yellow) for each hypotheses (bottom).

Table 4.11 presents the Cam Clay parameters found for the H2O, 1EU12B and 1EU2T protocols.

Finally, with the results from this study it possible to define the parameters to calibrate an adequate constitutive model for the biocemented soil, which can be used for the design of biocement solutions. Table 4.11 presents the calibration parameters of Cam Clay model found for the H2O, 1EU12B and 1EU2T protocols, although this constitutive model is not adequate for sandy soils. Cam Clay was chosen because it is used to start building many other elastoplastic constitutive models for soils.

Table 4.11 – Cam Clay parameters that can be used for the design of biocemented soil solutions.

Protocol	CSL slope (M _c)	Elastoplastic compressibility (λ)	Swelling compressibility (κ)		
1EU12B	1.16	0.169	0.022		
1EU2T	1.23	0.148	0.033		
H2O	1.24	0.078	0.028		

10 Final considerations

10.1 Conclusions

A new biocementation chamber was developed, offering advantages over conventional methods found in the literature for preparing laboratory test samples, particularly when compared to the steel chamber previously used by the research group. These advantages include (i) the small size, which reduces the volume of fluids and soil; (ii) the capacity of injection up to 350 kPa of pressure; (iii) the use of a peristaltic pump to control the flow of the treatment fluids; (iv) the non-corrosive material; (v) accessibility of inlets/outlets for cleaning; (vi) the optimized method to demould with reduced perturbations and (vii) the transparent design allowing for visual monitoring of the soil sample.

The determination of calcium carbonate content (CCC) on samples from biocementation chamber indicated a lightly biocemented level across all samples The amount of precipitated biocement has not increased significantly by increasing the number of treatment cycles, and probably this number had to be doubled or tripled. This analysis allowed an exploration of factors influencing the homogeneous distribution of biocement, identifying pre-saturation and top injection as contributors to achieve a homogeneous distribution. Based on these findings, protocols 1EU2T and 1EU12B were selected as representative of more and less homogeneous biocementation, respectively, for a completer hydro-mechanical characterization.

The SEM images and EDS results provide valuable information of the distribution of biocement on the treated samples. Control samples shown untreated sand grains with angular edges and no detectable calcium carbonate crystals, while samples treated with biocementation protocols exhibited cubic-shaped minerals indicative of calcite presence. On middle sample of the biocemented protocols, a smoother texture observed, which may contribute to reduce friction.

The triaxial and oedometer tests results allowed to understand the mechanical behaviour of biocemented sand samples treated with 1EU2T and 1EU12B protocols. The resulting Mohr-Coulomb envelopes revealed that, contrary to expectations, the friction angle at critical state was kept the same after the biocementation treatment. This may be attributed to variations in sample preparation procedures and the low level of biocement. Additionally, the presence of biocement had not resulted in cohesion at the peak state due to the relatively small percentage of biocement formed. Interestingly, the dilatancy angle measured for untreated samples was higher compared to treated samples, suggesting that the effect of initial void ratio was dominant. Additionally, the effective stress paths indicate a reduction in liquefaction with biocementation treatment, as evidenced by the parallelism to the Critical State Line (CSL) and the confirmation of dilatancy instead of cohesion caused by biocement bonds.

The oedometer tests revealed a significant increase in elastoplastic compressibility and yielding stress. These results contrast with previous assumptions, which suggested that biocementation of soil increases stiffness. This highlights the need for further investigation to clarify the fundamental mechanisms behind these unexpected outcomes.

In this chapter, the friction angle after the was kept the same after the biocementation treatment, maintaining the cohesionless nature of the sand, while also showing an increase in compressibility, indicating a particle level phenomenon. This observation is supported by SEM images revealing particles rounder and smoother after biocementation treatment.

10.2 Future studies

This study provided a hydro-mechanical characterization of two protocols, serving as a valuable starting point for samples prepared in the new biocementation chamber. However, further characterization of additional protocols is recommended to ensure consistency of results.

Regarding the new biocementation chamber, a deeper investigation into the relationship between protocol variables and biocement distribution is suggested. These variables include those proposed in this study as well as new ones, such as the initial void ratio, flow rate, and other types of biocementation treatment (e.g., MICP). The versatility of the new biocementation chamber allows for testing various variables, such as different sample heights, the circulation of the treatment solution, and simultaneous injection of two solutions.

The identification of issues with the previous steel chamber, the development of the new biocementation chamber, and the experience gained in demoulding samples are the starting points for future studies to characterize the hydro-mechanical properties of biocemented samples. However, the demoulding procedure can be further optimized, and chambers with standardized sample dimensions for laboratory tests can be developed.

Finally, further investigation on the spatial arrangement of biocement and how it interferes with the geometry of the grains is necessary to fully understand strength mobilization mechanisms. Such analysis has been done by others using tomography analysis, for example, but was not explored in this work.

The possibility that biocement precipitation can reduce particles roughness and therefore decrease friction angle could be investigated to check if there is a threshold value of CCC above which the biocement will no longer contribute to smooth the particles but will be in excess and may start creating new asperities, or even bonds. Such hypothesis must be investigated in the future.

Chapter 5

Final considerations

Each chapter concludes with a summary of its main findings and suggestions of future studies. This chapter aim to present a final overview of how the strategies for the design of biocementation treatment investigated can contribute to the implementation of this technique.

The main findings when exploring the three strategies are highlighted below:

- The analyses of clay minerals on biocementation contributes to understand their phyco-chemical influence on treatment efficiency. The interaction between clay and bacteria was identified as a critical factor, influencing biocementation treatment. The positive influence of clay minerals found suggest that fixed small amounts of clay minerals can be added to the treatment to improve its efficiency.
- The need to quantify the real amount of enzyme hydrolysing urea revealed to be fundamental to understand the results, as the mechanical and hydraulic improvements depend on the amount of calcium carbonate precipitated (CCC). This was possible with the help of the biosensor optimized to detect the usual concentrations of urease enzyme. This sensor has an huge potential as a monitoring tool of biocementation at small scale, and it offers promising prospects for real-time evaluation and management of biocementation processes. There are various potential applications across biocementation field inside and outside geotechnical scoop.
- The development of a new biocementation chamber represents a significant advancement specially when the amount of biocement precipitated is low, because it improves the sample preparation method. The preparation of good quality samples and as much identical as possible is fundamental for experimental testing, therefore allowing more accurate characterization of treated samples. A complete hydro-mechanical characterization allowed to understand the behaviour of biocemented samples.-The changes observed were explained by the presence of biocement.

As part of future studies, the continuation on investigating clay-bacteria interaction aiming at extending the treatment to clayey soils, or even use clay to optimize the treatment is proposed. To understand deeply the impact of clay on biocementation effects, it is suggested to conduct a complete hydro-mechanical characterization of samples prepared with sand and fixed percentages of clay. The new biocementation chamber developed can be used for such samples as well. The experience earned in demoulding samples reducing perturbation is a key factor to produce good quality samples for experimental tests.

The investigation on the changes on the mechanical properties of the soil investigated after biocementation treatment confirmed the need to analyse the soil at particle level. Such micromechanical analysis, done by many through tomography tests, must consider the real geometry of the particles and precipitated biocement, as well as spatial distribution. This is naturally associated with grading size distribution and void ratio at preparation.

Such information is very relevant as it will allow explaining why different results are achieved when the same treatment protocol is applied to different samples of the same soil. The use of such imaging technique can be explored further to investigate if the asperity and roughness of the grains can be modified by the presence of the precipitate, and then to impact stiffness and strength.

One of the main features of the chamber developed is the possibility to collect fluid outflow. This feature was designed specifically considering the future use of the biosensor to investigate these fluids. Data of urease monitored with the biosensor on EICP samples prepared on the chamber correlated with the hydro-mechanical parameters will be a great step into understanding better how to use the biosensor as a monitoring tool. These correlations can define abacus-like plots relating biosensor reads with relevant hydro-mechanical properties. Unfortunately, this investigation was not yet made in this thesis, however it is proposed as future study.

Finally, biocementation treatment remains a promising solution for soil stabilization and offers an alternative to more pollutant traditional methods. Overall, this thesis contributes to advancing our understanding of biocementation and its practical applications in soil engineering.

References

- Al Qabany, A., & Soga, K. (2013). Effect of chemical treatment used in MICP on engineering properties of cemented soils. *Géotechnique*, *4*, 107–115. https://doi.org/10.1680/bcmpge.60531.010
- Albuquerque, D. C. (2017). *Optimization and quantification of Urease in a magnetoresistive biochip platform with integrated Microfluidics*. Universidade de Lisboa Instituto Superior Técnico.
- Albuquerque, D. C., Cardoso, R., Monteiro, G. A., Duarte, S. O. D., Martins, V. C., & Cardoso, S. (2019). Towards a portable magnetoresistive biochip for urease-based biocementation monitoring. *2019 IEEE 6th Portuguese Meeting on Bioengineering (ENBENG)*, *4*, 1–4. https://doi.org/10.1109/ENBENG.2019.8692505
- Almajed, A., Khodadadi Tirkolaei, H., & Kavazanjian, E. (2018). Baseline Investigation on Enzyme-Induced Calcium Carbonate Precipitation. *Journal of Geotechnical and Geoenvironmental Engineering*, *144*(11), 1–11. https://doi.org/10.1061/(ASCE)GT.1943-5606.0001973
- Anker, H. T., Baaner, L., Backes, C., Keessen, A., & Möckel, S. (2018). *Comparison of ammonia regulation in Germany, the Netherlands and Denmark legal framework* (Issue 276). https://ifro.ku.dk/english/staff/?pure=en%2Fpublications%2Fcomparison-of-ammonia-regulation-ingermany-the-netherlands-and-denmark(dca73ad9-a1c2-4fed-b245-b6d27bae8d7d).html
- Arboleda-Monsalve, L. G., Zapata-Medina, D. G., & Galeano-Parra, D. I. (2019). Compressibility of biocemented loose sands under constant rate of strain, loading, and pseudo K-triaxial conditions. *Soils and Foundations*, *59*(5), 1440–1455. https://doi.org/10.1016/j.sandf.2019.06.008
- Bhaskar, S., Anwar Hossain, K. M., Lachemi, M., Wolfaardt, G., & Otini Kroukamp, M. (2017). Effect of self-healing on strength and durability of zeolite-immobilized bacterial cementitious mortar composites. *Cement and Concrete Composites*, 82, 23–33. https://doi.org/10.1016/j.cemconcomp.2017.05.013
- Bing, L. (2015). Geotechnical Properties of Biocement Treated Sand and Clay. Nanyang Technological University.
- Bolton, M. D. (1986). The strength and dilatancy. *Geotechnique*, 36(I), 65–78.
- Borges, I., Albuquerque, D. C., Cardoso, S., & Cardoso, R. (2023). Towards a monitoring tool to quantify urease during biocementation treatment at microscale. *Proceedings of the 8th International Symposium on Deformation Characteristics of Geomaterials (IS-PORTO 2023), September*. https://www.issmge.org/publications/publication/towards-a-monitoring-tool-to-quantify-urease-during-biocementation-treatment-at-microscale
- Borges, I., & Cardoso, R. (2023). Capacidade resistente de um solo arenoso tratado com a técnica de biocimentação the load bearing capacity of a sandy soil treated with biocementation tecnhique. 18° Congresso Nacional de Geotecnia (18CNG).
- Borges, I., Milhomens, N., Braz de Oliveira, S., Duarte, S. O. D., Monteiro, G. A., Quintela Cruz, M., & Cardoso, R.

- (2020). Estudo da biocimentação como técnica de tratamento superficial de taludes para evitar ravinamento. 17º Congresso Nacional de Geotecnia (17CNG), #121.
- Burdalski, R. J., Ribeiro, B. G. O., Gomez, M. G., & Gorman-Lewis, D. (2022). Mineralogy, morphology, and reaction kinetics of ureolytic bio-cementation in the presence of seawater ions and varying soil materials. *Scientific Reports*, *12*(1), 17100. https://doi.org/10.1038/s41598-022-21268-3
- Cabalar, A. F., Karabash, Z., & Erkmen, O. (2018). Stiffness of a biocemented sand at small strains. *European Journal of Environmental and Civil Engineering*, 22(10), 1238–1256. https://doi.org/10.1080/19648189.2016.1248791
- Calheiros, F. (2022). *Quantificação dos efeitos da bio-cimentação em solos arenosos*. Universidade de Lisboa Instituto Superior Técnico.
- Cardoso, R., Borges, I., Vieira, J., Duarte, S. O. D., & Monteiro, G. A. (2023). Interactions between clay minerals, bacteria growth and urease activity on biocementation of soils. *Applied Clay Science*, *240*(May). https://doi.org/10.1016/j.clay.2023.106972
- Cardoso, R., Oliveira, M., Borges, I., Pinto, M., Cruz, M. Q., Gonzalez, I., Rodrigues, A. T., Anjos, B., Sapin, L., & Filet, A. E. (2023). Tratamento de um talude real para evitar ravinamento: primeiro caso-estudo português em biocimentação Treatment of a real slope to prevent ravine formation: first portuguese case-study on biocementation. 18° Congresso Nacional de Geotecnia (18CNG).
- Cardoso, R., Pedreira, R., Duarte, S. O. D., & Monteiro, G. A. (2020). About calcium carbonate precipitation on sand biocementation. *Engineering Geology*, *271*, 105612. https://doi.org/10.1016/j.enggeo.2020.105612
- Cardoso, R., Pires, I., Duarte, S. O. D., & Monteiro, G. A. (2018). Effects of clay's chemical interactions on biocementation. *Applied Clay Science*, *156*(January), 96–103. https://doi.org/10.1016/j.clay.2018.01.035
- Centeno Dias, F., Borges, I., Duarte, S. O. D., Monteiro, G. A., & Cardoso, R. (2020). Comparison of experimental techniques for biocementation of sands considering homogeneous volume distribution of precipitated calcium carbonate. *E3S Web of Conferences*, *195*, 05004. https://doi.org/10.1051/e3sconf/202019505004
- Cheng, L. (2012). Innovative Ground Enhancement by Improved Microbially Induced CaCO3 Precipitation Technology. March, 251.
- Cheng, L., & Cord-Ruwisch, R. (2012). In situ soil cementation with ureolytic bacteria by surface percolation. *Ecological Engineering*, 42, 64–72. https://doi.org/10.1016/j.ecoleng.2012.01.013
- Cheng, L., Cord-Ruwisch, R., & Shahin, M. A. (2013). Cementation of sand soil by microbially induced calcite precipitation at various degrees of saturation. *Canadian Geotechnical Journal*, *50*(1), 81–90. https://doi.org/10.1139/cgj-2012-0023
- Cheng, L., Shahin, M. A., & Chu, J. (2019). Soil bio-cementation using a new one-phase low-pH injection method.

 **Acta Geotechnica*, 14(3), 615–626. https://doi.org/10.1007/s11440-018-0738-2

- Cheng, L., Shahin, M. A., & Mujah, D. (2017). Influence of Key Environmental Conditions on Microbially Induced

 Cementation for Soil Stabilization. *Journal of Geotechnical and Geoenvironmental Engineering*, *143*(1), 1–

 11. https://doi.org/10.1061/(asce)gt.1943-5606.0001586
- Choi, S.-G., Park, S.-S., Wu, S., & Chu, J. (2017). Methods for Calcium Carbonate Content Measurement of Biocemented Soils. *Journal of Materials in Civil Engineering*, 29(11), 1–4. https://doi.org/10.1061/(ASCE)MT.1943-5533.0002064
- Choi, S.-G., Wu, S., & Chu, J. (2016). Biocementation for Sand Using an Eggshell as Calcium Source. *Journal of Geotechnical and Geoenvironmental Engineering*, *142*(10), 2–5. https://doi.org/10.1061/(ASCE)GT.1943-5606.0001534
- Chu, J., Ivanov, V., Stabnikov, V., & Li, B. (2013). Microbial method for construction of an aquaculture pond in sand. *Géotechnique*, *63*(10), 215–219. https://doi.org/10.1680/bcmpge.60531.020
- Cuadros, J. (2017). Clay minerals interaction with microorganisms: a review. *Clay Minerals*, *52*(2), 235–261. https://doi.org/10.1180/claymin.2017.052.2.05
- Cui, M.-J., Zheng, J.-J., Chu, J., Wu, C.-C., & Lai, H.-J. (2021). Bio-mediated calcium carbonate precipitation and its effect on the shear behaviour of calcareous sand. *Acta Geotechnica*, *16*(5), 1377–1389. https://doi.org/10.1007/s11440-020-01099-0
- Cui, M.-J., Zheng, J.-J., Zhang, R.-J., Lai, H.-J., & Zhang, J. (2017). Influence of cementation level on the strength behaviour of bio-cemented sand. *Acta Geotechnica*, *12*(5), 971–986. https://doi.org/10.1007/s11440-017-0574-9
- D 4373. (1996). Standard test method for calcium carbonate content of soils. In *ASTM-Standards*. https://doi.org/10.1520/D4373-14
- D2435-96. (1996). Standard test method for one-dimensional consolidation properties of soils. In *ASTM-Standards* (Vol. 04, Issue August, pp. 196–205).
- D4767-95. (1988). Standard Test Method for Consolidated Undrained Triaxial Compression Test for Cohesive Soils (D 4767-95). *Astm*, *04*(January), 1–15. https://doi.org/10.1520/D4767-11R20.2
- Darby, K. M., Hernandez, G. L., DeJong, J. T., Boulanger, R. W., Gomez, M. G., & Wilson, D. W. (2019). Centrifuge Model Testing of Liquefaction Mitigation via Microbially Induced Calcite Precipitation. *Journal of Geotechnical and Geoenvironmental Engineering*, 145(10), 1–13. https://doi.org/10.1061/(ASCE)GT.1943-5606.0002122
- DeJong, J. T., Fritzges, M. B., & Nüsslein, K. (2006). Microbially Induced Cementation to Control Sand Response to Undrained Shear. *Journal of Geotechnical and Geoenvironmental Engineering*, *132*(11), 1381–1392. https://doi.org/10.1061/(ASCE)1090-0241(2006)132:11(1381)
- DeJong, J. T., Martinez, B. C., T. R. Ginn, 3 C. Hunt, Major, D., & Tanyu, B. (2014). Development of a Scaled

- Repeated Five-Spot Treatment Model for Examining Microbial Induced Calcite Precipitation Feasibility in Field Applications. *Geotechnical Testing Journal*, *37*(3). https://doi.org/10.1520/GTJ20130089
- DeJong, J. T., Mortensen, B. M., Martinez, B. C., & Nelson, D. C. (2010). Bio-mediated soil improvement. *Ecological Engineering*, *36*(2), 197–210. https://doi.org/10.1016/j.ecoleng.2008.12.029
- Demas, V., & Lowery, T. J. (2011). Magnetic resonance for in vitro medical diagnostics: superparamagnetic nanoparticle-based magnetic relaxation switches. *New Journal of Physics*, *13*(2), 025005. https://doi.org/10.1088/1367-2630/13/2/025005
- Dixit, C. K. (2016). Microfluidics for Biologists. In C. K. Dixit & A. Kaushik (Eds.), *Microfluidics for Biologists:*Fundamentals and Applications. Springer International Publishing. https://doi.org/10.1007/978-3-319-40036-5
- Feng, K., & Montoya, B. M. (2016). Influence of Confinement and Cementation Level on the Behavior of Microbial-Induced Calcite Precipitated Sands under Monotonic Drained Loading. *Journal of Geotechnical and Geoenvironmental Engineering*, 142(1), 1–9. https://doi.org/10.1061/(ASCE)GT.1943-5606.0001379
- Feng, K., & Montoya, B. M. (2017). Quantifying Level of Microbial-Induced Cementation for Cyclically Loaded Sand. *Journal of Geotechnical and Geoenvironmental Engineering*, 143(6), 1–4. https://doi.org/10.1061/(ASCE)GT.1943-5606.0001682
- Ferreira Cardoso, S. M. (2015). *Development of a Urease Quantification Biosensor to Monitor Biocementation Processes in Soils*. Universidade de Lisboa Instituto Superior Técnico.
- Filet, A. E., Gadret, J.-P., Loygue, M., & Borel, S. (2012). Biocalcis and its applications for the consolidation of sands. *Grouting and Deep Mixing*, 1767–1780.
- Filet, A. E., Gutjahr, I., Garandet, A., Viglino, A., Béguin, R., Monier, J. M., Oxarango, L., Emeriault, F., & Castanier Perthuisot, S. (2020). BOREAL, Bio-reinforcement of embankments by biocalcification. *E3S Web of Conferences*, 195, 1–6. https://doi.org/10.1051/e3sconf/202019505001
- Fomina, M., & Skorochod, I. (2020). Microbial Interaction with Clay Minerals and Its Environmental and Biotechnological Implications. *Minerals*, *10*(10), 861. https://doi.org/10.3390/min10100861
- Freitas, P., Cardoso, F. A., Martins, V. C., Martins, S. A. M., Loureiro, J., Amaral, J., Chaves, R. C., Cardoso, S., Fonseca, L. P., Sebastião, A. M., Pannetier-Lecoeur, M., & Fermon, C. (2012). Spintronic platforms for biomedical applications. *Lab on a Chip*, *12*(3), 546–557. https://doi.org/10.1039/c1lc20791a
- Gao, Y., Hang, L., He, J., & Chu, J. (2019). Mechanical behaviour of biocemented sands at various treatment levels and relative densities. *Acta Geotechnica*, *14*(3), 697–707. https://doi.org/10.1007/s11440-018-0729-3
- Germano, J., Martins, V. C., Cardoso, F. A., Almeida, T., Sousa, L., Freitas, P., & Piedade, M. (2009). A Portable and Autonomous Magnetic Detection Platform for Biosensing. *Sensors*, *9*(6), 4119–4137. https://doi.org/10.3390/s90604119

- Ghosh, T., Bhaduri, S., Montemagno, C., & Kumar, A. (2019). Sporosarcina pasteurii can form nanoscale calcium carbonate crystals on cell surface. *PLOS ONE*, *14*(1), e0210339. https://doi.org/10.1371/journal.pone.0210339
- Gingine, V. L. (2017). Consolidation and decontamination of clayey soils using electrokinetic treatment [Instituto Superior Técnico Universidade de Lisboa]. https://scholar.tecnico.ulisboa.pt/records/EZF19zP8Lw9TV-Szp7C6LfGE-9Q3pK8o8851
- Gomez, M. G., & DeJong, J. T. (2017). Engineering Properties of Bio-Cementation Improved Sandy Soils Michael. *Grouting 2017 GSP 288*, 23–33.
- Gomez, M. G., DeJong, J. T., & Anderson, C. M. (2018). Effect of Bio-cementation on Geophysical and Cone Penetration Measurements in Sands Author. *Canadian Geotechnical Journal*, 1–53.
- Gomez, M. G., Martinez, B. C., DeJong, J. T., Hunt, C. E., DeVlaming, L. A., Major, D. W., & Dworatzek, S. M. (2015). Field-scale bio-cementation tests to improve sands. *Proceedings of the Institution of Civil Engineers Ground Improvement*, *168*(3), 206–216. https://doi.org/10.1680/grim.13.00052
- Gowthaman, S., Nakashima, K., & Kawasaki, S. (2020). Freeze-thaw durability and shear responses of cemented slope soil treated by microbial induced carbonate precipitation. *Soils and Foundations*, *60*(4), 840–855. https://doi.org/10.1016/j.sandf.2020.05.012
- Harkes, M. P., van Paassen, L. A., Booster, J. L., Whiffin, V. S., & van Loosdrecht, M. C. M. (2010). Fixation and distribution of bacterial activity in sand to induce carbonate precipitation for ground reinforcement. *Ecological Engineering*, 36(2), 112–117. https://doi.org/10.1016/j.ecoleng.2009.01.004
- Islam, M. T., Chittoori, B. C. S., & Burbank, M. (2020). Evaluating the Applicability of Biostimulated Calcium Carbonate Precipitation to Stabilize Clayey Soils. *Journal of Materials in Civil Engineering*, *32*(3), 1–11. https://doi.org/10.1061/(ASCE)MT.1943-5533.0003036
- Ivanov, V. (2010). Environmental Microbiology for Engineers. In *Environmental Microbiology for Engineers* (Issue November). https://doi.org/10.1201/9781439895009
- Ivanov, V., Stabnikov, V., Stabnikova, O., & Kawasaki, S. (2019). Environmental safety and biosafety in construction biotechnology. *World Journal of Microbiology and Biotechnology*, *35*(2), 1–11. https://doi.org/10.1007/s11274-019-2598-9
- Krajewska, B. (2018). Urease-aided calcium carbonate mineralization for engineering applications: A review. *Journal of Advanced Research*, 13, 59–67. https://doi.org/10.1016/j.jare.2017.10.009
- Lapierre, F. M., Schmid, J., Ederer, B., Ihling, N., Büchs, J., & Huber, R. (2020). Revealing nutritional requirements of MICP-relevant Sporosarcina pasteurii DSM33 for growth improvement in chemically defined and complex media. *Scientific Reports*, *10*(1), 22448. https://doi.org/10.1038/s41598-020-79904-9
- Lee, M. L., Ng, W. S., & Tanaka, Y. (2013). Stress-deformation and compressibility responses of bio-mediated

- residual soils. Ecological Engineering, 60, 142-149. https://doi.org/10.1016/j.ecoleng.2013.07.034
- Li, W., Liu, L., Chen, W., Yu, L., Li, W., & Yu, H. (2010). Calcium carbonate precipitation and crystal morphology induced by microbial carbonic anhydrase and other biological factors. *Process Biochemistry*, *45*(6), 1017–1021. https://doi.org/10.1016/j.procbio.2010.03.004
- Lin, T. H. (2016). Microbial Modification of Soil for Ground Improvement. Lehigh University.
- Lin, T. H., Suleiman, M. T., Brown, D. G., & Kavazanjian, E. (2016). Mechanical Behavior of Sands Treated by Microbially Induced Carbonate Precipitation. *Journal of Geotechnical and Geoenvironmental Engineering*, 142(2), 1–13. https://doi.org/10.1061/(ASCE)GT.1943-5606.0001383
- Liu, B., Zhu, C., Tang, C.-S., Xie, Y.-H., Yin, L.-Y., Cheng, Q., & Shi, B. (2020). Bio-remediation of desiccation cracking in clayey soils through microbially induced calcite precipitation (MICP). *Engineering Geology*, *264*(February 2019), 105389. https://doi.org/10.1016/j.enggeo.2019.105389
- Ma, G., He, X., Jiang, X., Liu, H., Chu, J., & Xiao, Y. (2021). Strength and permeability of bentonite-assisted biocemented coarse sand. *Canadian Geotechnical Journal*, *58*(7), 969–981. https://doi.org/10.1139/cgj-2020-0045
- Ma, L., Pang, A.-P., Luo, Y., Lu, X., & Lin, F. (2020). Beneficial factors for biomineralization by ureolytic bacterium Sporosarcina pasteurii. *Microbial Cell Factories*, *19*(1), 12. https://doi.org/10.1186/s12934-020-1281-z
- Mahawish, A., Bouazza, A., & Gates, W. P. (2018). Effect of particle size distribution on the bio-cementation of coarse aggregates. *Acta Geotechnica*, *13*(4), 1019–1025. https://doi.org/10.1007/s11440-017-0604-7
- Margesin, R., Zimmerbauer, A., & Schinner, F. (2000). Monitoring of bioremediation by soil biological activities. *Chemosphere*, 40(4), 339–346. https://doi.org/10.1016/S0045-6535(99)00218-0
- Martinez, B. C., DeJong, J. T., Ginn, T. R., Montoya, B. M., Barkouki, T. H., Hunt, C. E., Tanyu, B., & Major, D. (2013). Experimental Optimization of Microbial-Induced Carbonate Precipitation for Soil Improvement. *Journal of Geotechnical and Geoenvironmental Engineering*, 139(4), 587–598. https://doi.org/10.1061/(ASCE)GT.1943-5606.0000787
- Martins, V. C., Germano, J., Cardoso, F. A., Loureiro, J., Cardoso, S., Sousa, L., Piedade, M., Fonseca, L. P., & Freitas, P. (2010). Challenges and trends in the development of a magnetoresistive biochip portable platform.

 Journal of Magnetism and Magnetic Materials, 322(9–12), 1655–1663.

 https://doi.org/10.1016/j.jmmm.2009.02.141
- Mitchell, J. K., & Santamarina, J. C. (2005). Biological Considerations in Geotechnical Engineering. *Journal of Geotechnical and Geoenvironmental Engineering*, 131(10), 1222–1233. https://doi.org/10.1061/(ASCE)1090-0241(2005)131:10(1222)
- Montoya, B. M., & DeJong, J. T. (2015). Stress-Strain Behavior of Sands Cemented by Microbially Induced Calcite Precipitation. *J. Geotech. Geoenviron. Eng*, 1–10. https://doi.org/10.1061/(ASCE)GT.1943-5606

- Montoya, B. M., DeJong, J. T., & Boulanger, R. W. (2014). Dynamic response of liquefiable sand improved by microbial-induced calcite precipitation. In *Bio- and Chemo-Mechanical Processes in Geotechnical Engineering* (Vol. 63, Issue 4, pp. 125–135). ICE Publishing. https://doi.org/10.1680/bcmpge.60531.012
- Montoya, B. M., DeJong, J. T., Boulanger, R. W., Wilson, D. W., Gerhard, R., Ganchenko, A., & Chou, J.-C. (2012). Liquefaction Mitigation using Microbial Induced Calcite Precipitation. *GeoCongress 2012 © ASCE 2012*, 1918–1927.
- Morales, L., Garzón, E., Romero, E., & Sánchez-Soto, P. J. (2019). Microbiological induced carbonate (CaCO 3) precipitation using clay phyllites to replace chemical stabilizers (cement or lime). *Applied Clay Science*, 174(March), 15–28. https://doi.org/10.1016/j.clay.2019.03.018
- Mueller, B. (2015). Experimental Interactions Between Clay Minerals and Bacteria: A Review. *Pedosphere*, *25*(6), 799–810. https://doi.org/10.1016/S1002-0160(15)30061-8
- Mujah, D., Cheng, L., & Shahin, M. A. (2019). Microstructural and Geomechanical Study on Biocemented Sand for Optimization of MICP Process. *Journal of Materials in Civil Engineering*, *31*(4), 1–10. https://doi.org/10.1061/(ASCE)MT.1943-5533.0002660
- Ni, M., & Ratner, B. D. (2008). Differentiating calcium carbonate polymorphs by surface analysis techniques—an XPS and TOF-SIMS study. *Surface and Interface Analysis*, 40(10), 1356–1361. https://doi.org/10.1002/sia.2904
- NP_E-196. (1996). Análise granulométrica (peneiração e sedimentação).
- NP-E196-1996. (1966). Solos Analise Granulometrica. *Normas-LNEC, E 196 1966*.
- O'Donnell, S. T., Jr, E. K., & Rittmann, B. E. (2018). MIDP: Liquefaction Mitigation via Microbial Denitrification as a Two-Stage Process. II: MICP. *J. Geotech. Geoenviron. Eng.*, 143(12), 1–12. https://doi.org/10.1061/(ASCE)GT.1943-5606.0001806.
- Rezende, I. M., Prietto, P. D. M., Thomé, A., & Dalla Rosa, F. (2022). Mechanical Behavior of Microbially Induced Calcite Precipitation Cemented Sand. *Geotechnical and Geological Engineering*, *40*(4), 1997–2008. https://doi.org/10.1007/s10706-021-02006-4
- Rodríguez, R. F., & Cardoso, R. (2022). Relationship between Enzyme Concentration and Carbonate Precipitation in a Sand Treated By Biocementation Using Enzyme. *Proceedings of the 7th World Congress on Civil, Structural, and Environmental Engineering, April*. https://doi.org/10.11159/icgre22.240
- Roy, N., Frost, J. D., & Terzis, D. (2023). 3-D contact and pore network analysis of MICP cemented sands. *Granular Matter*, *25*(4), 1–16. https://doi.org/10.1007/s10035-023-01347-6
- Røyne, F. (2017). Life Cycle Assessment of BioZEment Concrete production based on bacteria. In *SP Technical Research Institute of Sweden*.

- Safdar, M. U., Mavroulidou, M., Gunn, M. J., Purchase, D., Gray, C., Payne, I., & Garelick, J. (2022). Towards the Development of Sustainable Ground Improvement Techniques Biocementation Study of an Organic Soil Content courtesy of Springer Nature, terms of use apply. Rights reserved. Content courtesy of Springer Nature, terms of use apply. Rights r. *Circular Economy and Sustainability*, 2022(2), 1589–1614.
- Salek-Maghsoudi, A., Vakhshiteh, F., Torabi, R., Hassani, S., Ganjali, M. R., Norouzi, P., Hosseini, M., & Abdollahi, M. (2018). Recent advances in biosensor technology in assessment of early diabetes biomarkers. *Biosensors and Bioelectronics*, *99*, 122–135. https://doi.org/10.1016/j.bios.2017.07.047
- Salifu, E., MacLachlan, E., Iyer, K. R., Knapp, C. W., & Tarantino, A. (2016). Application of microbially induced calcite precipitation in erosion mitigation and stabilisation of sandy soil foreshore slopes: A preliminary investigation. *Engineering Geology*, 201, 96–105. https://doi.org/10.1016/j.enggeo.2015.12.027
- Saneiyan, S., Ntarlagiannis, D., Werkema, D. D., & Ustra, A. (2018). Geophysical methods for monitoring soil stabilization processes. *Journal of Applied Geophysics*, *148*, 234–244. https://doi.org/10.1016/j.jappgeo.2017.12.008
- Schofield, A., & Wroth, P. (1968). Critical state soil mechanics. In *Engineer* (Vol. 16, Issues 3–4). https://api.semanticscholar.org/CorpusID:128155099
- Ševčík, R., Šašek, P., & Viani, A. (2018). Physical and nanomechanical properties of the synthetic anhydrous crystalline CaCO3 polymorphs: vaterite, aragonite and calcite. *Journal of Materials Science*, *53*(6), 4022–4033. https://doi.org/10.1007/s10853-017-1884-x
- Stabnikov, V., Jian, C., Ivanov, V., & Li, Y. (2013). Halotolerant, alkaliphilic urease-producing bacteria from different climate zones and their application for biocementation of sand. *World Journal of Microbiology and Biotechnology*, 29(8), 1453–1460. https://doi.org/10.1007/s11274-013-1309-1
- Stanier, Y., Doudoroff, M., & Adelberg, E. A. (1958). General microbiology. *General Microbiology, July*, 3–5. https://www.cabidigitallibrary.org/doi/full/10.5555/19581102009
- Stocks-Fischer, S., Galinat, J. K., & Bang, S. S. (1999). Microbiological precipitation of CaCO3. *Soil Biology and Biochemistry*, *31*(11), 1563–1571. https://doi.org/10.1016/S0038-0717(99)00082-6
- Stroes-Gascoyne, S. (2010). Microbial occurrence in bentonite-based buffer, backfill and sealing materials from large-scale experiments at AECL's Underground Research Laboratory. *Applied Clay Science*, *47*(1–2), 36–42. https://doi.org/10.1016/j.clay.2008.07.022
- Sun, X., Miao, L., & Chen, R. (2019). Effects of Different Clay's Percentages on Improvement of Sand-Clay Mixtures with Microbially Induced Calcite Precipitation. *Geomicrobiology Journal*, *36*(9), 810–818. https://doi.org/10.1080/01490451.2019.1631912
- Terzis, D. (2017). Kinetics, Mechanics and Micro-structure of Bio-cemented Soils [ÉCOLE POLYTECHNIQUE FÉDÉRALE DE LAUSANNE]. In *Geomechanics for Energy and the Environment* (Vol. 8).

- https://doi.org/https://www.semanticscholar.org/paper/50ba53a5fce26f7f4a18704ca6b221c9bc2b000b
- Terzis, D., Bernier-Latmani, R., & Laloui, L. (2016). Fabric characteristics and mechanical response of bio-improved sand to various treatment conditions. *Géotechnique Letters*, *6*(1), 50–57. https://doi.org/10.1680/jgele.15.00134
- Terzis, D., & Laloui, L. (2018). 3-D micro-architecture and mechanical response of soil cemented via microbial-induced calcite precipitation. *Scientific Reports*, 8(1), 1416. https://doi.org/10.1038/s41598-018-19895-w
- Terzis, D., & Laloui, L. (2019a). Cell-free soil bio-cementation with strength, dilatancy and fabric characterization.

 Acta Geotechnica, 14(3), 639–656. https://doi.org/10.1007/s11440-019-00764-3
- Terzis, D., & Laloui, L. (2019b). A decade of progress and turning points in the understanding of bio-improved soils: A review. *Geomechanics for Energy and the Environment*, 19, 100116. https://doi.org/10.1016/j.gete.2019.03.001
- Vail, Zhu, C., Tang, C.-S., Anderson, Moroski, & Montalbo-Lomboy. (2019). Desiccation Cracking Behavior of MICP-Treated Bentonite. *Geosciences*, *9*(9), 385. https://doi.org/10.3390/geosciences9090385
- Valentim, J. P. P. (2016). *Optimization of a Lab-On-Chip Device to Study the Biocementation of Soils: Vol. MSc.*Instituto Superior Técnico Universidade de Lisboa.
- van Paassen, L. A. (2009). *Biogrout: ground improvement by microbially induced carbonate precipitation*. Delft University of Technology.
- van Paassen, L. A. (2011). Bio-Mediated Ground Improvement: From Laboratory Experiment to Pilot Applications. *Geo-Frontiers 2011*, 4099–4108. https://doi.org/10.1061/41165(397)419
- van Paassen, L. A., Ghose, R., van der Linden, T. J. M., van der Star, W. R. L., & van Loosdrecht, M. C. M. (2010).

 Quantifying biomediated ground improvement by ureolysis: Large-scale biogrout experiment. *Journal of Geotechnical and Geoenvironmental Engineering*, 136(12), 1721–1728.

 https://doi.org/10.1061/(ASCE)GT.1943-5606.0000382
- van Paassen, L. A., Harkes, M. P., Van Zwieten, G. A., Van Der Zon, W. H., Van Der Star, W. R. L., & Van Loosdrecht, M. C. M. (2009). Scale up of BioGrout: A biological ground reinforcement method. *Proceedings of the 17th International Conference on Soil Mechanics and Geotechnical Engineering: The Academia and Practice of Geotechnical Engineering*, 3, 2328–2333. https://doi.org/10.3233/978-1-60750-031-5-2328
- Vandevivere, P., Welch, S. A., & Ullman, W. J. (1994). MICROBIAL. 241–251.
- Vargas-Bernal, R., Rodrguez-Miranda, E., & Herrera-Prez, G. (2012). Evolution and Expectations of Enzymatic Biosensors for Pesticides. In R. P. Soundararajan (Ed.), *Pesticides Advances in Chemical and Botanical Pesticides*. InTech. https://doi.org/10.5772/46227
- Volpatti, L. R., & Yetisen, A. K. (2014). Commercialization of microfluidic devices. Trends in Biotechnology, 32(7),

- 347-350. https://doi.org/10.1016/j.tibtech.2014.04.010
- Wang, Y., Soga, K., DeJong, J. T., & Kabla, A. J. (2019). Microscale Visualization of Microbial-Induced Calcium Carbonate Precipitation Processes. *Journal of Geotechnical and Geoenvironmental Engineering*, *145*(9), 1–13. https://doi.org/10.1061/(ASCE)GT.1943-5606.0002079
- Wei, S., Cui, H., Jiang, Z., Liu, H., He, H., & Fang, N. (2015). Biomineralization processes of calcite induced by bacteria isolated from marine sediments. *Brazilian Journal of Microbiology*, *46*(2), 455–464. https://doi.org/10.1590/S1517-838246220140533
- Weil, M. H., DeJong, J. T., Martinez, B. C., & Mortensen, B. M. (2012). Seismic and resistivity measurements for real-time monitoring of microbially induced calcite precipitation in sand. *Geotechnical Testing Journal*, 35(2). https://doi.org/10.1520/GTJ103365
- Whiffin, V. S. (2004). Microbial CaCO3 Precipitation for the production of Biocement. In *Midwives chronicle*. School of Biological Sciences & Biotechnology Murdoch University Western Australia.
- Whiffin, V. S., van Paassen, L. A., & Harkes, M. P. (2007). Microbial Carbonate Precipitation as a Soil Improvement Technique. *Geomicrobiology Journal*, *24*(5), 417–423. https://doi.org/10.1080/01490450701436505
- Wise, K. (2006). Preparing Spread Plates Protocols. American Society for Microbiology.
- Wu, S., Li, B., & Chu, J. (2021). Stress-Dilatancy Behavior of MICP-Treated Sand. *International Journal of Geomechanics*, 21(3), 1–12. https://doi.org/10.1061/(ASCE)GM.1943-5622.0001923
- Wu, Y., Ajo-Franklin, J. B., Spycher, N., Hubbard, S. S., Zhang, G., Williams, K. H., Taylor, J., Fujita, Y., & Smith, R. (2011). Geophysical monitoring and reactive transport modeling of ureolytically-driven calcium carbonate precipitation. *Geochemical Transactions*, *12*(1), 7. https://doi.org/10.1186/1467-4866-12-7
- Xiao, Y., Long, L., Matthew Evans, T., Zhou, H., Liu, H., & Stuedlein, A. W. (2019). Effect of Particle Shape on Stress-Dilatancy Responses of Medium-Dense Sands. *Journal of Geotechnical and Geoenvironmental Engineering*, 145(2), 1–15. https://doi.org/10.1061/(ASCE)GT.1943-5606.0001994
- Xiao, Y., Wu, B., Shi, J., Wang, L., & Liu, H.-L. (2023). Acoustic Emission of Biocemented Calcareous Sand Base. International Journal of Geomechanics, 23(9), 1–10. https://doi.org/10.1061/IJGNAI.GMENG-8817
- Yasuhara, H., Neupane, D., Hayashi, K., & Okamura, M. (2012). Experiments and predictions of physical properties of sand cemented by enzymatically-induced carbonate precipitation. *Soils and Foundations*, *52*(3), 539–549. https://doi.org/10.1016/j.sandf.2012.05.011
- Yin, T., Zhang, Z., Huang, X., Shire, T., & Hanley, K. J. (2021). On the morphology and pressure-filtration characteristics of filter cake formation: Insight from coupled CFD–DEM simulations. *Tunnelling and Underground Space Technology*, 111(February), 103856. https://doi.org/10.1016/j.tust.2021.103856
- Yu, T., Souli, H., Pechaud, Y., & Fleureau, J. M. (2021). Review on engineering properties of micp-treated soils.

- Geomechanics and Engineering, 27(1), 13-30. https://doi.org/10.12989/gae.2021.27.1.013
- Zhao, Y., Zhang, P., Fang, H., Guo, C., Zhang, B., & Wang, F. (2021). Bentonite-assisted microbial-induced carbonate precipitation for coarse soil improvement. *Bulletin of Engineering Geology and the Environment*, 80(7), 5623–5632. https://doi.org/10.1007/s10064-021-02302-6
- Zhu, Y., Li, Y., Lu, A., Wang, H., Yang, X., Wang, C., Cao, W., Wang, Q., Zhang, X., Pan, D., & Pan, X. (2011). Study of the Interaction Between Bentonite and a Strain of Bacillus Mucilaginosus. *Clays and Clay Minerals*, *59*(5), 538–545. https://doi.org/10.1346/CCMN.2011.0590511